# Characteristics of Forced Convection Heat Transfer to R125 at Supercritical State in a Horizontal Tube

# Kenmerken van warmteoverdracht in gedwongen convectie naar R125 in de superkritische toestand in een horizontale buis

Marija Lazova

Supervisors: prof. dr. M. De Paepe, prof. dr. S. Lecompte
Dissertation submitted in fulfillment of the requirements for the degree of Doctor of Electromechanical Engineering

Department of Electromechanical, Systems and Metal Engineering
Chairman: prof. dr. P. De Baets
Faculty of Engineering and Architecture
Ghent University
Academic year 2020-2021

GHENT UNIVERSITY

# Examination board

Prof. Dr. ir. Patrick De Baets (Ghent University, Chair)

Prof. Dr. ir. Michel De Paepe (Ghent University, Promoter)

Prof. Dr. ir. Steven Lecopmte (Ghent University, Co-promoter)

Prof. Dr. ir. Josua Meyer (University of Pretoria, South Africa)

Prof. Dr. ir. Dimitris Manolakos (Agricultural University of Athens, Greece)

Dr. ir. Marnix Van Belleghem (Belgian Boiler Company)

Prof. Dr. ir. Jelle Laverge (Ghent University)

Prof. Dr. ir. Sebastian Verhelst (Ghent University, Secretary).

# Acknowledgement

First of all, I would like to thank God for giving me the strength to go through this unique life path.

Then, I would like to thank to everyone, to everyone who had a positive "touch" and contributed this chapter of my life to have such an end.

Last but not least, I would like to thank to the most important category of my life. That category is "f-n-f". Without my family and friends, it would have been absolutely impossible to cross the finish line of this "PhD marathon". I would like to thank them for their sincere support, shared love and chocolates :). Thank you for constantly reminding me how strong the MACEDONIAN heart is.

# Благодарност

Пред се' би сакала да му се заблагодарам на Господ што ми даде сила да го изодам овој посебен пат.

Потоа, би сакала да им се заблагодарам на сите, на сите што допридонесоа ова поглавје од мојот живот да има ваков завршеток.

На крај, би сакала да и' се заблагодарам на најважната категорија во мојот живот. Тоа е категоријата „с-и-п“. Без моето семејство и пријатели, ќе беше апсолутно невозможно да се премине целта на овој „докторандски маратон“. Би сакала да им се заблагодарам за искрената поддршка, споделена љубов и чоколади :). Ви благодарам што постојано ме потсетувавте колку е силно МАКЕДОНСКОТО срце.

# Contents

# List of Figures

# List of Tables

# Nomenclature

**Symbols**

| | | |
|---|---|---|
| $A$ | Heat transfer surface area | $[m^2]$ |
| $a$ | Annular diameter ratio | $[-]$ |
| $C$ | Constant | $[-]$ |
| $c_p$ | Specific heat capacity | $[J/(kgK)]$ |
| $d$ | Diameter of inner tube | $[m]$ |
| $D$ | Diameter of annulus | $[m]$ |
| $f$ | Friction factor | $[-]$ |
| $g$ | Gravitational acceleration | $[m/s^2]$ |
| $G$ | Mass flux | $[kg/(m^2s)]$ |
| $h$ | Enthalpy | $[J/kg]$ |
| $HTC$ | Heat transfer coefficient | $[W/(m^2K)]$ |
| $L$ | Length | $[m]$ |
| $LMTD$ | Log Mean Temperature Difference method | $[-]$ |
| $\dot{m}$ | Mass flow rate | $[kg/s]$ |
| $P$ | Constant | $[-]$ |
| $p$ | Pressure | $[bar; Pa]$ |
| $R$ | Thermal resistance | $[K/W]$ |
| $T$ | Temperature | $[C; K]$ |
| $\dot{q}$ | Heat flux | $[W/m^2]$ |
| $Q$ | Heat transfer rate | $[W]$ |
| $U$ | Overall heat transfer coefficient | $[W/(m^2K)]$ |

**Subscripts**

| | | |
|---|---|---|
| $b$ | Bulk | |
| $bot$ | Bottom (surface) | |
| $cr$ | Critical | |
| $e$ | Entrance (tube) | |
| $hf$ | Heating fluid | |
| $hy$ | Hydraulic | |
| $i$ | Inner | |
| $in$ | Inlet condition | |
| $loc$ | Local condition | |
| $n$ | Discretization step | |
| $o$ | Outer | |
| $out$ | Outlet condition | |
| $pc$ | Pseudocritical | |
| $t$ | Thickness | |
| $top$ | Top (surface) | |
| $w$ | Wall | |
| $wf$ | Working fluid | |

**Greek Symbols**

| | | |
|---|---|---|
| $\beta$ | Turbulent mixing coefficient | $[-]$ |
| $\delta$ | Thermal boundary layer | $[-]$ |
| $\kappa$ | Thermal conductivity | $[W/(mK)]$ |
| $\mu$ | Dynamic viscosity | $[Pas]$ |
| $\nu$ | Kinematic viscosity | $[m^2s]$ |
| $\rho$ | Density | $[kg/m^3]$ |

**Dimensionless numbers**

| | | |
|---|---|---|
| $E$ | Eckert number | $[-]$ |
| $Gr$ | Grashof number | $[-]$ |
| $Nu$ | Nusselt number | $[-]$ |

| | | |
|---|---|---|
| $Pr$ | Prandtl number | [–] |
| $Re$ | Reynolds number | [–] |

**Abbreviations**

| | |
|---|---|
| $DHT$ | Deteriorated Heat Transfer |
| $EHT$ | Enhanced Heat Transfer |
| $EU$ | European Union |
| $GWP$ | Global Warming Potential |
| $IEA$ | International Energy Agency |
| $iSCORe$ | SuperCritical Organic RankinE |
| $NHT$ | Normal Heat Transfer |
| $ODP$ | Ozone Depletion Potential |
| $ORC$ | Organic Rankine Cycle |
| $SCW$ | Supercritical Water |
| $SCWR$ | Supercritical Water Reactor |

# Summary

In the last 100 years, the energy use has risen significantly in various sectors. Up to 42% of the worldwide energy is used in industry. However, of this share 50% could be recovered as residual heat (i.e. waste heat). Therefore, there is a huge potential for waste heat recovery from industry. However, the temperature of this heat is usually lower than 200°C and cannot be used in the classical thermal processes for electricity production. A promising technology that can convert low-to-medium temperature heat (90-250°C) into electricity is the organic Rankine cycle (ORC).

The ORC is a thermodynamic power cycle that resembles the classical Clausius-Rankine cycle but instead of water it uses an alternative working fluid (e.g. refrigerants). The ORC consists of four basic components: a pump, a heat exchanger (an evaporator or a vapour generator), a condenser and an expander. The working fluid is at first pressurized and transported to the evaporator. In the evaporator the working fluid is heated at constant pressure to superheated or saturated vapour. Then there is an expansion process in the expander/turbine to extract the mechanical work. By dissipating the heat, the working fluid is condensed to saturated liquid in the condenser. The condensed liquid is pumped again to the desired pressure with which the cycle closes and the process repeats again.

Even though the ORC is well known technology there is still room for improving the efficiency and the performance. One possible way to achieve this is to ensure supercritical heat transfer in the vapour generator. The heat addition in the heat exchanger occurs at a near constant pressure which is above the critical pressure of the working fluid. This means that the two-phase region of the saturation curve is omitted and the heat addition is accompanied by a temperature increase of the working fluid. The benefit lays in a reduced temperature difference between the heat source and the working fluid temperature profile. The supercritical vapour expands in the turbine/expander and generates mechanical work. The working fluid is cooled down in the condenser up to saturated liquid. Then the working fluid is pressurized with the pump and the cycle is closed. Hence, operating with supercritical pressure can lead to improved cycle efficiency. This thermodynamic cycle, with supercritical heat addition and subcritical heat rejection is called a transcritical cycle.

Research activities on heat transfer to fluids at supercritical pressures started in the early $20^{th}$ century. In these early works the focus was mainly on inves-

tigating supercritical heat transfer of water and $CO_2$. Furthermore, the scope of the earlier experimental investigations was limited to vertical flow directions (upward and downward flow) in small tube diameters. There are many heat transfer correlations available in literature. However, their use for practical applications is limited because they are mainly validated with the specific data that they were derived for. Furthermore, there is little information in literature available about supercritical heat transfer to refrigerants circulating in horizontal flow and in large tube diameters. Additionally, the buoyancy has a different effect in horizontal and vertical flow direction. Therefore, experimental investigation of forced convection heat transfer to refrigerants at supercritical pressure is necessary.

Particularly for this thesis, a new test facility was built. The aim was performing heat transfer measurements to supercritical refrigerants under organic Rankine cycle conditions. More specifically, this means heat transfer measurements at low temperatures (heat fluxes) of the heating fluid (90-125°C). On a component level, the test facility 'iSCORe' is similar to an organic Rankine cycle but instead of an expander and expansion valve was used. Furthermore, the configuration of the test section was a horizontal tube-in-tube heat exchanger with a counter-current flow. The working fluid was flowing in the central tube while the heating fluid in the annulus. The central tube has an outer diameter of 28 $mm$ and inner diameter of 24 $mm$. Moreover, the test facility was equipped with a number of pressure and temperature sensors needed for control and measurements purposes.

A number of measurements were performed by varying the inlet parameters (mass flux, heat flux, pressures). The mass flux was in the range of 400-650 $kg/(m^2s)$, the heat flux was between 14-28 $kW/m^2$ and the pressure of the working fluid was (1.05-1.15)$p_{cr}$. A real challenge when working with fluids at supercritical state is closing the heat balance over the test section. In certain operating conditions the deviation of the energy balance can reach up to 20%. This is especially noticeable when the fluid is near the pseudocritical point. Moreover, the reliability of the test facility was verified by repeating several different measurements.

Based on the experimental results the supercritical heat transfer is strongly affected by the mass fluxes and the heat fluxes. Higher mass flux and lower heat flux lead to enhanced heat transfer. However, there was one deviation noticed on this trend. The heat transfer shows enhancement at lower mass flux when the fluid is close to the pseudocritical temperature. This could be due to the rapid changes of the thermophysical properties. Furthermore, at pressure closer to the critical pressure of the working fluid enhanced heat transfer is observed. Moreover, it was determined that the buoyancy effect cannot be neglected in horizontal flow.

Furthermore, the results from the measurements were compared with heat transfer correlations from literature. Even though the heat transfer correlations have a correction factor in order to account for the drastic property changes, they do not show good agreement with the experimental results in the entire range. Therefore, for deriving general heat transfer correlation that will be

applicable for wider operating conditions it is important the heat transfer correlation to be validated with extensive experimental data.

In conclusion, first set of measurements for supercritical R125 was obtained. The reproducibility tests prove good operation of the test facility. There were proposed suggestions for practical improvements to the test facility and to lower the uncertainties in the measurements.

# Samenvatting

In de afgelopen 100 jaar is het energieverbruik in verschillende sectoren drastisch gestegen. Meer bepaald wordt ook 42% van de wereldwijde energie gebruikt in de industrie. Alle industriële processen gaan echter gepaard met restwarmte die tot 50% recuperatie toelaat. Daarom is er een opmerkelijk potentieel voor energierecuperatie. De temperatuur van de afgevoerde warmte is echter meestal lager dan 200°C en kan niet worden gebruikt in de klassieke thermische processen voor elektriciteitsproductie. Een veelbelovende technologie die warmte van lage tot gemiddelde temperatuur (90-250°C) kan omzetten in elektriciteit is de organische Rankine-cyclus (ORC).

De ORC is een thermodynamische energiecyclus die lijkt op de klassieke Clausius-Rankine-cyclus, maar in plaats van water gebruikt hij een alternatief werkingsmedium. De ORC bestaat uit 4 basiscomponenten: een pomp, een warmtewisselaar (een verdamper of een dampgenerator), een condensor en een expander. De werkvloeistof wordt eerst onder druk gezet en naar de verdamper getransporteerd. In de verdamper wordt de werkvloeistof onder constante druk verhit tot oververhitte of verzadigde damp. Dan is er een expansieproces in de expander / turbine om het mechanische werk te onttrekken. Door de warmte af te voeren wordt de werkvloeistof in de condensor gecondenseerd tot verzadigde vloeistof. De gecondenseerde vloeistof wordt weer naar de gewenste druk gepompt waarmee de cyclus sluit en het proces herhaalt zich weer.

Hoewel de ORC een bekende technologie is, is er nog steeds ruimte om de efficiëntie van een dergelijke cyclus te verbeteren. Een mogelijke manier om dit te bereiken is door te zorgen voor superkritische warmteoverdracht in de warmtewisselaar (de dampgenerator). Het warmtetoevoegingsproces in de warmtewisselaar vindt plaats bij bijna constante druk die boven de kritische druk van de werkvloeistof ligt. Dit betekent dat het tweefasige gebied van de verzadigingskromme wordt weggelaten en dat de warmtetoevoeging gepaard gaat met een temperatuurverhoging van de werkvloeistof. Het voordeel ligt in een verminderd temperatuurverschil tussen de warmtebron en het temperatuurprofiel van de werkvloeistof. De superkritische damp zet uit in de turbine / expander en genereert arbeid. De werkvloeistof wordt in de condensor afgekoeld tot verzadigde vloeistof. Vervolgens wordt de werkvloeistof onder druk gezet met de pomp en wordt de cyclus gesloten. Daarom kan werken met superkritische druk leiden tot een verbeterde cyclusefficiëntie. Deze thermodynamische

cyclus die warmte ontvangt bij superkritische condities en warmte afgeeft bij subkritische toestand wordt ook wel een transkritische ORC genoemd.

Onderzoeksactiviteiten met betrekking tot warmteoverdracht naar vloeistoffen bij superkritische druk begonnen in het begin van de $20^e$ eeuw. Bij deze eerste onderzoeken lag de focus echter vooral op het onderzoeken van superkritische warmteoverdracht naar water en $CO_2$. Bovendien was het eerdere experimentele onderzoek beperkt tot verticale stromingsrichtingen (opwaartse en neerwaartse stroming) in kleine buisdiameters. Er zijn veel correlaties voor warmteoverdracht beschikbaar in de literatuur. Het gebruik ervan voor praktische toepassingen is echter beperkt omdat ze voornamelijk bruikbaar zijn met de gegevens waarvoor ze zijn afgeleid. Daarenboven is er in de literatuur weinig informatie beschikbaar over superkritische warmteoverdracht naar koelmiddelen die circuleren in horizontale stroming en in grote buisdiameters. Bovendien heeft de invloed van de zwaartekracht een ander effect in horizontale en verticale stroomrichting. Daarom is experimenteel onderzoek naar de warmte overdracht bij geforceerde convectie betreffende ORC koelmiddelen bij superkritische druk noodzakelijk.

Speciaal voor dit proefschrift is een nieuwe testfaciliteit gebouwd. Het doel was het uitvoeren van metingen van superkritische warmteoverdracht naar koelmiddelen ORC omstandigheden. Meer specifiek betekent dit metingen van warmteoverdracht bij lage temperaturen (warmtefluxen) van de verwarmingsvloeistof (90-125°C). Op componentniveau lijkt de testfaciliteit 'iSCORe' op een organische Rankine-cyclus, maar in plaats van een expander wordt een expansieklep gebruikt. Verder bestond de testsectie uit een horizontale buis-in-buis tegenstroom warmtewisselaar. Het werkmedium stroomde in de centrale buis terwijl de thermische olie in de annulus stroomde. De centrale buis had een buitendiameter van 28 $mm$ en een binnendiameter van 24 $mm$. Bovendien was de testfaciliteit uitgerust met een aantal druk- en temperatuursensoren die nodig zijn voor de aansturing en de metingen.

Een aantal metingen werd uitgevoerd door de inlaatparameters (massaflux, warmteflux, drukken) te variëren. De massaflux was in het bereik van 400-650 $kg/(m^2s)$, de warmteflux was tussen 14-28 $kW/m^2$ en de druk van de werkvloeistof was (1,05-1,15) $p_{cr}$. Een echte uitdaging bij het werken met vloeistoffen in superkritische toestand is het sluiten van de warmtebalans over het testgedeelte. Onder bepaalde bedrijfsomstandigheden kan de afwijking van de energiebalans oplopen tot 20 %. Dit is vooral opvallend wanneer de vloeistof zich nabij het pseudokritische punt bevindt. Daarnaast werd de betrouwbaarheid van de testfaciliteit ook geverifieerd door verschillende metingen te herhalen.

Op basis van de experimentele resultaten wordt de superkritische warmteoverdracht sterk beïnvloed door de massflux en de warmteflux. Een hogere massaflux en een lagere warmteflux leiden tot een verbeterde warmteoverdracht. Er werd echter één afwijking opgemerkt. De overgedragen warmte kan ook worden verbeterd bij een lagere massaflux wanneer de vloeistof dicht bij de pseudokritische temperatuur ligt. Dit komt waarschijnlijk door de snelle veranderingen van de thermofysische eigenschappen. Bovendien wordt bij een

druk dichter bij de kritische druk van de werkvloeistof een verbeterde warmteoverdracht waargenomen. Bovendien werd bepaald dat het effect van de zwaartekracht niet kan worden verwaarloosd bij horizontale stroming.

Uiteindelijk werden de resultaten van de metingen vergeleken met correlaties van warmteoverdracht uit de literatuur. Hoewel de warmteoverdrachtscorrelaties een correctiefactor hebben om rekening te houden met de drastische eigenschapsveranderingen, vertonen ze geen goede overeenkomst met de experimentele resultaten in het hele bereik. Daarom is het voor het afleiden van algemenere correlaties van warmteoverdracht belangrijk om deze te valideren met uitgebreide experimentele gegevens.

Concluderend werd de eerste set metingen voor superkritisch R125 verkregen. De reproduceerbaarheidstests bewijzen een goede werking van de testfaciliteit. Er zijn suggesties gedaan voor praktische verbeteringen aan de testfaciliteit en om de onzekerheden in de metingen te verminderen.

# 1. Introduction

## 1.1 Current trends in energy use and environmental impact

Energy is important in all aspects of life. The energy use, by various sectors (industry, transport and building) has risen exponentially in the last 100 years. It is a result of a considerable increase in the world's population, industrial activity and technological development. Starting from the industrial revolution and continuing during the digital revolution, fossil fuels (crude oil, coal, natural gas) have been used as primary energy source for electricity generation. Figure 1.1. presents the increase of electricity production on a global level in the period between 1973 till 2015 [1] by using different energy sources. In four decades the electricity generation worldwide has increased by 45%. The category 'other' includes electricity generated from solar, geothermal, wind and other renewable sources.

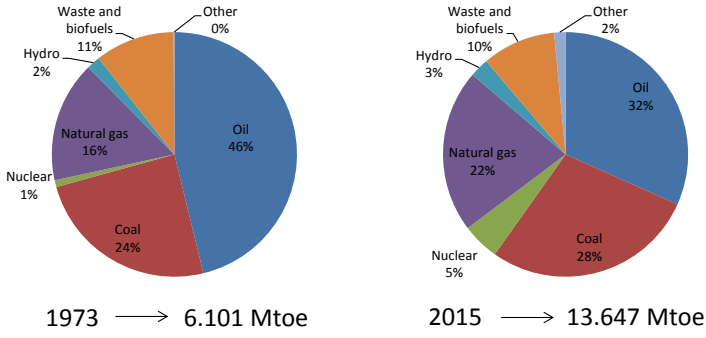


**Figure 1.1:** Global electricity production from 1973 till 2015, data retrieved from International Energy Agency (IEA) [1].

However, the wide use of conventional energy sources (fossil fuels) through the decades has led to their depletion on one hand and environmental concerns

like global warming potential (GWP), ozone depletion potential (ODP) and atmospheric pollution on the other [2].

Currently, almost 42% of the worldwide primary energy (730 $Mtoe/yr$) is used in industry [1]. This is illustrated in Figure 1.2. However, in Europe alone, the primary energy use in the industry is 275 $Mtoe/yr$ which is equivalent to 25% of the total share [3]. A large part of this energy is still available as flue gasses, exhaust air of drying installations, cooling water, afterburners, etc. This exhaust heat is available in the cement, chemical, glass, food, paper, plastic and steel industry. The potential of waste heat recovery from industry is remarkable. According to the statistical investigations up to 50% can be recovered as thermal energy [4]. In the European Union (EU) the annual unused waste heat potential has been estimated at 300-370 $TWh/year$ [4], [5]. The temperature level at which the waste heat is rejected from the industrial processes is usually lower than 200°C [5].

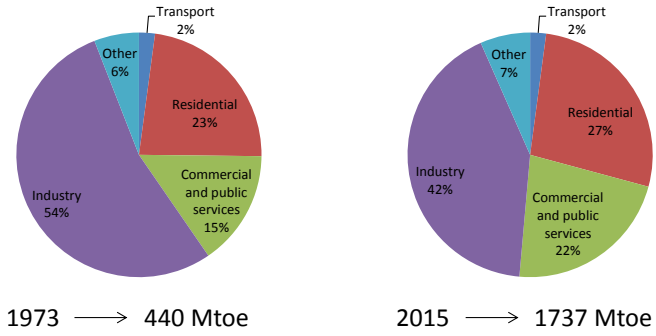


**Figure 1.2:** World electricity use from 1973 till 2015 by different sectors, Data retrieved from International Energy Agency (IEA) [1].

According to the International Energy Agency [1], energy prices have risen because of the increased use of fossil fuels and the difficulty to exploit these traditional energy sources. One way to mitigate the use of the conventional resources is possible by utilizing renewable energy sources for electricity production. However, this measure is projected to lead to increased energy prices [6].

Moreover, instead of focusing solely on the supply side, the demand can be reduced by incorporating energy efficiency measures. In the last decades, there is much effort in using renewable energy sources like solar, geothermal, wind and biomass. Also, waste heat from various industrial processes can be made valuable. The common practice in the past was discarding the excess (waste) heat, instead of exploiting it in various processes. All these energy resources are mainly available at low-to-medium temperatures and their potential for electricity generation is still not fully exploited [3].

Figure 1.3 illustrates the temperature ranges where <80°C is considered as very low, 90-150°C and 150-250°C as low-to-medium and 250-500°C as high temperature sources. Moreover, for each temperature range a possible thermodynamic cycle that can be used is indicated.


**Figure 1.3:** Temperature ranges of waste heat.

Low-to-medium temperature sources are considered within the range of 90-250°C and the utilization in conventional heat to electricity concepts is not cost-effective. Recovering or utilizing this energy, would considerably reduce the use of the conventional energy sources and would help to cope with the increased energy demand on global level [3]. On the other hand, in Europe it will help to comply with the 'Energy roadmap 2050 plan'[1] [7].

Depending on the characteristics like temperatures, mass flow rates, availability/uniformity etc. low-temperature heat can be utilized in a number of ways. The possible applications include district heating, heat-to-power, upgrading heat to higher temperature levels, etc. These applications indicate that there is an opportunity for developing suitable technical solutions for utilizing low-to-medium temperature heat sources.

Moreover, transportation of large quantities of heat over long distances is not always practical and presents a significant technological challenge in the near future. Therefore, low temperature heat-to-power cycles, attract a lot of interest in industry and research centers worldwide. This became especially clear in the last decade. One of the promising technologies that can be used for conversion of low-to-medium temperature heat into electricity is the organic Rankine cycle (ORC) [8–10].

## 1.2 Introducing the transcritical organic Rankine cycle

A thermodynamic power cycle is a cycle that converts heat into electricity while varying pressure, temperature and other state variables and eventually returning the system to its initial state [11]. The organic Rankine cycle (ORC) is a power cycle that can utilize low-to-medium temperature heat for electricity production. This cycle resembles the classical Clausius-Rankine cycle but instead of water, an alternative working fluid is used.

1. The EU goal to cut greenhouse gas emissions by 80–95% by 2050.

The main use of ORCs is to valorize low-to-medium temperature heat sources. In this category belong all the resources that cannot be utilized by traditional power steam cycles (Figure 1.3). Hence, there are many potential heat sources (solar energy, biomass, geothermal and waste heat) that can be exploited in ORC's.

In continuation a simple description of an ORC is presented. It consists of the following basic components: a pump, a heat exchanger (an evaporator or a vapour generator), a condenser and an expander. The corresponding component layout is depicted in Figure 1.4.

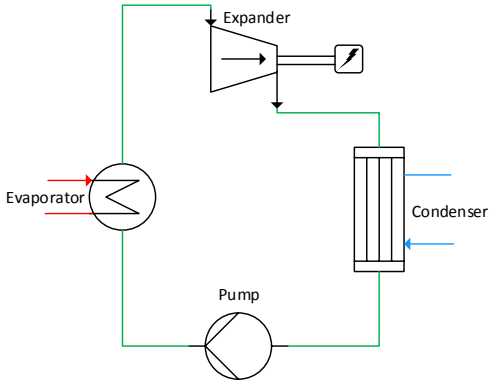


**Figure 1.4:** Basic layout of the organic Rankine cycle.

Concerning the operating conditions, the ORC can, amongst other types be classified as subcritical, transcritical and supercritical. The thermodynamic processes of the subcritical and the transcritical organic Rankine cycles is depicted in Figure 1.5 and is represented on a temperature-entropy (T-s) diagram.

In the ***subcritical cycle*** all four thermal processes (pressurization, evaporation, expansion, condensation) appear at a pressure lower than the critical pressure of the working fluid. The following thermodynamic processes occur at subcritical operating conditions (marked with "'"): the working fluid is pressurized (1-2') and transported to the evaporator (2'-3'). In the evaporator the working fluid is heated at constant pressure to superheated or saturated vapour by undergoing the two-phase region of the saturation curve. Then there is a non-isentropic expansion process in the expander/turbine to extract the mechanical work (3'-4'). By dissipating the heat, the working fluid is condensed to saturated liquid in the condenser (4'-1). The condensed liquid is pumped again to the desired pressure with which the cycle closes and the process repeats again.

The efficiency of a subcritical ORC with an isothermal evaporation is $\sim$ 20% [3]. Nevertheless, this efficiency, depends on many factors (heat source temperature, working fluid, thermal stability, etc. [12]). However, improving

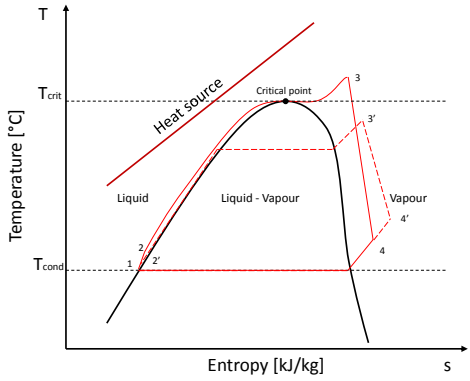


**Figure 1.5:** Temperature-entropy (T-s) diagram of subcritical and transcritical organic Rankine cycle.

the efficiency of such cycle is possible by using zeotropic mixtures as working fluids [13]. Zeotropic mixtures have a property referred as 'temperature slip' in the evaporation and condensation process which enables a better thermal match in the heat exchangers. This can potentially reduce the exergy destruction rate because of temperature differences and thus lead to higher efficiencies.

However, a better match between the temperature profiles of the heating and the working fluid is possible when ensuring supercritical heat transfer in the main heat exchanger. Thus, this cycle is referred as transcritical ORC. Moreover, the distinction between the subcritical and the transcritical cycles lies in the heat addition process.

In a ***transcritical cycle*** the fluid is first pressurized up to the desired pressure, that is above the critical pressure of the working fluid (1-2) [14], [15], (Figure 1.5). The heat addition process in the heat exchanger at the hot side (referred to as a vapour generator) occurs at constant pressure. The heat transfer at supercritical conditions is introduced in Chapter 2. The two-phase region of the saturation curve (2-3), is omitted and heat addition is accompanied by a temperature increase of the working fluid. The supercritical vapour expands in the turbine/expander and generates mechanical work (3-4). At constant pressure, the working fluid is cooled down in the condenser up to saturated liquid (4-1). The working fluid is pressurized with the pump and the cycle is closed.

As already mentioned, this leads to a reduced temperature difference between the heat source and the working fluid temperature profile [12]. Hence, a better thermal match between the temperature glides of both fluids is achieved in the heat exchanger. This can be used to reach higher net power output and improved cycle efficiency. In such a case, the system's irreversibility is reduced [12] which leads to minimization of the exergy losses and exergy destruction in the heat exchanger. Concerning the efficiency of a transcritical ORC, an

improvement of about 8% was observed for supercritical conditions compared to subcritical conditions due to the higher second law efficiency [3], [14], [15].

On the other hand, for the ***supercritical cycles***, the working fluid is at supercritical conditions in both the condenser (heat sink) and the vapour generator (heat source) [16]. However, in literature this distinction is not used strictly and transcritical cycles are sometimes referred as supercritical cycles.

Performance evaluation of the transcritical ORC was done by several researcher using different fluids [14], [17–19]. According to the comparative theoretical study of Chen et al. [17] the transcritical cycle has higher performance because there is a better thermal match between the temperature profiles of the heating and the working fluid. In their studies, $CO_2$ was considered as a working fluid in a transcritical ORC and R123 as working fluid in a subcritical ORC. Furthermore, Schuster at al. [14] made a comparison of the subcritical ORC and the transcritical ORC with the working fluid R245fa at constant superheated vapour temperature. Even for constant conditions, the heat input is at higher average temperature in the case of supercritical operation. The enthalpy change (Figure 1.6) is larger than in the subcritical process for the same condensing pressure. In comparison, the feed pump's additional specific work to reach supercritical pressure is increased (Figure 1.6). Therefore, the gain provided by the supercritical vapour generator in minimizing the temperature difference between working fluid and heat source should be leveraged. In reality, keeping a small temperature difference between the heat source and the working fluid is not always cost effective because of the huge heat transfer area required. Low heat transfer coefficients make this even more detrimental.

Larjola et al. [20] pointed out that for a cycle that uses waste heat at a low-to-medium inlet temperature (90–250°C) as heat source, the best efficiency and highest power output usually is obtained when there is a good thermal match between the working fluid and the heating fluid profiles. This means, the system will have a better performance if the temperature difference between the heat source and the temperature of the working fluid in the heat exchanger is reduced, because of the lower system's 'irreversibility [2]

Figure 1.6 shows the different thermal match for R152a in a subcritical ORC and R143a in a transcritical ORC for the same maximum temperature and pinch point temperature difference [12] in order to produce the same power output of 1 $MW$. However, for obtaining the same power output the mass flow rate of the heating fluid is lower in the transcritical cycle. From the analysis can be concluded that the selection of a proper working fluid and the operating conditions have an effect on the thermal efficiency. By using R143a at supercritical pressure of 40 $bar$ ($p_{cr}$ = 37.6 $bar$), the thermal efficiency increases by a factor of 2.

Investigating the transcritical ORC represents a challenge and attracts the attention of many researchers. The focus can be on the performance enhance-

2. According to the second law of thermodynamics, it can be interpreted that entropy is produced by system's irreversibilities. In this case the better thermal match of the fluids provides reduced entropy creation because of the finite temperature heat transfer.

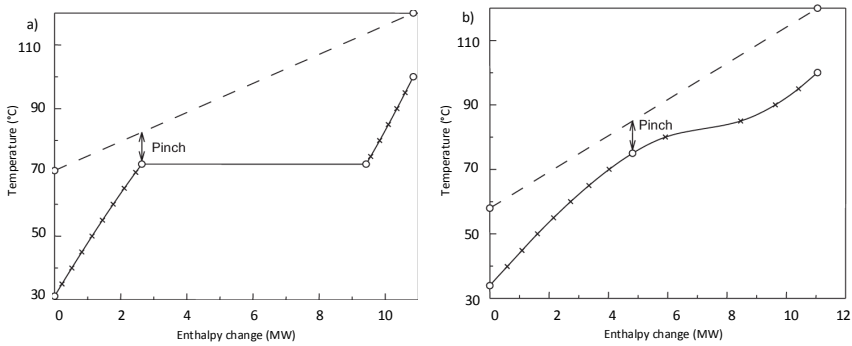


**Figure 1.6:** Thermal match in a subcritical and transcritical organic Rankine cycle in a QT diagram. (a) Heating R152a in a subcritical ORC at 20 *bar* from 31.16°C to 100°C. (b) Heating R143a in a transcritical ORC at 45 *bar* from 33.93°C to 100°C [15].

ment of each component, an appropriate working fluid selection [18], [19], [21] and determination of optimal cycle operation conditions [22]. In practice, a combination of all these aspects will lead to improved cycle efficiency. However, the heat exchanger at the hot side has a vital role in the transcritical ORC. Therefore, determining the behavior of the working fluid in the heat exchanger operating at supercritical pressures and temperatures is of primary interest in this thesis.

### 1.2.1 Applications using a fluid at supercritical state

There are many different applications that use fluids at supercritical state. Increasing the operational pressure and temperature of the working fluids typically lead to higher cycle efficiency (i.e. Carnot efficiency). Several coal power plants worldwide use supercritical water at a pressure of 330 *bar* [23], [24]. An improvement of the thermal efficiency from 40% to 50% is achieved in these coal-fired power plants. Additionally, the use of fluids at supercritical state as coolant has been proposed in the nuclear reactor designs (Supercritical Water Reactor - SCWR). Most of the studies have been done in the USA and USSR in the 1960's. Furthermore, this idea regained interest in 1990's when the Generation IV advanced nuclear reactors were developed [25]. Superconductivity effects were obtained by cooling the conductor with fluids (helium) at supercritical state [26]. There are many other fields where fluids at supercritical state can be applied. Rockets and military aircraft are cooled using fuel at supercritical pressure as an on-board coolant. Additionally, supercomputer elements, magnets, power transmission cables and highly loaded machine elements such as gas turbine blades are cooled with supercritical fluids.

The transcritical ORC is considered as a promising low-to-medium heat utilization technology. Research activities of a solar receiver coupled to an ORC

engine for maximizing the thermal efficiency by using toluene as working fluid is one of the first investigations regarding transcritical ORC [27]. On the other hand, the first commercial transcritical ORC was installed in Oregon, USA, in 2012 [28]. Low-temperature heat from a geothermal brine with a temperature of 138°C is recovered by using R134a as working fluid. R134a had been chosen over other hydrocarbons because of the ability to recover low temperature heat sources for generating electricity, due to the low critical temperature and pressure (101°C and 41 *bar*). This refrigerant is non-flammable, non-toxic, has an ODP of 0 but has a GWP of 1430. The designed capacity of the binary power cycle is 22 $MW$, but it exceeded expectations. The current total output of net base load power is 29.7 $MW$. This has been achieved thanks to a good selection of the working fluid operating under supercritical conditions.

In 2013 in Canada, South of the city of Calgary on Crowsnest Pass, another transcritical ORC for waste heat recovery started its operation [29]. The waste heat from jet turbines heats up the working fluid R600 (butane) up to 250°C expanding it in the turboexpander at supercritical conditions. The critical pressure and temperature of R600 are 38 *bar* and 152°C respectively. The capacity of this installation is 7.5 $MW$, of which 6.5 $MW$ is sent to the grid.

Besides, there is one more relevant example for a solar transcritical ORC, where the construction of the heat exchanger (vapour generator) was done in collaboration with industry [30]. The vapour generator was of a shell-and-tube type with a large tube diameter ($d_o = 28\ mm$). The heating source temperature was in the range of 80-100°C and mass flux of the working fluid (R404A) between 300-640 $kg/m^2s$. However, it should be highlighted that for designing the vapour generator, heat transfer correlations from literature were used. In order to account for the uncertainties of the heat transfer correlations, the heat exchanger was oversized by 20%. Therefore, for more accurate design there is a need to develop a general heat transfer correlation with improved accuracy. Usually, the heat exchangers in the ORCs are with horizontal flow arrangements and in Section 2.4, the effect of the flow direction on the supercritical heat transfer is elaborated.

## 1.3 Working fluids - for transcritical organic Rankine cycle

Many different fluids can be considered as potential working medium for the ORC, besides water/steam that is used in the classical Rankine power cycle. For an optimal selection of working fluids several selection criteria can be employed.

In general, the proper selection is linked with the system efficiency, operating conditions, environmental impact, the economic feasibility (cost of the fluid and the system) and the safety aspects. As promising working media are considered the fluids (with $C$ atoms) used in the refrigeration systems [12], [31], [32]. Furthermore, the selection of the working fluid depends on the temperature

profile of the heat source [18]. Vetter et al. [33], observed in a theoretical study that for optimal power output the critical temperature of working fluid should be 20% lower than the heat source temperature. The reason is to ensure that the working fluid will be heated above its critical temperature. In case of a lower heating fluid temperature, the working fluid will remain at a temperature below the critical temperature. On the other hand, if the heating fluid is at a much higher temperature than the critical temperature of the working fluid, the cycle will show reduced performance.

Fulfilling all the criteria when selecting a working fluid for an ORC system is very difficult. Therefore, there is always a trade-off between aforementioned requirements. Furthermore, there is no consensus or an optimal choice for the best working fluid that can satisfy all the measures.

Table 1.1 gives an overview of working fluids that are potential candidates for a transcritical ORC based on the temperature range of the waste heat stream [12], [31], [32]. The refrigerants have large molecular weight and low boiling temperature and pressure. Furthermore, the critical point of the refrigerants is obtained at lower temperatures and pressures, compared to water. These are one of the characteristics that make the refrigerants potential candidates for ORC's.

**Table 1.1:** Potential working fluids for a transcritical ORC's.

| *Fluid* | $T_{cr}$ (°C) | $p_{cr}$ (bar) | $ATL(yr)$ | $ODP$ | $GWP(100yr)$ |
|---|---|---|---|---|---|
| R1233zd(E) | 166.45 | 36.24 | / | 0 | 1 |
| R125 | 66.02 | 36.2 | 29 | 0 | 3,500 |
| R134a | 101.03 | 40.56 | 14 | 0 | 1,430 |
| R143a | 72.73 | 37.64 | 52 | 0 | 4,470 |
| R152a | 113.5 | 44.95 | 1.4 | 0 | 124 |
| R227ea | 101.74 | 29.29 | 34.2 | 0 | 3,220 |
| R236ea | 139.22 | 34.12 | 10.7 | 0 | 1,370 |
| R23 | 26.14 | 48.3 | 270 | 0 | 14,800 |
| R245fa | 154.05 | 36.4 | 7.6 | 0 | 900 |
| R245ca | 174.42 | 39.25 | 6.2 | 0 | 693 |
| R32 | 78.11 | 57.83 | 4.9 | 0 | 550 |
| R404A | 72.14 | 37.35 | 40.36 | 0 | 3,922 |
| R407C | 86.79 | 45.97 | 15,657 | 0 | 1,800 |
| R410A | 70.2 | 47.9 | 16.95 | 0 | 2,088 |
| R747 (CO2) | 31.1 | 73.8 | >50 | 0 | 1 |
| R218 | 71.89 | 26.8 | 2,600 | 0 | 8,830 |
| R318 | 115.2 | 27.78 | 3,200 | 0 | 10,250 |
| R31-10 | 113.18 | 23.2 | 2,600 | 0 | 8,600 |
| R41-12 | 147.41 | 20.5 | 4,100 | 0 | 9,160 |

In many theoretical studies, related to low-to-medium temperature transcritical ORC cycles, the working fluid R125 is considered as potential medium [32], [34–38]. The advantages of using R125 are the beneficial thermophysical

properties and the low critical pressure and temperature (36.2 *bar* and 66°C). In a number of comparative studies for transcritical ORCs [34–38], R125 is compared with many other fluids including $CO_2$. Due to the lower critical pressure the required pumping power is lower compared to the other fluids. Therefore, R125 is the fluid of interest in the present study.

R125 was selected to be used as working medium because of good thermophysical properties. Furthermore, R125 is a pure fluid (not a blend) with a relatively low critical pressure. Additionally, because of the low critical temperature it was possible to test low-to-medium (90-150°C) heating fluid temperatures.

## 1.4 Thermophysical fluid properties at supercritical state

### 1.4.1 Nomenclature and definitions for fluids at supercritical state

A pressure-temperature diagram of R125 is depicted in Figure 1.7. All important terms related to a fluid at supercritical state are illustrated in the same figure.

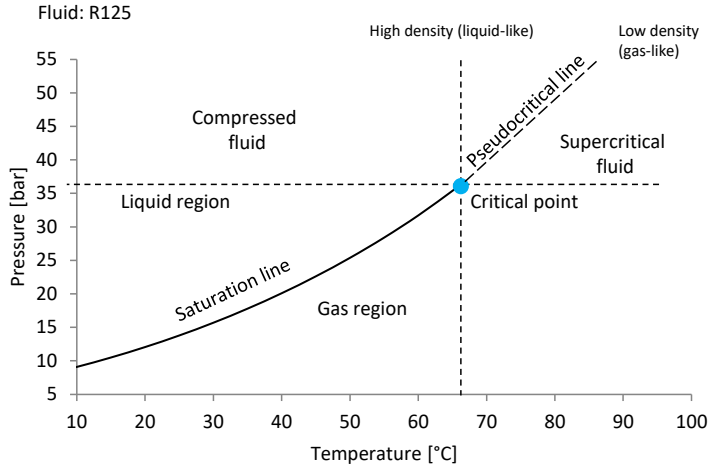


**Figure 1.7:** Pressure-temperature diagram of R125 indicating the saturation line, liquid region, gas region and supercritical region.

A fluid at *supercritical state* exceeds the values of pressure and temperature above its critical point. The *critical point* is the region where the distinction between the liquid and vapour of the fluid no longer exists. The critical point

is defined by the state parameters ($p_{cr}, T_{cr}, V_{cr}$) that have unique values for each fluid and are determined experimentally. To uniquely define the critical point only two state parameters are necessary (i.e $p_{cr}$ and $T_{cr}$ (see Figure 1.7).

The *pseudocritical point* corresponds to the maximum value (locus) of the specific heat capacity occurring at corresponding pressures and temperatures. The pseudocritical line connects the pseudocritical points. At each supercritical pressure, the specific heat capacity has its local maximum. This occurs at *pseudocritical temperature* $T_{pc}$, where the specific heat capacity $c_p$ reaches a peak and then falls steeply. The pseudocritical temperature is higher than the critical temperature ($T_{pc} > T_{cr}$) of a fluid and is determined at each particular pressure. (The correlation for determining the pseudocritical temperature of R125 is given in Section 3.6.5.)

Furthermore, the *near-critical region* is defined as the narrow area around the (pseudo)critical point, where all thermophysical properties show strong variations.

### 1.4.2 Variations of the thermophysical fluid properties at supercritical state

Typical for fluids at supercritical state or at near-critical region is the strong variations of the thermophysical properties (density, $\rho$, viscosity, $\mu$, thermal conductivity, $\kappa$, specific heat capacity, $c_p$) [39]. Moreover, the properties of a fluid are strongly dependent on temperature, particularly in the critical or pseudocritical temperature range, where the specific heat capacity reaches a local maximum $c_p$. Below the pseudocritical temperature the fluid has more liquid-like properties while above it behaves more like a vapour [40].

Figure 1.8 gives an overview of the variation of (a) the specific heat capacity, $c_p$, (b) the density, $\rho$, (c) the viscosity, $\mu$, and (d) the thermal conductivity, $\kappa$ of the fluid R125 at different supercritical ($(1.05\text{-}1.15)p_{cr}$) pressures. The pseudocritical line for R125 connecting the pseudocritical points obtained at different pressures is illustrated in Figure 1.8 (a). Starting from the critical point the pressure and the temperature increase along the pseudocritical line but the local maximum (peak) of the specific heat capacity decreases till it is barely visible. The pseudocritical temperature $T_{pc}$ rises as well but the local maximum value of the specific heat $c_p$ becomes smaller and the variations of the other thermophysical properties are less pronounced. Furthermore, it can be noticed in Figure 1.8 (b) and in Figure 1.8 (c) that the density and the viscosity have dropped significantly, almost in a vertical line (i.e 90% and 110%, respectively), while the thermal conductivity of the fluid reaches a peak near the critical and pseudocritical region.

However, the magnitude of these variations is less pronounced with increase in pressure (far from the supercritical pressure of the designated fluid).

Under supercritical pressure, a fluid shows rather similar flow regimes to the conventional single-phase flow, with no phase change. Understanding the behavior of the thermophysical properties of a fluid progressing from subcritical

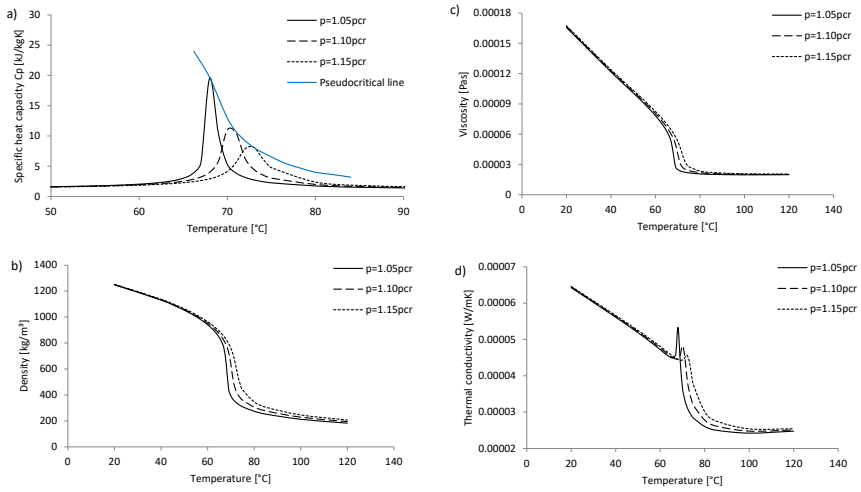


**Figure 1.8:** Variation of the thermophysical properties of R125 at supercritical pressure.

to supercritical state is important to correctly assess the heat transfer phenomena and presents a big challenge. Considerable effects on the heat transfer are expected due to strong property variations in the range of (1.01-1.2)$p_{cr}$ [41]. This is especially relevant when designing a heat exchanger suitable to operate under supercritical conditions. The value of the heat transfer coefficients (HTCs) and pressure drop depend on the thermophysical fluid properties. Due to the strong changes in thermophysical properties of the fluid during supercritical heating or cooling, the HTCs and the pressure drop are greatly dependent on the local fluid temperature and the inner wall temperature. All these changes influence the heat transfer mechanisms [30], [42], systematically elaborated in Chapter 2.

## 1.5 Objective of the study

Transcritical or supercritical thermodynamic cycles rely on the proper design and operation of their vapour generators. Yet, knowledge on this topic is scarce. It is generally accepted that there is an intricate interaction between the fast changing fluid properties and the fluid mechanics but the phenomena and the resulting impact is not understood.

The main focus of this thesis is to get a better understanding of heat transfer to refrigerants at supercritical state by experimental research, where the heating fluid of interest has a low-to-medium temperature (and a low heat flux). Concerning the heat exchanger design, the shell-and-tube configuration in horizontal layout is considered more suitable for the transcritical ORC

[30], [43], [44]. The tube diameters, the flow direction and the heating fluid temperature that are targeted in this thesis are also within the range of practical (industrial) applications [28–30].

According to the author's knowledge, experimental data for determining heat transfer characteristics of refrigerants (HFC's) is largely missing in open literature. Most of the studies related to heat transfer at supercritical state were done for water or $CO_2$ in vertical circular tubes [45], because of the interest in large scale thermal power plants.

Additionally, to date, there is no heat transfer correlation derived for working fluids (refrigerants) in horizontal flow during heating at relatively low heat fluxes and in large diameter tubes. This conclusion is also valid for R125 that is considered as suitable to be used in a transcritical ORC. The reason for using R125 is the low critical pressure and temperature and the beneficial thermophysical properties.

From the elaborated considerations above, it is clear that there is a need for extensive experimental work on supercritical heat transfer to refrigerants in horizontal orientation and this for relative large diameter tubes. Additional details about the gaps in literature can be found in Chapter 2.

Hence, the objective of this thesis can be summarized in the following points:

1. Defining the heat transfer characteristics of R125 in a horizontal flow with a tube diameter of 28 $mm$.
2. Determining the parameters that have an influence on the heat transfer coefficients.
3. Determining the suitability of existing heat transfer correlations to predict experimental heat transfer data of supercritical R125.

## 1.6 Outline

The chapters in this manuscript are organized in the following order.

In Chapter 2, a literature review of heat transfer at supercritical state is presented. At the beginning, the different heat transfer mechanisms typical for fluids at supercritical state are explained. Furthermore, a detailed study is made on different parameters that have an effect on the heat transfer. Determining the onset of deteriorated heat transfer is very important. In this chapter there is also a summary of the most significant heat transfer correlations derived for water and $CO_2$. Additionally, an overview of all heat transfer correlations derived for refrigerants is also presented.

Chapter 3 discusses the development of novel test facility 'iSCORe'. The control strategies and the experimental procedures are explained as well. Details about acquiring steady-state conditions followed by the performance validation of the test facility and the data reduction method are included as well. The uncertainty analysis are elaborated in Appendix A.

The experimental results of the local heat transfer coefficients obtained with R125 are presented in Chapter 4. Furthermore, the results are compared and evaluated with data from literature. Also, suggestions are given for improving the measurements.

Finally, the conclusions of this thesis are presented in Chapter 5. Furthermore, some recommendations for future work are also proposed.

# 2. Forced convection heat transfer to fluids at supercritical state

Fluids at supercritical state have always been present in nature. One typical example is the occurrence of supercritical water in underwater volcanoes in the oceans. Below the ocean depth of 2200 $m$ the pressure exceeds the critical point of water (22 $MPa$). The surrounding water that cools the lava is actually a fluid at supercritical state [46]. Another phenomenon found in nature are the minerals in aqueous solutions that have been processed at near or above the critical point of water. Starting from the $19^{th}$ century, this method, called hydrothermal processing has been used in the laboratories worldwide for producing high quality crystals [46] and is still used today. Moreover, the atmosphere of the planet Venus is mainly composed of supercritical carbon dioxide, [47], the atmosphere of Jupiter consists mostly of supercritical hydrogen and that of Saturn of supercritical helium [48].

Investigation on heat transfer to fluids at supercritical pressures started in the early 30's of the $20^{th}$ century. Until now, there is a lot of data in literature obtained for forced convection heat transfer to fluids under supercritical conditions. These studies are mainly considering water, carbon dioxide and cryogenic fluids, like hydrogen and helium, in either heating or cooling applications. Besides these commonly used fluids, there were also some experiments done on refrigerants. Most of the available data is for circular tubes and only a few studies were done in annuli, rectangular channels and bundles [25]. These fluids were mainly tested in small tube diameters in a vertical flow. Common for all heat transfer experiments at supercritical state is the complexity of achieving accurate measurements because of extreme variations in thermophysical properties with temperature. Additional difficulties occur due to the high operating pressures. At these operating conditions, the density, the specific heat capacity, the viscosity and the thermal conductivity of a fluid vary drastically at very small pressure and temperature deviations (Figure 1.8). Also, due to the rapid changes of the specific heat capacity, the enthalpy cannot be predicted correctly near the critical point and that has an effect on the predicted heat transfer.

Despite the intense research related to supercritical heat transfer there is

still a gap in understanding the behavior of refrigerants at supercritical state under low heat fluxes, horizontal flow and in large tube diameters. These conditions are for example encountered in ORC applications.

## 2.1 Heat transfer regimes

There are three heat transfer regimes that occur in a developing flow heated up to its supercritical state: normal heat transfer (NHT), enhanced heat transfer (EHT) and deteriorated heat transfer (DHT).

Figure 2.1 illustrates the heat transfer regimes appearing along a heated length of a (vertical) tube, for a given temperature and heat transfer coefficients profiles of water [24].

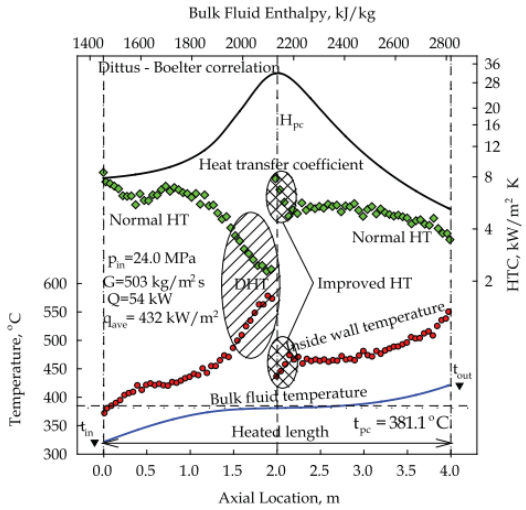


**Figure 2.1:** Heat transfer regimes of a fluid at supercritical state [24].

Typical for the *normal heat transfer* (NHT) regime is that the wall heat transfer coefficients (HTC) are similar to the convection HTCs that are determined by the conventional single-phase Dittus-Boelter heat transfer correlation. The *enhanced heat transfer* (EHT) is characterized with higher values of the heat transfer coefficient compared to the NHT. On the other hand, for the *deteriorated heat transfer* (DHT) regime the values of the wall temperature are higher and the heat transfer coefficient is lower compared to the NHT.

The EHT and the DHT occur when the bulk fluid temperature approaches the pseudocritical region. The peak of the specific heat capacity and the decrease in viscosity yield an enhanced heat transfer from the heated wall to the bulk of the fluid flow. However, the decrease of the thermal conductivity in this region leads to deteriorated heat transfer. Furthermore, a fluid at supercritical state undergoes a significant velocity profile transformation as the bulk fluid

goes through the pseudocritical region (even when considering a fully developed flow). The change of the velocity profiles is induced by a change in shear stress due to the viscosity changes and in turn has an effect on the heat transfer.

Additionally, in literature two other definitions for heat transfer phenomena for supercritical flow can be found. Namely, pseudo-boiling and pseudo-film boiling, which were developed in the past. The aim was to establish an analogy between EHT and the two-phase boiling and DHT and the film boiling. However, these two phenomena lost popularity because there was a lack of successful models to predict the heat transfer coefficients. *Pseudo-boiling* appears at supercritical pressures and is similar to subcritical nucleate boiling. This physical phenomenon appears if the bulk fluid temperature is below the pseudocritical temperature $T_{pc}$ of the fluid but some layers of the fluid near the heating surface may reach higher temperatures than $T_{pc}$. The wall heat transfer coefficient usually increases during the pseudo-boiling. The *pseudo-film boiling* is a phenomenon that appears at supercritical pressures and is similar to the film boiling typical for subcritical pressures. At pseudo-film boiling, the fluid at a temperature above the $T_{pc}$ prevents the fluid at temperatures lower than the $T_{pc}$ to reach the heated surface. This leads to the deteriorated heat transfer regime, elaborated in detail in Section 2.1.1.

### 2.1.1 Enhanced and deteriorated heat transfer

It should be emphasized that the two heat transfer regimes (mechanisms), the enhanced heat transfer EHT and the deteriorated heat transfer DHT, always occur side by side [40], [49–55]. Enhanced heat transfer occurs when the thermophysical property of the thermal boundary layer of the fluid is near the pseudocritical temperature rather than the bulk fluid property. The EHT near the pseudocritical temperature is mainly due to the increase in the specific heat capacity.

Figure 2.2 illustrates a thermal boundary layer in a circular tube developed near its entrance.

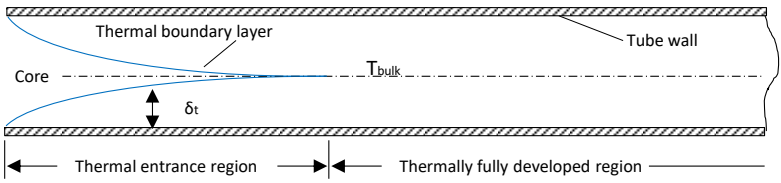


**Figure 2.2:** Thermal boundary layer in a circular tube developed near its entrance.

When considering heat transfer, the wall surface of a tube is either heated or cooled. At the entrance of the tube, the bulk fluid (usually written as $T_b$)

stays at the inlet temperature and does not contribute in the heat transfer. In the entrance region a thermal boundary layer is created. The thickness of the thermal boundary layer '$\delta_t$' increases far away from the inlet and is fully developed after a certain distance. This length is identified as thermal entrance region $L_e$. In the thermally fully developed region (after the thermal entrance region) all the fluid layers participate in the heat transfer. For reaching the fully developed flow region (hydrodynamically and thermally) the thermal entrance region $L_e$ in a turbulent flow is recommended to be $L_e = 10D$. This is important for defining the occurrence of the enhanced EHT and deteriorated heat transfer DHT. Furthermore, as criterion for classifying both heat transfer regimes the ratio of the heat flux and the mass flux is used $\dot{q}/\dot{G}$ (see Section 2.1.2).

The heat transfer rate from the wall to the fluid depends on the thermal resistance at the thermal boundary layer, which is a function of the thermal conductivity and the thickness of the thermal boundary layer. The conductivity of the fluid decreases (despite the small peak) with temperature near the pseudocritical region and tends to reduce the heat transfer. However, the increase of the specific heat capacity and the viscosity decrease overcome the effect of the decreased thermal conductivity which yields EHT [40], [49], [50]. As already mentioned the $c_p$ has a local maximum and the range of the peak is not constantly dominant over the other thermophysical properties. However, apart from EHT at certain conditions (e.g. at high heat fluxes and low mass flux) near the pseudocritical region a DHT can occur.

The phenomenon of deteriorated heat transfer, at low mass fluxes was first observed by Shitsman [51]. At the onset of DHT a pressure pulsation was observed when the bulk fluid temperature was near the pseudocritical temperature. From the experimental data, several heat transfer correlations were developed for predicting the heat transfer coefficients, the onset of deteriorated heat transfer and the frictional pressure drop.

In literature, there is no unique definition for the onset of deteriorated heat transfer DHT. However, a common conclusion is that DHT occurs at high heat fluxes and low mass fluxes resulting in a strong decrease in the heat transfer coefficient. Additionally, deteriorated heat transfer was observed at the following temperature conditions $T_b < T_{pc} < T_w$.

Vikhrev and Lokshin [52] performed one of the earliest studies regarding supercritical heat transfer to water in horizontal flow in a single tube and this was the first attempt to quantitatively formulate the deteriorated heat transfer DHT.

Furthermore, the onset of the DHT was observed in the work of Ackermann [53] by determining pseudo-film boiling phenomenon appearing near the critical heat flux. However, Ackermann [53] attempted to make a comparison with the phenomenon occurring at subcritical heat transfer by using the term 'critical heat flux' in pseudo-film boiling.[1]. Additionally, the 'critical heat flux' at

1. Critical heat flux characterizes the thermal limit of a phenomenon where a phase change takes place during heating. This leads into reduced heat transfer and occurrence of a high temperature increase of the heated surface.

the start of DHT increases by raising the pressure and the mass flux and by decreasing the tube diameter. It was concluded that this phenomenon is affected by the heat flux, the pressure, the mass flux and the tube diameter. Yamagata et al. [54] expressed that the onset of the DHT occurs at high heat fluxes, while at low heat fluxes there is EHT when the bulk fluid temperature is near the pseudocritical region.

Shiralkar and Griffith [55] studied the effects of different parameters on the DHT and consequently on the heat transfer coefficient. It was pointed out that the onset of the DHT depends on mass flux, pressure, tube diameter and the flow direction. However, the conclusion was based on numerical results that actually over-predict the DHT.

### 2.1.2 Determining the onset of deteriorated heat transfer

In literature, there are several correlations for determining the start of deteriorated heat transfer and to quantify this heat transfer mechanism. One of the criteria for identifying DHT is the ratio of the heat and the mass flux $\dot{q}/\dot{G}$. It is difficult to identify DHT because the wall temperature increase and the HTCs decrease appear rather smooth compared to film boiling (at subcritical conditions) for which a much larger increase in the wall temperature takes place.

Kondrat'ev [56] proposed the following correlation for calculating the heat flux and the onset of DHT:

$$\dot{q}_{DHT} = 5.815 \cdot 10^{-17} Re_b^{1.7} \Big( \frac{p}{0.101325} \Big)^{4.5} \tag{2.1}$$

This criterion is applicable for pressure $p = (23.3 - 30.4)MPa$, Reynolds number $Re_b = (30 - 100) \cdot 10^3$ and the heat flux $\dot{q} = (116.3 - 1163)kW/m^2$.

In the numerical work of Koshizuka et.al. [57] the onset of the DHT was quantified with Eq.(2.2)

$$\frac{HTC}{HTC_0} < 0.3 \tag{2.2}$$

where $HTC_0$ is the ideal or reference heat transfer coefficient determined by using the Dittues-Boelter heat transfer correlation ($Nu = Re^{0.8} Pr^{0.4}$). In the conclusion of Koshizuka et al. [57] it was indicated that the calculation results agree with the experimental work of Yamagata et al. [54] at high mass fluxes.

Furthermore, Yamagata et.al. [54] proposed the following correlation for determining the heat flux at the start of DHT:

$$\dot{q}_{DHT} = 0.2 \dot{G}^{1.2} \tag{2.3}$$

In 1973, Protopopov et al. [58] based on experimental data, proposed a non-dimensional coefficient $K$ for defining the beginning of the DHT:

$$K = \frac{C(\rho_b - \rho_w)^4 \rho_b Pr_b}{\mu_b \dot{G} \sqrt{\xi} \Big( \frac{Gr}{Re^3} \Big)^{0.23}} \tag{2.4}$$

There are two values for the constant $C$ for this correlation, determined for water ($C = 8 \cdot 10^{-14}$) and for $CO_2$ ($C = 1 \cdot 10^{-14}$). Furthermore, heat transfer deterioration occurs when the coefficient $K$ reaches $K_{cr} \approx 1.35 \cdot 10^4$.

Taking into account the ratio of the heat flux and mass flux, Protopopov and Silin [59] proposed the correlation:

$$\left(\frac{\dot{q}}{\dot{G}}\right)_{DHT} = \frac{1.3}{(T_{pc} - T_b)c_{pb}\left(\frac{\xi}{8}\right)\left(\frac{\nu_w}{\nu_{pc}}\right)^{1.3}} \tag{2.5}$$

where the specific heat capacity $c_p$ was calculated at bulk fluid temperature.

Pethukhov et al. [60] experimentally investigated the friction and acceleration factors during heating of water in upward flow. For determining the starting point of deteriorated heat transfer the following correlation is proposed:

$$\left(\frac{\dot{q}}{\dot{G}}\right)_{DHT} = 0,034\sqrt{\frac{f}{8}}\left(\frac{c_p}{\beta}\right)_{pc} \tag{2.6}$$

where $\beta$ is the turbulent mixing coefficient, $\dot{G}$ is the mass flux of the fluid and $f$ is the friction factor determined by using the Filonenko definition:

$$f = (1.82lgRe_b - 1.64)^{-2} \tag{2.7}$$

where the viscosity in the $Re$ number should be determined at the temperature of the onset of DHT.

Mokry et al. [61] proposed a correlation for determining the start of the DHT

$$\dot{q}_{DHT} = -58.97 + 0.745\dot{G} \tag{2.8}$$

and it is valid for the following ranges: $\dot{q} \leq 1250kW/m^2$, $\dot{G} = 200 - 1500kg/m^2$, $p = 240bar$, $T_{in} = 320 - 350C$ and $D = 10mm$.

The onset of the deteriorated heat transfer for R22 was determined [62] with the ratio of the heat and mass flux $\dot{q}/\dot{G}$ and is in the range:

$$\dot{q}/\dot{G} = 0.0571 - 0.0712kJ/kg \tag{2.9}$$

The first number corresponds to the higher inlet temperature of R22. With the appointed measurement approach [62] it was found that the DHT is strongly dependent on the inlet temperature while this is not the case for the heat transfer enhancement.

As already mentioned (Section 2.1.1) the DHT occurs when the following condition '$T_b < T_{pc} < T_w$' is fulfilled. The thermophysical properties of the working fluid near the (pseudo)critical temperature have an effect on the HTCs (and $T_b$ and $T_w$). Moreover, the HTCs and the temperature differences ($T_b$ and $T_w$) of the working fluid are influenced by the mass flux $\dot{G}$ as well. Therefore, the correlation for defining the onset of DHT should incorporate the effect of

the thermophysical changes at $T_b$ and $T_w$. Moreover, it is very important the correlation for determining the onset to incorporate all (the pressure, the tube diameter, the flow direction and the buoyancy) parameters that have an effect on the DHT [56] [58–60].

For example, the correlation for determining the start of DHT of Protopopov et al. [58] considers the density and viscosity changes, the Prandtl, the Reynolds and the Grashof numbers and two other coefficients. However, because this correlation was determined with data fitting, based on experimental data for water and $CO_2$, it is better to be verified if it can be used for other (experimental) data sets for different fluids. This conclusion is valid for the correlations that are given as a function of the heat flux and mass flux as well.

## 2.2 Literature review

### 2.2.1 An overview of studies investigating supercritical heat transfer to water and $CO_2$

Research activities regarding heat transfer to fluids at supercritical pressure started from the 30's of the $20^{th}$ century. There are several comprehensive reviews of experimental studies and correlations for heat transfer and pressure drop of supercritical water and $CO_2$. The first one was published by Petukhov [63] in 1970, presenting a summary of the state-of-the-art. Furthermore, in the reviews of Jackson and Hall [40, 64], a comparison of several heat transfer correlations with the experimental data was done and a new semi-empirical correlation was proposed. Their heat transfer correlation incorporates the effect of buoyancy on the heat transfer at supercritical pressure and gave empirical estimations about the onset boundaries of the buoyancy effect. On the other hand, Polyakov [65] extended the literature survey of Petukhov [63]. In his work the heat transfer mechanisms appearing at supercritical state were explained by using mathematical modeling of turbulent heat transfer. Also numerical analysis under different boundary conditions as well as the onset of the deteriorated heat transfer were discussed [63]. In 2000, Kirillov [66] reviewed the research done in Russia about heat and mass transfer of supercritical water and a new correlation was presented.

More recent literature reviews were published by Pioro et al. [23, 25, 45, 67], giving an overview of (all) studies related to heat transfer at supercritical state by using water, $CO_2$, helium and other fluids, including a summary of the existing heat transfer correlations. A brief literature review of water, $CO_2$ and hydrofluorocarbons was made by Huang et al. [68], emphasizing that the predictive heat transfer correlations derived for one working fluid cannot be directly applied to another. Recently, Cabeza et al. [69] published a comprehensive review for the work done regarding supercritical $CO_2$, concluding that there is a need of a unique heat transfer correlation for each geometry that can have a practical application.

One of the pioneers in the field of supercritical heat transfer was Schmidt and his associates. They investigated free convection heat transfer to fluids at near-critical region. The aim was to apply it in a new effective cooling system for turbine blades in jet engines. Furthermore, Shitsman [70], Dickinson [71] and Krasnoshchekov [72] developed a concept of using supercritical water for increasing the total thermal efficiency in the steam generators/turbines in fossil-fuel power plants. The difference of working at supercritical conditions compared to working at subcritical pressure is that there is no liquid–vapor phase transition. Therefore, there is no such phenomenon occurring like critical heat flux and dry-out. Moreover, in the period of 1950s until 1980s several researchers [52], [54], [73], from the former USSR and USA did research on supercritical water as a coolant in nuclear reactors. The primary objectives were increasing the thermal efficiency of modern nuclear power plants from 30% to 45% or even higher and secondly decreasing the operational and capital cost.

Furthermore, the focus in the experimental work [53], [54], [71] was on supercritical water for the design of supercritical fossil power plants. The tests were done in tube diameter of 7.5-24 $mm$ at maximum temperature of 450°C. Dickinson [71] compared the experimental results with the Dittus-Boelter ($Nu = CRe^m Pr^n$) heat transfer correlation and a good fit was observed at wall temperatures of maximum 350°C. In contrast, when the wall temperature was in the range of 350-450°C, there was a large deviation with the Dittus-Boelter heat transfer correlation. As already introduced, Ackerman [53] and Yamagata et al. [54] experimentally determined the occurrence of the deteriorated heat transfer in their experiments.

Recently, heat transfer to supercritical water in vertical bare tubes was conducted by Mokry et al. [61]. Several heat transfer correlations of Dittus-Boelter type were compared and it was concluded that they overestimate the HTC especially in the pseudocritical region.

The focus in the past was mainly on conducting investigations and experiments in test sections with vertical (upward, downward) flow direction. Hence, the experimental parameters cover wide ranges: heat fluxes of 70–4,500 $kW/m^2$, mass fluxes of 135–5,100 $kg/m^2s$, and inner diameters of 2–24.4 $mm$ for water pressures of 220–450 $bar$. The data that is matching with the focus of the present study is limited and is linked only with the mass fluxes and the tube diameter but not with the other parameters [53], [54], [56], [61], [73–76].

As already mentioned (Section 1.5), the objective of this study is to investigate supercritical heat transfer in horizontal flow. Therefore, in continuation, a chronological overview of the achievements in horizontal flow are presented as well. Vikhrev and Lokshin (1964) [52], did one of the earliest studies on heat transfer to supercritical water in a tube diameter of 6 $mm$. Their research was a first attempt to quantitatively define deteriorated heat transfer in horizontal flow at supercritical conditions.

In Figure 2.3 the temperature distribution as a function of enthalpy in a horizontal flow is presented; at various heat fluxes (699 $kW/m^2$, 582 $kW/m^2$,

465 $kW/m^2$, 349 $kW/m^2$), constant mass flux (700 $kg/(m^2s)$) and supercritical pressure.

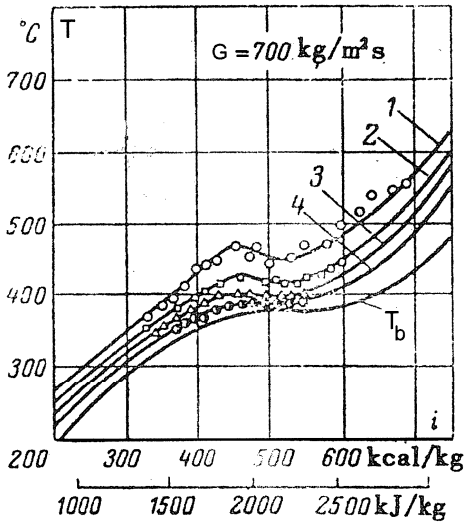


**Figure 2.3:** Temperature distribution in a horizontal flow at various heat fluxes (1. 699 $kW/m^2$, 2. 582 $kW/m^2$, 3. 465 $kW/m^2$, 4. 349 $kW/m^2$) and constant mass flux (700 $kg/(m^2s)$) [52].

The DHT in horizontal flow is less distinct than in the vertical upward flow direction. In a horizontal layout, the heat transfer is more complex. There is non-uniform temperature profiles in the circumferential direction of the tube caused by gravity force that is perpendicular to the flow direction. Therefore, there is a temperature difference occurring between the top and bottom tube surface and the tube temperature is sensitive to the heat flux. This temperature variation leads to reduction in the heat transfer coefficient at the top surface compared to the one obtained at the bottom surface and there is higher temperature difference.

When compared with a downward heated flow there is a continuous enhancement in the heat transfer as buoyancy effect becomes relatively stronger [77]. This behavior has been found with many other fluids at supercritical pressure. Not only the heat transfer is improved (enhanced), but also wall temperatures are less sensitive to the heat flux.

Miropol'skii and Shitsman [74] measured the temperature distribution for supercritical water in a horizontal and vertical 16 $mm$ diameter tube. The

function of the wall temperature and the bulk enthalpy is depicted in Figure 2.4.

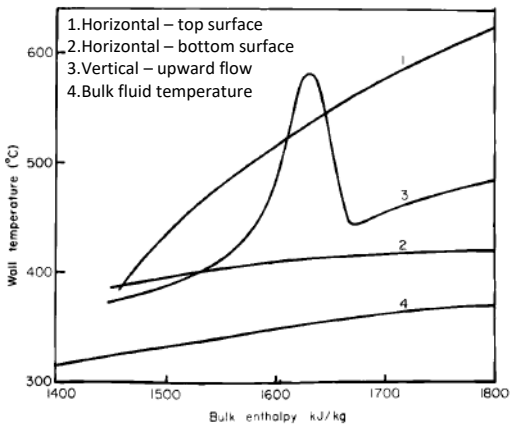


**Figure 2.4:** Wall temperature distribution as a function of local bulk enthalpy for water at $1.11p_{cr}$ in horizontal and vertical flow [74].

In the critical region the temperature difference between the bulk fluid temperature and the wall surface temperature on the top is a lot higher compared to the wall surface temperature at the bottom and the bulk fluid temperature. When the fluid is heated above the pseudocritical point the specific heat capacity is less dominant and the wall temperature increases. The temperature difference between the bulk fluid temperature (line 4) and the top (line 1) and bottom (line 2) surfaces is illustrated in Figure 2.4. This leads to a reduction in the heat transfer coefficient of about a factor of 4 when comparing the top surface to the bottom one. The measurements were done at pressure of 245 $bar$ ($1.11p_{cr}$) and the heat flux and the mass flux were 520 $kW/m^2$ and 600 $kg/(m^2s)$ respectively. This conclusion is valid when the ratio of the heat flux and mass flux rises and leads to DHT on the top surface.

Jackson and Hall [40, 64], proposed a 'model' to explain the buoyancy effect on the heat transfer. The dominant factor is the modification of the shear stress distribution across the tube, with a consequential change and causing turbulence. As mentioned in Section 2.3.6, buoyancy effects are present in horizontal flows due to a flow stratification. The hotter (less dense) fluid can be found in the upper part of the pipe. Also, there may be an effect on the heat transfer near the upper surface of a tube due to damping effect of the stabilizing density gradient on turbulence. At the lower surface, the heat transfer is frequently better than at the upper one for forced convection alone, suggesting that there may be some amplification of turbulence by the destabilizing density gradient in this region.

Belyakov et al. [78] performed measurements for heat transfer of supercrit-

ical water in a horizontal tube with a diameter of 20 $mm$ and length of 4 $m$ at wide ranges of heat and mass fluxes. Deteriorated heat transfer was observed on the top surface visible in Figure 2.5 (on top, location 4) at $\dot{q}/\dot{G} = 0.93\ kJ/kg$. This heat transfer regime appears progressively along the tube and does not show the sharp peaks that are attained in upward flow. As the ratio of the heat flux to the mass flux rises, the wall temperature and thus deterioration at the upper surface increases. However, the heat transfer coefficients at temperatures far below and above the critical point were not affected by the magnitude of the heat flux and the mass flux.

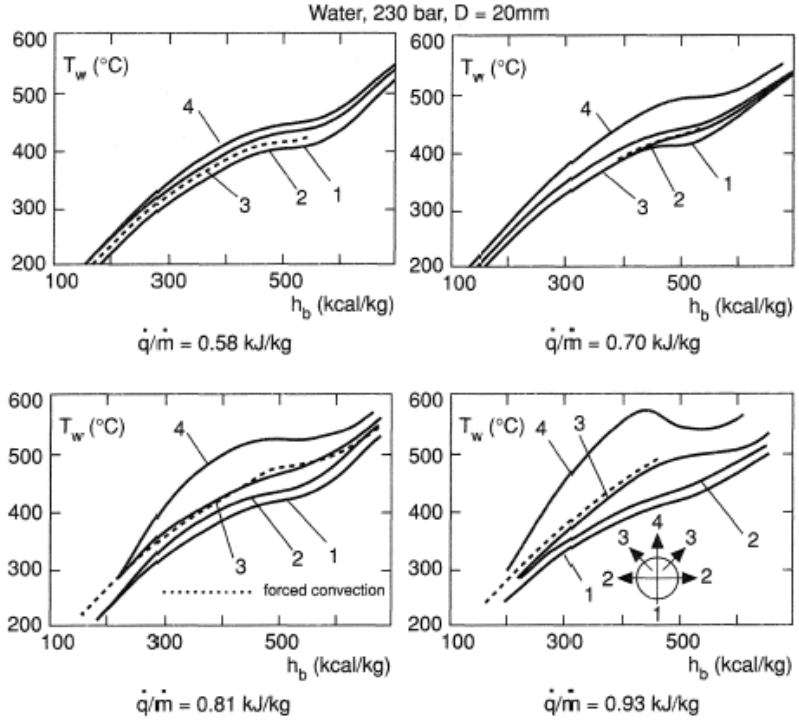


**Figure 2.5:** Wall temperature distribution as a function of the bulk enthalpy for water at $1.05p_{cr}$ in horizontal flow [78].

Yamagata et al. [54] made a comparison with the results of Belyakov et al. [78], concerning the horizontal and vertical flows of water. It was concluded that at low heat fluxes the same heat transfer coefficients were acquired in vertical and horizontal (top and bottom surfaces) flow. At higher heat fluxes, the highest heat transfer coefficient was obtained at bottom surface and the lowest HTC at the top surface of the horizontal flow. However, in vertical flow there was no peripheral temperature difference and the HTC was the second highest.

The experimental parameters of supercritical heat transfer in horizontal flow, cover smaller ranges: heat fluxes of 50–1,820 $kW/m^2$, mass fluxes of 300–3,391 $kg/m^2s$, and inner diameters of 6–43 $mm$ for water pressures of 230–310 $bar$. The data that is matching with the focus of the present study is limited and is linked only with the mass fluxes and the tube diameter but not with the other parameters [52], [71], [78–82]

$CO_2$ was at first used as a testing fluid instead of water [77, 83–86], in vertical flow, because of its lower critical pressure and temperature compared to water. However, in the last years there is an effort in exploiting supercritical $CO_2$ as a main working medium in various refrigeration and power cycle systems.

In 1976, Adebiyi and Hall [79] investigated the buoyancy effects and local acceleration due to density variations for $CO_2$. The measurements were done in vertical and horizontal flow. A wide range of wall temperature measurements at different heat fluxes and mass flow rates were made. Free convection could occur due to the relatively large diameter of 22.1 $mm$ of the tube (Figure 2.6).

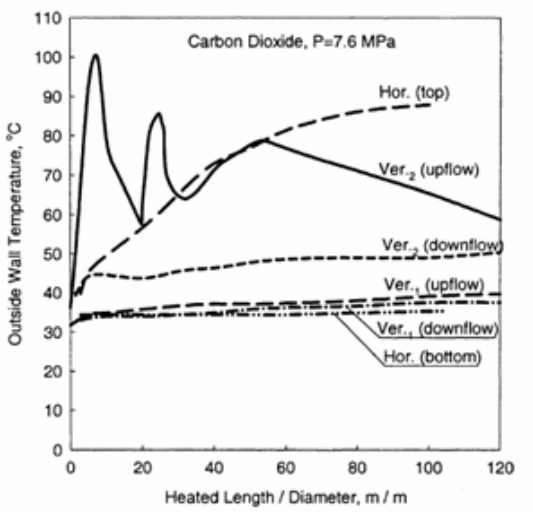


**Figure 2.6:** Wall temperature distribution along horizontal and vertical layout for $CO_2$ [79].

They noticed that the buoyancy effect does not only cause deteriorated heat transfer on the top surface of the tube, but also an enhancement at the bottom surface. Furthermore, buoyancy-free and buoyancy-dependent cases were distinguished.

Figure 2.6 shows a comparison of the wall temperature profiles along the heated tube in horizontal and vertical flow (upward and downward). For

comparison purposes the vertical flow data of Weinberg, was used, presented in Table 2.1. It can be noticed that there is a more gradual temperature distribution at horizontal flow rather than to those of vertical (upward) flow.

**Table 2.1:** Parameters used for comparison of horizontal and vertical flow.

| *Flow* | *Reference* | $D$, $mm$ | $T_{in}$, °C | $\dot{m}$, $kg/s$ | $q_w$, $kW/m^2$ |
|---|---|---|---|---|---|
| $Horizontal$ | Adebiyi, Hall 1976 | 22 | 20 | 0.121 | 27 |
| $Vertical_1$ | Weinberg, 1972 | 19 | 20 | 0.124 | 50 |
| $Vertical_2$ | Weinberg, 1972 | 19 | 20 | 0.124 | 30 |

When comparing the research activities of water and $CO_2$, it can be seen that there is a lot more data for vertical flow rather than for supercritical heat transfer in horizontal layout. Furthermore, it is important to be mentioned that not much attention was paid in defining if it is a buoyancy-free or buoyancy-dependent flow. There are several researchers that had an attempt to define the boundary conditions for the onset of buoyancy [40, 64] [77] [79]. This is very important and the effect of the density changes should be considered, especially when deriving a heat transfer correlation.

Table 2.2, shows a summary of the experimental investigations carried out for water and $CO_2$ that are considered in this thesis. Concerning the experimental ranges, there is a large deviation between the test conditions; heat flux is in the range of 2-11,000 $kW/m^2$ and mass flux between 100-22,000 $kg/(m^2s)$. Furthermore, the experiments were done in a tube diameter range of 0.7-43 $mm$. The pressure for supercritical water was in the range of 220-441 $bar$ and for supercritical $CO_2$ between 74-120 $bar$. Some of the investigated parameters i.e the mass flux and the diameter are in the range of the interest of this work.

**Table 2.2:** A summary of investigated parameters for water and $CO_2$.

| *Ref.* | *Fluid* | $q$, $kW/m^2$ | $G$, $kg/(m^2s)$ | $D$, $mm$ | $L$, $m$ | $p$, $bar$ | $T_{in}$, °C | *Orientation* |
|---|---|---|---|---|---|---|---|---|
| Vikhrev, Lokshin[52] | | 349-699 | 700 | 6 | | | | Horizontal |
| Adebiyi, Hall[79] | | 230-1,400 | 300-3,000 | 22.1 | | 230 | | Horizontal |
| Belyakov et al.[78] | | 232-1,396 | 300-3,000 | 20 | 4 | | 135-225 | Horizontal |
| Yu et al.[80] | | 50-400 | 300-1,000 | 26; 43 | 2 | 250 | | Horizontal |
| Bazargan et al.[81] | | 310 | 330-1,230 | 6.3 | 3 | 230-270 | | Horizontal |
| Dickinson[71] | | 880-1,820 | 2,170-3,391 | 7.62 | 1.6 | 240; 310 | 104-538 | Horizontal |
| Miropol'skii[74] | | <1,600 | 300-1,500 | 16 | 1.5 | 220-250 | <450 | Vertical, horizontal |
| Yamagata et al.[54] | | 116-930 | 310-1,830 | 7.5; 10 | 1.5-2 | 226-294 | 230-540 | Vertical |
| Bishop et al.[73] | *Water* | 310-3,500 | 651-3,662 | 2.5; 5.1 | | 226-276 | 282-527 | Vertical, annulus |
| Ackerman[53] | | 120-1,700 | 135-2,170 | 9.4-24.4 | | 227-441 | 77-482 | Vertical |
| Mokry et al.[61] | | 1,250 | 200-1,500 | 10 | 4 | 240 | 320-350 | Vertical |
| Gupta et al.[75] | | 70-1,250 | 200-1,500 | 10 | 4 | 240 | 320-350 | Vertical |
| Swenson et al.[76] | | 200-1,800 | 542-2,150 | 9.42 | 1.83 | 228-414 | 70-576 | Vertical |
| Kondrat'ev[56] | | 120-1,200 | | 12.02 | 0.52 | 228-304 | 260-560 | Vertical |
| Domin [82] | | 580-4,500 | 600-5,100 | 2; 4 | 1.08; 1.23 | 220-250 | 220-260 | Horizontal |
| Adebiyi, Hall[79] | | 5-40 | ≤391 | 22.1 | 2.4 | 76 | 10-31 | Horizontal |
| Liao, Zhao[26] | | 10-200 | ≤910 | 0.7; 1.4; 2.16 | 0.11 | 74-120 | 20-110 | Vertical, horizontal |
| Li et al.[83] | | 6.5-52 | | 2 | 0.29 | 78-95 | 25-40 | Vertical |
| Shiralkar, Griffith[55] | | 125-190 | 680-2,710 | 6.35 | 1.52 | 76-79 | 10-32 | Vertical, annulus |
| Kline et al.[87] | $CO_2$ | 2-450 | 200-1,500 | 4.6, 8; 22 | 1.2, 1.94; 2 | 77.6; 83.5 | 0-40 | Vertical |
| Kim et al.[88] | | ≤150 | 400-1,200 | 7.8 | 1.2 | 80 | 15-32 | Vertical channel |
| Petukhov et al.[89] | | | | 6.7 | 0.67 | 88-108 | $\Delta T$=4-50 | Vertical |
| Bringer, Smith[90] | | 31-310 | 100-1,300 | 4.57 | 0.61 | 83 | 21-49 | Vertical |
| Krasnoshchekov[91] | | 7,500-11,000 | 22,000 | 2.05 | 0.095 | 100 | 26-45 | Horizontal |

### 2.2.2 Review of experimental studies related to potential working fluid candidates for transcritical ORC

For more than 30 years, experimental investigation on supercritical heat transfer decreased due to the high operating pressures and temperatures (of the tested fluids: water, $CO_2$) and corresponding cost of the equipment. However, in the last decade it regained the interest of many researchers and industry in a broader sense, including: transcritical ORCs, Brayton cycles, refrigeration cycles, heat pumps, etc. As already mentioned in the previous section there are several comprehensive reviews considering supercritical water and $CO_2$ as working fluid. According to the knowledge of the author there is a lack of comprehensive data for supercritical heat transfer to refrigerants (including R125) that can be potentially used in a transcritical ORC. However, this does not mean that the importance of the work done for water and $CO_2$ is negligible. Due to the unique fluid properties and the thermophysical property variations in the critical region, there is a need of separate investigation.

In this section an overview of the achievements of supercritical heat transfer to refrigerants available in literature is presented.

Many of the refrigerants that were used in the refrigeration systems in the past are discarded due to environmental concerns. However, the data found concerning the supercritical heat transfer of these fluids is included because of their insights into the thermophysical behavior.

#### *R12 - Dichlorodifluoromethane*

Several experimental studies used R12 ($p_{cr}$=41.36 bar, $T_{cr}$=111.97°C) as a working fluid instead of water [92, 93], for designing supercritical water cooled nuclear reactors (SCWRs). The tests were done in a vertical flow but the ranges (mass flux, diameter, pressure and temperature) vary significantly. Back in 1960, Holman and Boggs [94] determined the occurrence of the pseudo-boiling effect. However, Richards et al. [93] considered to do experiments in a more complex geometry (7-element tube bundle). Three different heat transfer mechanisms for forced convection heat transfer were distinguished by Richards et al. [93]. The result from this study was novel and DHT can occur in bundles cooled with supercritical fluid. Furthermore, the 1-dimensional heat transfer correlations from literature do not predict accurately the data and the uncertainty is within ±50%.

Gorban' et al. [92] used R12 as working fluid for vertical flow in replacement of water. The test section was a circular tube with a diameter of 10 $mm$ and length of 1 $m$. A new heat transfer correlation was derived for a wide range of parameters (6-290 $kW/m^2$, 500-2000 $kg/(m^2s)$, 20-140°C, 10.8-44.6 $bar$).

#### *R134a - Tetrafluoroethane*

In the literature, R134a ($p_{cr}$=40.56 bar, $T_{cr}$=101.03°C) was used the most compared to other refrigerants. Due to the lower critical pressure and temperature (compared to water) it represents a suitable working fluid for recovering

low-to-medium temperature heat sources, i.e in a transcritical ORC. The test sections comprise tube diameters in the range of 4-16 $mm$, mainly positioned vertically. Furthermore, the experimental investigation was done at pressures (1.01-1.2)$p_{cr}$ and various ranges of heat fluxes and mass fluxes but in some cases up to 10 times lower than the tested conditions for water (Table 2.2).

Experiments on heat transfer near the critical pressure in an internally-heated vertical annular channel cooled by R134a was performed by Hong et al. [95]. As a result it was reported that the 'critical heat flux' decreased very fast when the operating pressure was approaching the supercritical pressure, in the near critical region. At supercritical pressures this phenomenon is no longer present.

Kang and Chang [39] performed two type of experiments with R134a, steady-state and transient. A heat transfer correlation at steady-state conditions was proposed. The results showed a good agreement with the previous studies obtained for water and $CO_2$. Zhang et al. [96] did experimental investigation of R134a at higher supercritical pressures (4.3-4.7 $MPa$) compared to the work of Kang and Chang [39]. The effect of different parameters; mass flux (600-2500 $kg/(m^2s)$), heat flux (20-180 $kW/m^2$), inlet temperature (71-115°C) on the heat transfer were tested. New heat transfer correlations of the Dittus-Boelter type were proposed that incorporate the acceleration parameter of Cheng et al. [97]. Furthermore, they determined the occurrence of DHT at high heat fluxes and low mass fluxes.

Experimental investigation for transcritical ORC at similar test conditions but at different flow directions was made by Cui and Wang [98] and Tian et al. [43]. Cui and Wang [98] derived heat transfer correlations suitable for designing heat exchangers (vapour generators) applicable for transcritical ORC. The tests were conducted in upward and downward flow and the influence of different parameters was tested. In most of the tested cases the heat transfer is improved (enhanced) in downward flow rather than in upward flow, due to the buoyancy effect. Furthermore, the experimental results were compared to three different dimensionless 'Buoyancy numbers' and fitted with the experimental data. The new heat transfer correlation was assessed with 6 other representative heat transfer correlations from literature and a new correlation was fitted with the experimental data. Only two heat transfer correlations derived by Tarsitano et al. [99] and Bishop et al. [73] show good agreement for upward flow. While the new heat transfer correlation of Cui and Wang [98] showed significant improvements in prediction accuracy for upward and downward flow. On the other hand Tian et al. [43] reported that due to the buoyancy effect, caused by the density variations, there is a non-uniformity of the wall temperature in circumferential direction. Heat transfer deterioration is detected on the top surface of the tube at high heat fluxes, while at the bottom surface there is heat transfer enhancement for all tested conditions. New heat transfer correlations are proposed from the experimental data, that are as well compared with heat transfer correlations from literature.

The results of Zhang et al. [96], Cui and Wang [98] and Feuerstein et al. [100] showed that the heat transfer correlations derived for water showed

a significant deviation with the experimental data for R134a. The large discrepancies were dominant as the enthalpy was approaching the pseudocritical region.

Investigation in horizontal flow of supercritical R134a was made by several researchers [43, 101, 102]. Zhao and Jiang [101] used R134a as working fluid for heat transfer measurements at supercritical pressure during cooling. The results showed that the mass flux, the pressure and the temperature of R134a had a significant impact on the heat transfer characteristics.

Detailed experimental investigation of the heat transfer of R134a in a horizontal flow at supercritical pressures for application in a transcritical ORC was made by Wang et al. [102]. The experimental results of Wang et al. [102] for micro-fin tube were compared with the work done by Tian et al. [43] for the smooth tube. The aim was to provide data and heat transfer correlations for designing micro-fin tube heat exchanger for transcritical ORC's. Furthermore, the buoyancy effect is greatly reduced in the micro-fin tube which yields better heat transfer coefficient (1.68 time larger on the top and 1.59 time larger on the bottom compared to the smooth tube). Furthermore, Wang et al. [44] determined the heat transfer characteristics of R134 in a horizontal ribbed tube at different parameter ranges.

***R22 - Chlorodifluoromethane***

There are several experimental studies concerning heat transfer measurements at supercritical conditions that consider R22 ($p_{cr}$=49.9 bar, $T_{cr}$=96.15°C) as a working fluid. R22 is considered a favorable fluid for transcritical ORC's [32]. However, the experiments were done with small tube diameters (1-13.5 $mm$) and in vertical flow direction. Mori et al. [103] used R22 as a working fluid instead of water for development of supercritical water cooled reactor (SCWR) in sub-bundle channels in vertical flow.

Comparison of the heat transfer characteristics of R22 and ethanol ($p_{cr}$=63.9 bar, $T_{cr}$=243.1°C) were determined at supercritical pressures by Jiang et al. [104]. The frictional pressure drop depends on the viscosity and density variations during heating. The viscosity of ethanol decreases rapidly while the density changes are very small. In contrary, the density of supercritical R22 undergoes sharp changes with the temperature. The friction correlations do not consider the density and viscosity changes and under-predict the frictional pressure drop. This is the case for both fluids. At pressures (73-100 $bar$) far from the critical pressure of R22 the local wall temperature increases with the temperature and the enthalpy rises but the local heat transfer coefficient decreases. A minimum local heat transfer coefficient occurs at the location with maximum wall temperature. At high heat fluxes, when the pressure of R22 is 55 $bar$ ($1.10p_{cr}$), and the mass flux is relatively low there is a significant temperature gradient of 200°C between the wall temperature $T_w$ and the fluid temperature. Near the tube wall, the density, the specific heat capacity and the thermal conductivity are low which yields reduced (deteriorated) heat transfer between the wall and the tube. The same counts for the local heat

transfer coefficient. Enhanced heat transfer is occurring when considering ethanol because the viscosity abruptly decreases as the temperature rises and the density changes with temperature are relatively small. A completely different approach was made by Dubey et al. [62]. The aim was to determine the local heat transfer coefficients and heat transfer correlations of R22 by using a thermal camera. The test sections were electrically heated by using Joule heating. With this measurement technique it was found that the deteriorated heat transfer DHT is strongly dependent on the inlet temperature while this is not the case for the enhanced heat transfer EHT. There is a sharp increase of the wall temperature when it reaches a value just above the pseudocritical temperature. The derived heat transfer correlation of Dittus-Boelter type is multiplied with a correction factor.

### *R245fa - Pentafluoropropane*

Heat transfer measurements of supercritical R245fa ($T_{cr}$=154.05°C, $p_{cr}$=36.4 bar) under heating conditions in a vertical upward flow were made by He et al. [105]. Wide ranges of heat fluxes (15-100 $kW/m^2$), mass fluxes (400-800 $kg/m^s$) and inlet pressures (40-50 $bar$) were considered for the tests. The results were compared with the heat transfer correlation of Yamagata et al. [54]. A prediction of 70% of the measured data was acquired within uncertainty of 30%. Furthermore, it is highlighted that further improvement of the heat transfer correlations is needed when considering strong heat transfer deterioration conditions. However, it has to be taken into account that the heat transfer correlation of Yamagata et al. [54] was derived for water. At higher pressures in respect to the critical pressure the thermophysical property's variation is less prominent and the heat transfer coefficient decreased in the vicinity of the pseudocritical temperature. Furthermore, in forced convection the local heat transfer coefficient had a maximum value when the local bulk temperature was close to the pseudocritical temperature.

### *R1233zd(E)*

The working fluid R1233zd(E) ($p_{cr}$=36.24 bar, $T_{cr}$=166.45°C) is considered as an alternative for R245fa and R123, due to its beneficial environmental characteristics (GWP and ODP). He et al. [106] experimentally investigated the heat transfer characteristics of R1233zd(E) at supercritical pressures (1.10-1.23)$p_{cr}$ and at lower heat fluxes and mass fluxes compared to R245fa. A comparison of the heat transfer coefficients of both fluids was conducted and a higher heat transfer coefficient was obtained for R1233zd(E) in the supercritical region. Furthermore, the results were compared with existing heat transfer correlations where the one of Petukhov et al. [60] shows the best predictability. Moreover, at these conditions heat transfer deterioration for the fluid R1233zd(E) was not detected.

***R404A and R410A***

Experimental investigation regarding supercritical heat transfer to blends, R404A ($p_{cr}$=37.8 bar, $T_{cr}$=161.68°C) and R410A ($p_{cr}$=47.9 bar, $T_{cr}$=70.2°C) in horizontal flow and for cooling applications was performed by Garimella et al. [107]. Small diameter tubes in the range between 0.76–9.4 $mm$ were tested and the proposed heat transfer correlation is applicable for pressure (1.0-1.2)$p_{cr}$. The heat transfer coefficients were compared with several heat transfer correlations from literature. It was concluded that the heat transfer correlations derived for water and $CO_2$ cannot be used for the blends within an acceptable level of accuracy.

$C_4F_{10}$ ***- Perfluorobutane***

Supercritical $C_4F_{10}$ - Perfluorobutane ($C_4F_{10}$) ($p_{cr}$=23.24 bar, $T_{cr}$=113.2°C) was tested in two plate-type heat exchangers with different corrugated angles [108]. It was found out that the results differ by those obtained using the Dittus-Boelter correlations. The effect of the wall-to-bulk property ratio has stronger influence to the heat transfer rate compared to that of the buoyancy effect. Therefore, the effect of the wall-to-bulk was accounted by deriving new heat transfer correlation using a correction factor. The majority of the experimental data points fall within 15% of those predicted using the correlation.

A comprehensive review of all experimental studies available in literature for refrigerants that can be used as potential fluid candidates in transcritical ORCs is presented. Table 2.3, illustrates a summary of the reviewed experimental heat transfer measurements to refrigerants.

The experimental investigations are for vertical (upward, downward) flow direction. Hence, the parameters cover wide ranges: heat fluxes of 6-1,800 $kW/m^2$, mass fluxes of 70–4,000 $kg/m^2s$, and inner diameters of 0.76–16 $mm$ in pressure ranges of 34.5–100 $bar$. This investigation (Section 2.2.2) shows that there is lack of experimental data for supercritical heat transfer to refrigerants in heated horizontal tubes.

In general, it can be concluded from the 'Literature review' (Section 2.2) that the focus was mainly for water and $CO_2$ while the refrigerants were scarcely experimentally tested. This conclusion is especially valid for the horizontal flow direction. According to the best knowledge of the author, experimental heat transfer investigation of supercritical R125 is scarce. Thus, there is lack of experimental data that describes the heat transfer characteristics of R125 in heated horizontal tube. The experimental range of interest is the following: heat fluxes of 15-28 $kW/m^2$, mass fluxes of 400–650 $kg/m^2s$, and inner diameters of 24 $mm$ in pressure ranges of 38-42 $bar$.

**Table 2.3:** A summary of experimental studies related to refrigerants.

| *Ref.* | *Fluid* | $q$, $kW/m^2$ | $G$, $kg/(m^2s)$ | $D$, $mm$ | $L$, $m$ | $p$, $bar$ | $T_{in}$, °C | *Orientation* |
|---|---|---|---|---|---|---|---|---|
| Gorban et al.[92] | | | | 10.92 | | 34.5-65.5 | 65.6-204.4 | Vertical |
| Richards et al.[93] | R12 | 6-290 | 500-2,000 | 10 | 1 | 10.8-44.6 | 20-140 | Vertical |
| Holman et al.[94] | | | 440-1,320 | 40x4 | 8 | 46.5 | 120 | Vertical tube bundle |
| Zhang et al.[96] | | 20-180 | 600-2,500 | 7.6 | 2.3 | 43-47 | 71-115 | Vertical |
| Kang and Chang[39] | | 160 | 600-2,000 | 9.4 | 2 | 41-45 | 50-110 | Vertical |
| Hong et al.[95] | | 69.6-239 | 500-1,504 | 9.54 | 1.84 | 41.4 | 85-56,05 | Vertical, annulus |
| Cui and Wang[98] | | 20-100 | 500-1,500 | 8 | 3 | 43-48 | | Vertical |
| Feuerstein et al.[100] | | 10-200 | 300-2,000 | 10 | 2.5 | 42.2-55.1 | 50-124 | Vertical |
| Chen et aL.[109] | R134a | 20-100 | 400-1,500 | 8.3 | 1.5 | 44-47 | | Vertical, rod bundle |
| Zhao and Jiang[101] | | | 70-405 | 4.01 | 1.12 | 45-55 | 80-140 | Horizontal |
| Tian et al.[43] | | 20-100 | 400-1,500 | 10.3, 16 | 2.5 | 41.5-49 | 70-95 | Horizontal |
| Wang et al.[102] | | 10-70 | 400-600 | 7.76-8 | 2.5 | 42.6-50 | 70-102 | Horizontal, ribbed tube |
| Wang et al.[44] | | 15-25 | 100-300 | 13.4-15.8 | 2.5 | 42.6-51 | 70-103 | Horizontal, ribbed tube |
| Mori et al.[103] | | 10-190 | 400-2,000 | 4.4 | 2 | 55 | | Vertical |
| Jiang et al.[104] | R22 | 110-1,800 | 2,000-4,000 | 1.004 | 0.152 | 55-100 | | Vertical |
| Kumar et al.[62] | | 9-60.5 | 530-1,000 | 6, 13.5 | 1.8 | 55-55.6 | 46.1-86.1 | Vertical |
| He et al.[105] | R245fa | 15-100 | 400-800 | 4 | 1.04 | 40-50 | 120 | Vertical |
| He et al.[106] | R1233zd(E) | 20-80 | 400-600 | 4 | 1.04 | 39.3-44 | 125 | Vertical |
| Garimella et al.[107] | R404A<br>R410A | | 200-800 | 0.76,9.4 | 0.5 | | 30-110 | Horizontal |
| Jiang et al.[104] | Ethanol | 110-1,800 | 2,000-4,000 | 1.004 | 0.152 | 55-100 | | Vertical |

## 2.3 Parameters influencing the heat transfer

Heat transfer to fluids at supercritical state is followed by complex heat transfer mechanisms such as normal heat transfer NHT, enhanced heat transfer EHT and deteriorated heat transfer DHT. In order to be able to determine the heat transfer regimes it is important to asses the effect that each parameter has on supercritical heat transfer. In the text below the influence of eight parameters is elaborated.

### 2.3.1 Effects of mass flux

The mass flux is an important parameter that has a significant effect on the convection heat transfer coefficients.

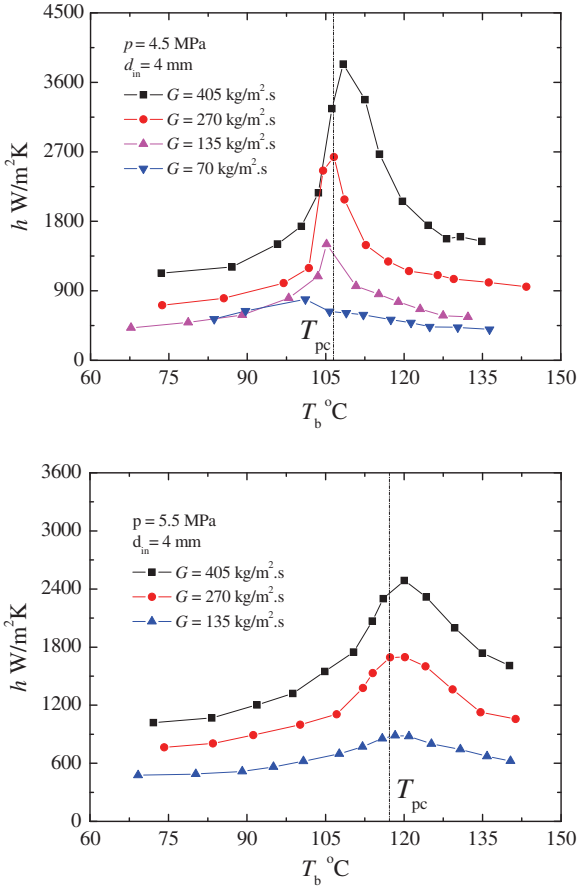


**Figure 2.7:** Heat transfer coefficient for various mass fluxes in horizontal flow of R134 and pressure of 4.5-5.5 $MPa$ [101].

At higher mass flow rate (Reynolds number) there is an increase of the heat transfer coefficient because of the increased turbulence. Vikhrev et al. [52], Bae et al. [77]. Bishop et al. [73] experimentally investigated this effect and it is valid for the entire range of the considered bulk fluid temperatures.

When the temperature of the working fluid is not in the vicinity of the pseudocritical temperature $T_{pc}$, then, the variation of the thermophysical properties is not that strong. In contrast, when the fluid temperature approaches the pseudocritical temperature $T_{pc}$, then the changes of the specific heat, the density, the viscosity and the thermal conductivity are large. This may give the unusual result that the HTC is higher at lower mass flux for example when the bulk fluid temperature is near the pseudocritical temperature. Figure 2.7 presents the measured in-tube heat transfer coefficient of R134a at various mass fluxes and at pressure of 45 *bar* and 55 *bar* respectively [101]. It can be seen that when the mass flux increases by factor 2 the HTC is higher by a factor of 1.9. The effect of the mass flux is more dominant when the bulk fluid temperature is near the pseudocritical temperature.

As a conclusion, at high mass fluxes and low heat flux, the heat transfer rate is usually improved because the Reynolds number is higher. Moreover, the fluid bulk temperature is close to the pseudocritical temperature which leads to strong property variations in the vicinity of this region. Hence, on one hand the viscosity drop yields increased velocity and turbulence of the fluid and together with the peak of the specific heat capacity this lead to enhanced heat transfer. However, at low mass fluxes but high heat flux the heat transfer rate is impaired (deteriorated).

### 2.3.2 Effects of heat flux

In many experimental studies it is pointed out that the heat transfer coefficient HTC increases at lower heat fluxes [110], [76], [77]. However, the HTC strongly depends on the heat flux, especially at the pseudocritical region. The HTC decreases at higher heat flux Swenson et al. [76]. At higher heat fluxes there is a bigger difference between the wall ($T_w$) and the bulk fluid ($T_b$) temperatures. Both temperatures ($T_w$ and $T_b$) increase at these conditions.

On the other hand, when the bulk temperature $T_b$ is near the pseudocritical temperature $T_{pc}$, the specific heat of the fluid will have a maximum value and the magnitude of the viscosity and the density will have a significant drop that will enhance the heat transfer. However, deteriorated heat transfer appears when the wall temperature is higher than the pseudocritical temperature $T_{pc}$. In that region the specific heat, the density and the thermal conductivity of the fluid are quite low which reduces the heat transfer between the wall and the fluid.

In Figure 2.8 the effects of the heat flux as a function of the heat transfer coefficients' ratio ($HTC/HTC_0$) and the ratio of the bulk and the pseudocritical temperature ($T_b/T_{pc}$) showed in reduced units are presented. The experimental data was obtained for methane ($p_{cr}$=45.95 *bar*, $T_{cr}$=-82.6°C) circulating in

horizontal flow Gu et al. [110]. The reference value of $HTC_0$ is determined by the Dittus-Boelter heat transfer correlation for mass flux of 11,000 $kg/(m^2s)$, temperature of -150°C and pressure of 100 $bar$.

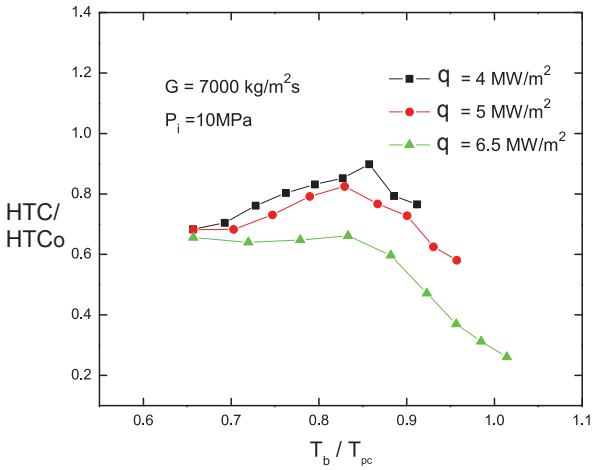


**Figure 2.8:** Heat transfer coefficient presented in reduced units for various heat fluxes in horizontal flow of methane [110].

In conclusion, the heat flux has a significant effect on the magnitude of the heat transfer coefficients. This is especially prominent in the pseudocritical region. Hence, when the heat flux is low (4 $MW/m^2$) Gu et al. [110] there is enhanced heat transfer because the temperature difference $T_w$ and $T_b$ is low. Additionally, at these conditions the bulk fluid temperature (methane) goes through the pseudocritical region. On the other hand, by increasing the heat fluxes (6.5 $MW/m^2$) the wall temperature is (2.6 times) higher than the pseudocritical temperature which leads to deteriorated heat transfer [110].

### 2.3.3 Effects of pressure

The pressure effect on the heat transfer coefficients is as prominent as the effects of the mass flux $\dot{G}$ and the heat flux $\dot{q}$, according to [76], [77], [101], [110].

However, the HTC increases at pressures close to the critical pressure of the fluid when the other conditions are fixed. This can be associated to the drastic thermophysical property changes at pressures near the critical pressure. At constant values of mass flux and heat flux, the wall $T_w$ and the bulk fluid $T_b$ temperatures change insignificantly with pressure. However, the pseudocritical temperature $T_{pc}$ is related to the pressure changes. Hence, the heat transfer coefficient varies at different pressures. At pressures close to the critical pressure of the working fluid and when the ratio of $\dot{q}/\dot{G}$ is low, then the bulk temperature $T_b$ is closer to the pseudocritical temperature $T_{pc}$ and the wall temperature $T_w$ is slightly higher than the $T_{pc}$. Therefore the variations of the thermophysical properties is stronger at lower pressure (closer to the critical pressure) than at

higher pressures. Thus, the magnitude of the HTC is higher at lower pressures. On the other hand, at different pressures, when the ratio $\dot{q}/\dot{G}$ is relatively high, the bulk fluid temperatures $T_b$ are near the pseudocritical temperature $T_{pc}$, but the wall temperatures $T_w$ are higher than the pseudocritical temperature $T_{pc}$ at lower pressures. At these conditions a deteriorated heat transfer occurs.

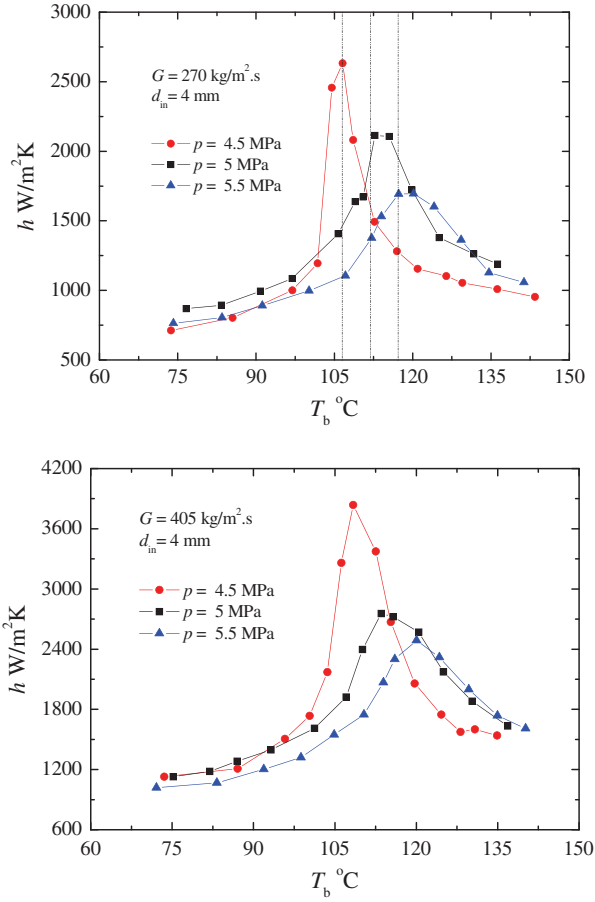


**Figure 2.9:** Heat transfer coefficient at different pressures in horizontal flow of R134 and mass fluxes of 270-405 $kg/(m^2s)$ [101].

In Figure 2.9 the measured in-tube heat transfer coefficient of R134a at various pressure and mass fluxes 270 $kg/(m^2s)$ and 405 $kg/(m^2s)$ is shown [101]. Zhao and Jiang [101] showed in their experimental investigation that at higher pressures the magnitude of the HTC is lower and shifted towards the higher temperature.

### 2.3.4 Effects of tube diameters

There are a number of studies investigating the effect of tube diameter on the heat transfer coefficient at supercritical conditions, [26, 77, 80, 86, 111, 112]. However, it is difficult to determine the tube diameter effect on the HTC's at DHT. Oh and Son [86] concluded that the heat transfer coefficient in $d_i = 4.55mm$ is 8-35.6% higher than in $d_i = 7.75mm$. A higher heat transfer coefficient is observed in smaller tube diameters for all temperatures.

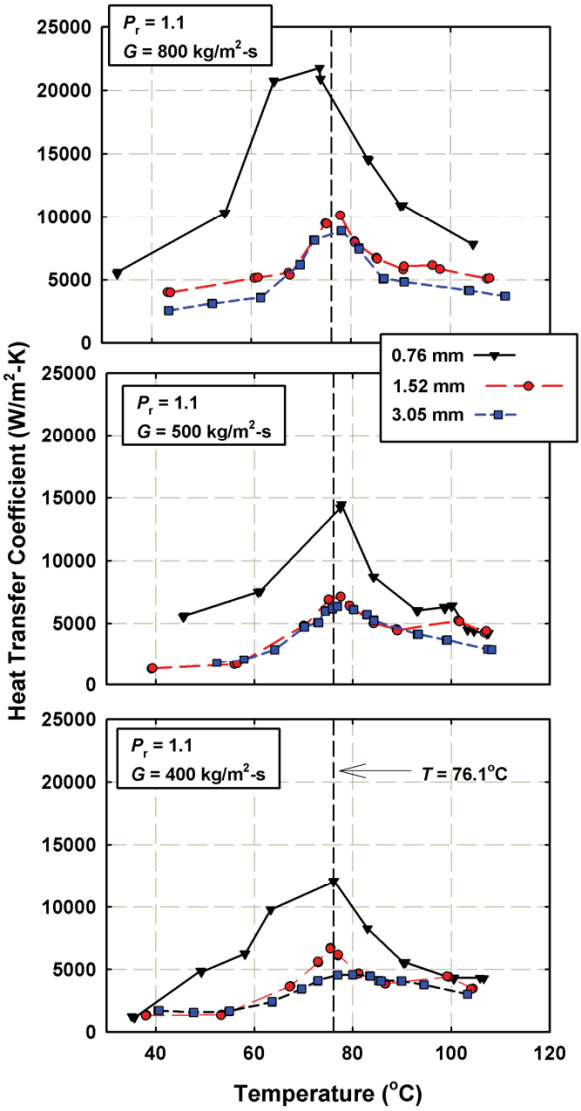


**Figure 2.10:** The tube diameter effect on the heat transfer [112].

In order to determine the tube diameter effect on the HTC, Yu at al. [80] compared their data with Yamagata et al [54]. Two tube diameters (26 $mm$ and 43 $mm$) were considered in horizontal flow of supercritical water being between 3.5-5.7 times larger than the tube diameter tested in the work of Yamagata et al. [54]. When the ratio of the $\dot{q}/\dot{G}$ is small, the tube diameter has insignificant effect on the heat transfer of supercritical water in horizontal flow. Furthermore, there is no large temperature difference between the top and the bottom surface of small tube diameter (7.5 $mm$) compared with the larger tube diameter (43 $mm$). At higher values of the ratio $\dot{q}/\dot{G}$, there is a discrepancy of the temperatures on the top and bottom surface of the tube diameters of 26 $mm$ and 7.5 $mm$. The temperature difference on top and bottom surface is greater when considering the larger tube diameter. This indicates that the buoyancy effect has a significant influence inside tubes with bigger diameters.

Garimealla [112] reported that the HTC increases with a diameter decrease for all mass fluxes. The results for constant pressure ($1.1p_{cr}$ of R410A) and various mass fluxes are presented in Figure 2.10. At higher mass fluxes it is evident that the heat transfer coefficients are significantly higher at the smallest considered diameter (0.76 $mm$) than in the larger tested diameter (3.05 $mm$).

### 2.3.5 Effects of flow direction

Since the flow direction has a significant effect on the heat transfer it was analyzed by several researchers, [26], [80], [83]. Yu et al. [80] compared the heat transfer characteristics of water at supercritical state in horizontal and vertical (inclined) flow directions. It was concluded that the DHT is more dominant in vertical flow rather than in horizontal. Results of this comparison are shown in Figure 2.11.

Experimental investigation in small tube diameters of supercritical $CO_2$ was done by Liao and Zhao [26] in horizontal and vertical directions. It was observed that the heat transfer coefficients in downward flow near the pseudocritical region were much lower compared to horizontal and upward flow. This is relevant for a fluid with constant thermophysical properties as well. However, the authors reported that this conclusion is inconsistent with results available in literature. Furthermore, from the results it was concluded that there is EHT in horizontal and vertical upward flow. Li et al. [83] also tested a tube diameter of 2 $mm$ in downward and upward flow of supercritical $CO_2$. At lower heat fluxes and higher mass fluxes ($Re_{in}$=9,000) local wall temperature increase was observed for downward and upward flow. However, for higher heat fluxes it was noticed that the local wall temperatures vary in a complex and nonlinear way in upward flow. It was also indicated that DHT was not detected in downward flows.

The effect of flow direction is mostly determined by buoyancy phenomena (Section 2.3.6). In laminar mixed convection for upward heating or downward cooling flow the heat transfer would be enhanced. However, for the opposite direction flow the heat transfer will be decreased due to the buoyancy effect.

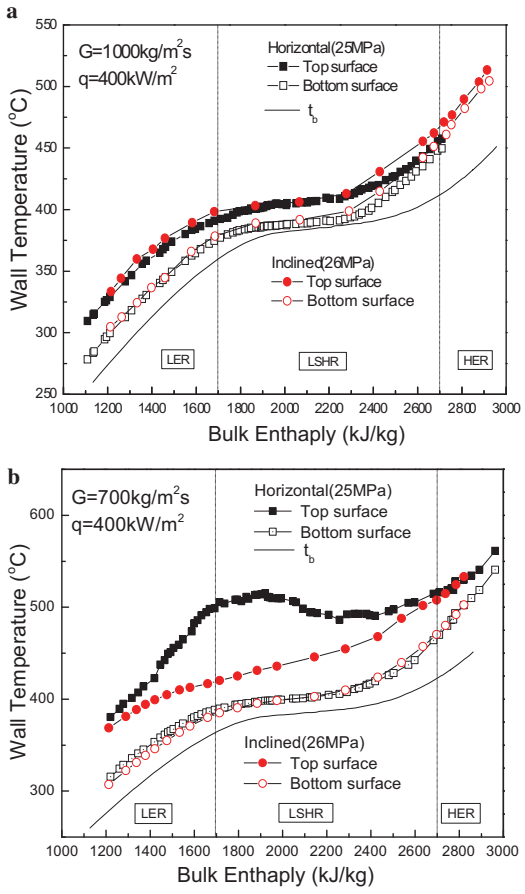


**Figure 2.11:** The variation of the wall temperature in horizontal and inclined tubes [80].

In contrary, for turbulent mixed convection, the heat transfer for downward heating was improved compared with the upward conditions [113].

### 2.3.6 Buoyancy effect

The buoyancy effect is important and it should be investigated if it has a significant or negligible influence on the heat transfer. However, the occurrence of the buoyancy depends on the flow direction (Subsection 2.3.5). Most of the analytical and experimental studies available in literature focus on vertical flow. There are very few criteria in literature for detecting buoyancy(-free) regions in a horizontal supercritical fluid flow [114].

This phenomenon is especially dominant at high heat flux or at low mass flux. There is a significant density difference when considering the temperature near the wall $T_w$ and at bulk temperature $T_b$. That results in a complex heat

transfer due to the buoyancy effect. The differences of the heat transfer characteristics in the upward and downward flow were attributed to the buoyancy effect [40, 54, 55, 64, 114–116]. Jackson and Hall [40], [64] pointed out that deteriorated heat transfer in upward flow is induced because of the localized laminarization of the flow caused by the buoyancy. Due to the buoyancy effect, there is a continuous heat transfer enhancement in downward flow whereas the wall temperatures are less sensitive to heat flux.

In horizontal flow of a fluid at supercritical state, at a pre-determined set of parameters, it is important to assess if the buoyancy effect is likely to be significant or not. Defining if this effect is essential is very important because in horizontal flow there is a differentiation between the top flow layers and the bottom flow layers. As a result there is a difference between the wall temperature and the bulk fluid temperature between the top and bottom. Hence, the less dense fluid raises to the upper layer of the tube and the denser (colder) fluid remains at the lower layer of the tube. This effect is bigger in tubes with relatively large diameters.

Investigating the effect of the density changes of water (buoyancy) in horizontal flow was done by Shitsman [111], and they proposed to use the product of Grashof and Prandtl number as a criterion for the buoyancy effect. However, this criterion for buoyancy could not be verified against any existing data but his own. Nevertheless, his study had a major impact on future work.

Vikhrev and Lokshin [52] and Yamagata et al. [54] experimentally compared the heat transfer characteristics of vertical and horizontal flows of water. From their results it was concluded that the HTC's and the temperature profiles from the horizontal (top and bottom) flow differ from that obtained in vertical directions. Therefore, direct application of the results obtained for different flow directions, even though in similar conditions can lead to a significant error. At low ratio of $\dot{q}/\dot{G}$ there is no significant temperature difference between the top and bottom surface of the tube, while at high ratio $\dot{q}/\dot{G}$ the top surface temperature is considerably higher, due to the buoyancy effect. Petukhov et al. [115] proposed a criterion for determining the buoyancy effect in horizontal flow. Bazargan et al. [81] investigated the buoyancy and acceleration effect in a horizontal flow and tube diameter of 6.6 $mm$. They concluded that the reason for considerable disagreement between the empirical heat transfer correlations and the experimental data is due to neglecting the buoyancy effect. Moreover, they proved the validity of the Petukhov and Polyakov [115] criterion for determining the buoyancy effec

***Criteria for determining the buoyancy effect***

The ratio of the two dimensionless numbers $Gr/Re^2$ is usually used as criteria for determining if there is buoyancy-free or buoyancy-dependent effect. Grashof number $Gr$ Eq.(2.10) can accurately estimate the effect of natural convection in a flow that doesn't undergo drastic property variations.

$$Gr = \frac{g\beta(T_w - T_b)d_{hy}^3}{\nu^2} \tag{2.10}$$

where $\beta$ is the bulk thermal expansion, $\nu$ is the kinematic viscosity of the considered fluid and $g$ is the gravitational acceleration. The Reynolds number is small at low mass flow rates. However, the density gradient and the radial temperature profile are larger. Hence, the Grashof number and the ratio $Gr/Re^2$ increase as well.

In order to distinguish the significance between the buoyancy-free region and the effect of natural convection, the term $Gr/Re^2$ is used. It is derived with dimensional analysis of mixed convection heat transfer. When the ratio $Gr/Re^2$ is in order of magnitude of unity or higher the buoyancy effect should be accounted for. This is valid for near-constant property flow.

Bazargan et al. [81] experimentally investigated if there is a buoyancy effect in 4 different set of experiments indicated as 4 different cases, depicted in Table 2.4. Case A is representing experimental data done at low mass flux and high heat flux where the buoyancy effect is significant. Near the critical region, the wall surface temperature difference $T_{w,top}$ and $T_{w,bot}$ is up to 70°C and the property variations and buoyancy effect are the biggest. The buoyancy effect is substantial because of the significant density gradient occurring between wall temperature $T_w$ and bulk fluid temperature $T_b$. However, at higher temperatures (670°C) far from the pseudocritical temperature, both wall surface temperatures at the top $T_{w,top}$ and the bottom $T_{w,bot}$ even up. Hence, there is less density variation between the wall and the bulk and the buoyancy effect diminishes. In other two sets of experiments (B and C) the mass fluxes were increased, with the aim to reduce the buoyancy effect. However, the surface temperature difference between the top and bottom $T_{w,top}$ and $T_{w,bot}$ was 35°C and 12°C for Case B and Case C, accordingly. These results are relevant for near the pseudocritical temperature. For Case B and Case C, the surface temperature differences vanished at 570°C and 460°C, respectively. However, in Case C, the wall temperature $T_w$ and bulk fluid temperature $T_b$ were 445°C (105 $kg/s$) and 400°C (150 $kg/s$). There is a density change of 35%. In Case D, the experiments were done at 965 $kg/(m^2s)$ the surface temperature difference was insignificant and the buoyancy effect was vanished.

Figure 2.12 illustrates the results from this investigation. Case A reaches unity and can be accounted as a criterion for buoyancy effects. Nevertheless, for Case C, the value of the ratio ($Gr/Re^2$=0.1) is less than 1 but there was density gradient detected which indicates that it is not buoyancy-free region and the buoyancy should be accounted. The density and the viscosity were estimated at bulk temperatures $T_b$ and the top surface temperature was used as wall temperature.

In Table 2.4, the summary of the test conditions from Bazargan et al. [81] is presented.

The heat flux was constant for all four set of measurements while the mass flux was in the range of 340-965 $kg/(m^2s)$. As a conclusion, this approach criterion should be validated with more experimental data if used for supercritical fluids because the peak values of the ratio $Gr/Re^2$ vary significantly.

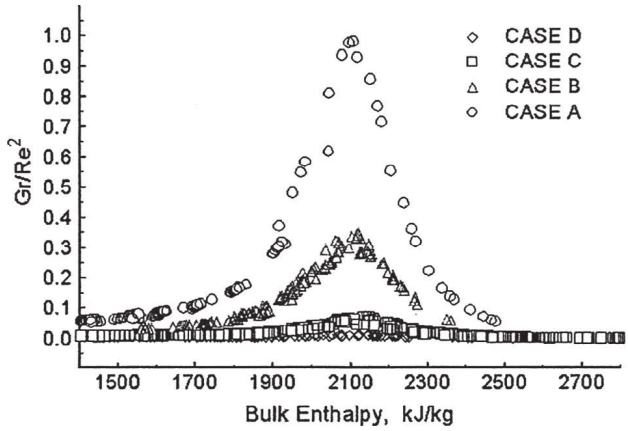


**Figure 2.12:** Variation of $Gr/Re^2$ with the bulk fluid enthalpy at constant heat flux [67].

**Table 2.4:** Summary of test conditions [67]

| *Heatflux* $q = 300$ $kW/m^2$ | *Massflux* $G$ $kg/(m^2s)$ | *Maximum* $\Delta(T_{w,top}\text{-}T_{w,bot})$, °C | *Wall Temp. Bo diminish* °C | *Ratio* $HTC_{w,top}/HTC_{w,bot}$ |
|---|---|---|---|---|
| Case A | 340 | 70 | 670 | 2.75 |
| Case B | 432 | 35 | 570 | 2.15 |
| Case C | 646 | 12 | 460 | 1.5 |
| Case D | 965 | 4 | 405 | 1.2 |

Jackson et al. [117] proposed a different standard to determine the buoyancy effect in vertical flow, $Gr/Re^{2.7} < 10^{-5}$. If this criterion is fulfilled then the buoyancy effect is negligible. However, Bazargan et al. [81] proved that this standard is not proper for determining the buoyancy effect in horizontal flow and under moderate buoyancy effect.

Another criterion to check the buoyancy effect was proposed by Petukhov and Polyakov [115]. They derived a threshold value for the Grashof number $Gr_{th}$ Eq.(2.2).

$$Gr_{th} = 3 \cdot 10^{-5} Re_b^{2.75} \overline{Pr}^{0.5} [1 + 2.4 Re^{-1/8} (\overline{Pr}^{2/3} - 1)] \tag{2.11}$$

where the Prandtl $Pr$ number is defined with Eq.(2.12)

$$\overline{Pr} = \frac{h_w - h_b}{T_w - T_b} \frac{\mu_b}{\kappa_b} \tag{2.12}$$

Considering the heat flux at the wall, the Grashof number is redefined with

Eq.(2.13)

$$Gr_q = \frac{g\overline{\beta}qd^4}{\nu_b^2\kappa_b} \tag{2.13}$$

where the bulk thermal expansion is defined with Eq.(2.14)

$$\overline{\beta} = \frac{1}{\rho_f}\frac{\rho_b - \rho_w}{T_w - T_b} \tag{2.14}$$

When $Gr_q < Gr_{th}$, then the buoyancy effect was negligible. This criterion was tested by Adebiyi and Hall [79] for supercritical $CO_2$ in horizontal flow and this criteria was complied. However, more test conditions should be compared since in the work of Adebiyi and Hall [79] the $Gr_q$ was always above the threshold. Bazargan et al., [81] showed that the criterion of Petukhov and Polyakov shows a very good accuracy, but in a conditions with a negligible acceleration effect.

### 2.3.7 Acceleration effect

The acceleration of a fluid flow is defined as the rate of the velocity variation caused by the position changes of the fluid particles.

The acceleration effect is significant in small tube diameters while for large tube diameters the buoyancy effect is more dominant. Therefore, the acceleration effect can be neglected with respect to the buoyancy. The acceleration in a tube occurs due to the density changes. In a heated section, at a continuous mass flow rate, lowering the density results in a raise of the volumetric flow rate. Jackson proposed a non-dimensional number $A_c$ for determining the acceleration effect in thermally-induced flow.

$$Ac = \frac{\beta_b q_w d}{k_b Re_b^{1.63} Pr_b} \tag{2.15}$$

If $A_c$ approaches the limit $10^{-6}$ then the acceleration effect should be included. Gu et al. [110] compared their experimental data and concluded that at high heat fluxes ($15\ MW/m^2$) $A_c$ approaches the limit $10^{-6}$. At these conditions the thermally-induced acceleration effect starts and the heat transfer is impaired. As a conclusion the Jackson criterion $A_c < 10^{-6}$ worked well in predicting the heat transfer deterioration.

Furthermore, Petukhov and Polyakov [115] proposed a criterion $J$ for determining the acceleration effect Eq.(2.16)

$$J = 4\frac{Re}{\overline{Pr}}\left(\frac{\rho_b - \rho_w}{T_w - T_b}\frac{qD\rho_b}{\kappa\rho_f^2}\right)^2 \tag{2.16}$$

The following relationship Eq.(2.17) was proposed by Petukhov and Polyakov to determine if the acceleration effect is negligible, but in vertical flow direction.

$$|\pm Gr_q + J| < 4\cdot 10^{-4} Re^{2.8}\overline{Pr} \tag{2.17}$$

where the negative sign − is for downward flow and the positive sign + for upward flow. However, Bazargan et al. [81] used this standard regardless the flow direction to check if the acceleration effect is negligible in supercritical horizontal fluid flow with inner tube diameter of 6.3 $mm$, and proved that it can be used with confidence.

### 2.3.8 Effects of inlet temperature

The effects of the inlet temperature is the least investigated and hence there is modest information in literature. Due to the fact that a fluid with supercritical flow is prone to drastic changes of the thermophysical properties, apart from the entry effect, it deserves an independent study [118].

Dubey et al. [62] reported that the inlet temperature has a significant effect in determining the location and the magnitude of the local peak of the specific heat capacity and consequently the peak of the local wall temperature. In his study it was highlighted that the EHT is independent of the inlet temperature $T_{in}$ but it has a strong effect on DHT. Furthermore, in the location where the maximum wall temperature occurs the bulk fluid temperature decreases by increasing the heat flux and reducing the inlet temperature.

Kline et al. [87] investigated the effect of the inlet temperature of supercritical $CO_2$ at three different heat fluxes and tube diameters of 4.6 $mm$, 8 $mm$ and 22 $mm$ in vertical flow. The inlet temperature varied between 5-35°C. This can have a significant effect at high heat fluxes and determining the onset of the deteriorated heat transfer. For fixed diameter $D$ and mass flux $G$, DHT occurred only when $T_{in}$ was within a limited range, which became wider as $q$ was increased.

From Section 2.3 it can be concluded that the heat flux and the mass flux are one of the parameters that have the most significant effect on the supercritical heat transfer. This effect becomes even more dominant near the critical region or more particularly when the fluid is approaching the pseudocritical temperature. Moreover, of key importance is the ratio $\dot{q}/\dot{G}$, because at high heat fluxes and low mass fluxes deteriorated heat transfer is detected.

The pressure of the working fluid is also a substantial parameter that influences the heat transfer, especially closer to the critical pressure of the working fluid. When the pressure is in the vicinity of the critical pressure of the respected fluid, the specific heat capacity reaches a sharp peak. While far from the critical pressure, the local maximum of the specific heat is milder. The changes of the specific heat are simultaneously followed by the changes of the density, viscosity and the thermal conductivity.

Another important parameter that has influence on the supercritical heat transfer is the buoyancy effect. This is especially relevant for horizontal flow. Therefore, the effects that these parameters have on supercritical heat transfer are investigated and determined from the measurement data.

## 2.4 Heat transfer correlations derived for forced convection

There are several reviews available in literature concerning heat transfer correlations [23], [67], [118]. The heat transfer correlations are validated for water and $CO_2$, tested at certain experimental conditions. The conclusion of these reviews is that there is no general heat transfer correlation that fits well with all experimental results, except in the conditions they were derived for.

Describing the heat transfer behavior of a fluid at supercritical pressure is a challenge because of the rapid thermophysical property variations with the temperature, appearing in radial direction of the tube. For correlating experimental heat transfer data with constant thermophysical properties the following general form of the heat transfer correlation presented in Eq.(2.18) can be used:

$$Nu = CRe^m Pr^n \tag{2.18}$$

where the Nusselt number $Nu$, is presented as a function of the Reynolds number $Re$ and the Prandtl number $Pr$. One of the most frequently used (cited) heat transfer correlation is the one of Dittus and Boelter (1930) Eq.(2.19) [119]

$$Nu_b = 0.023 Re_b^{0.8} Pr_b^n \tag{2.19}$$

where the subscript $b$ indicates to the bulk-fluid conditions, and the superscript is linked with either $n = 0.4$ used in heating or $n = 0.3$ in cooling applications.

This heat transfer correlation is derived for a wide range of experimental parameters at single-phase flows. Furthermore, it was developed for constant property flow that does not account for the rapid variations of the thermophysical and transport properties. Therefore, its use at supercritical state is limited. In order to account for effects of the fluid's extreme property variations additional property ratios should be considered.

There are a number of empirical heat transfer correlations derived from experimental data by using water, $CO_2$, helium, cryogenic fluids and recently there are some derived for refrigerants as well. Mainly, these heat transfer correlations are of Dittus-Boelter type, that encounter additional property terms. There are many different approaches but for most of the heat transfer correlations, the ratio of the fluid properties obtained at bulk and wall temperatures are considered. In contrary, Pethukov et al. [89] proposed an integral average specific heat to be used $\frac{h_w - h_b}{T_w - T_b}$ instead of the specific heat at bulk or wall fluid temperature. Furthermore, the heat transfer correlations can be calculated by considering the film temperature as well, which represents the average of the bulk and wall temperatures. The most frequently cited, as well as the most recent heat transfer correlations and the ranges of their use are presented below.

### 2.4.1 Supercritical water and $CO_2$

Back in 1957, Bringer and Smith [90] were the pioneers on experimental research for heat transfer to supercritical water and $CO_2$. Because of the rapid variations of thermal conductivity, viscosity and density they have found that the existing empirical and semi-theoretical correlations did not give accurate results. The prompt changes of the thermophysical properties were identified as the main reasons for the deviation between experimental results and predictions by the heat transfer correlation. However, the peak of the thermal conductivity near the pseudocritical temperature was not considered. The reason is that the occurrence of a peak in the thermal conductivity of water near the pseudocritical temperature was updated and officially recognized in 1990s. In general, the results for water showed a good agreement with a heat transfer correlations compared from literature. In contrast, there is a deviation of 30% when compared with measurements of $CO_2$ [90]. The discrepancy in the results is due to the fact that the measurements for $CO_2$ were close to the critical pressure ($p = 1.1p_{cr}$), while the pressures when testing water was far from the critical point ($p = 1.6p_{cr}$).

$$Nu_x = 0.02663 Re_x^{0.77} Pr_w^{0.55} \tag{2.20}$$

valid for $30,000 < Re < 300,000$ derived for water at a pressure of 34.5 $MPa$.

$$Nu_x = 0.0375 Re_x^{0.77} Pr_w^{0.55} \tag{2.21}$$

valid for $30,000 < Re < 300,000$ derived for $CO_2$ at a pressure of 8.2 $MPa$ The $x$ stands for the dependence on characteristic temperature for calculating the dimensionless groups:

$$T_x = T_b \text{ if } \frac{T_{pc} - T_b}{T_w - T_b} < 0;$$
$$T_x = T_{pc} \text{ if } 0 \leq \frac{T_{pc} - T_b}{T_w - T_b} \leq 1.0; \text{ and}$$
$$T_x = T_w \text{ if } \frac{T_{pc} - T_b}{T_w - T_b} > 1.0.$$

In the heat transfer correlation derived by Miropol'skii and Shitsman [74] they assumed that the thermal conductivity of water is a smooth decreasing function of the temperature near the critical and pseudocritical points. In this case the minimum value for the Prandtl number ($Pr_{min}$) was considered which is lower than $Pr_b$ and $Pr_w$.

$$Nu_b = 0.023 Re_b^{0.8} Pr_{min}^{0.8} \tag{2.22}$$

This heat transfer correlation is valid for pressure of 22.0-25.0 $MPa$ and mass flux of 300-1500 $kg/(m^2 s)$, derived for a tube diameter of 8 $mm$.

However, in the heat transfer correlation of Krasnoshchekov and Protopopov [72, 120], the variation of the thermophysical properties of water and $CO_2$ were considered by using the averaged specific heat capacity $\overline{c_p}$ and the $\overline{Pr}$ number. The proposed heat transfer correlation shows a maximum deviation of 15%, when compared with the work of Dickinson [71] and Miropol'skii[74].

$$Nu_b = Nu_{0,b}\Big(\frac{\overline{c_p}}{c_{p,b}}\Big)^{0.35}\Big(\frac{\mu_b}{\mu_w}\Big)^{0.11}\Big(\frac{\kappa_b}{\kappa_w}\Big)^{-0.33} \tag{2.23}$$

$$Nu_{0,b} = \frac{f_b/8 Re_b \overline{Pr}}{12.7\Big(\frac{f_b}{8}\Big)^{0.5}\Big(\overline{Pr}^{2/3}-1\Big)+1.07} \tag{2.24}$$

where the Filonenko friction factor is determined with Eq.(2.25)

$$f = (1.82 lg Re_b - 1.64)^{-2} \tag{2.25}$$

This heat transfer correlation is valid for $2\cdot 10^4 < Re < 8.6\cdot 10^5$; $0.85 < \overline{Pr}_b < 65$; $0.9\dfrac{\mu_b}{\mu_w} < 3.6$; $1 < \dfrac{\kappa_b}{\kappa_w} < 6$; $0.07 < \dfrac{\overline{c_p}}{c_{p,b}} < 4.5$.

Later, Krasnoshchekov and Protopopov [91] modified this heat transfer correlation into the form of Eq.(2.26)

$$Nu = Nu_0\Big(\frac{\rho_w}{\rho_b}\Big)^{0.3}\Big(\frac{\overline{c_p}}{c_{pb}}\Big)^{n} \tag{2.26}$$

where $Nu_0$ is Eq.(2.28) and $n$ is a function of the $T_w$ and $T_b$. This heat transfer correlation is valid $8\cdot 10^4 < Re < 5\cdot 10^5$; $0.85 < \overline{Pr}_b < 65$; $0.9\dfrac{\rho_w}{\rho_b} < 1.6$; $0.02 < \dfrac{\overline{c_p}}{c_{p,b}} < 4$; $0.9 < T_w/T_{pc} < 2.5$; $46 < q < 2600$ $(kW/m^2)$ and the ratio $x/D \geq 15$.

Furthermore, they added a correction factor in order to account for the entrance effect $f(x/D) = 0.95 + 0.95(x/D)^{0.8}$, which can be applied in the range of $2 \leq (x/D) \leq 15$.

The heat transfer correlation Eq.(2.28) was modified by Gnielinski for $CO_2$ in the form given with Eq.(2.31)

$$Nu_b = \frac{f/8(Re_b - 1000)Pr_b}{1 + 12.7(f/8)^{0.5}\Big(Pr^{2/3}-1\Big)} \tag{2.27}$$

and is valid for the following range $3\cdot 10^3 < Re < 5\cdot 10^6$; $0.5 < Pr_b < 2000$;

Moreover, Jackson and Fewster [117] modified the heat transfer correlation of Krasnoshchekov et al. Eq(2.23) in the Dittus-Boelter form given with Eq.(2.28) and can be applied to water and $CO_2$

$$Nu = 0.0183 Re_b^{0.82}\overline{Pr}^{0.5}\Big(\frac{\rho_w}{\rho_b}\Big)^{0.3} \tag{2.28}$$

Domin [82] derived two heat transfer correlations testing water in horizontal flow that are valid for two different wall temperatures $T_w$>350°C and $T_w$=250-350°C and pressure of 22-26 $MPa$. The test section had a length between 1.08-1.23 $m$ and a tube diameter of 2-4 $mm$. The heat flux and the mass flux were in the range of 580-4500 $kW/m^2$ and 600-5100 $kg/(m^2s)$.

1. $T_w \geq 350$°C

$$Nu_b = 0.1 Re_b^{0.66} Pr_b^{1.2} \tag{2.29}$$

2. $T_w = 250 - 350$°C

$$Nu_b = 0.036 Re_b^{0.8} Pr_b^{0.4} \left(\frac{\mu_b}{\mu_w}\right)^{0.11} \tag{2.30}$$

Forced convection heat transfer measurements with water at near critical temperatures and supercritical pressure was made by Bishop et al. [73]. The tests were performed in vertical upward inside flow and in annuli. The derived heat transfer correlation, Eq.(2.31), correlates the results from the measurements within a span of ±15% while considering the entrance effects. The bulk and film fluid temperature were considered for deriving the heat transfer correlation.

$$Nu_{b,x} = 0.00696 Re_{b,x}^{0.9} Pr_{b,x}^{0.66} \left(\frac{\rho_w}{\rho_b}\right)^{0.43} \left(1 + \frac{2.4D}{x}\right) \tag{2.31}$$

The experiments were performed in a wide range of pressure (226-276 $bar$), temperature (282-527°C), tube diameter (2.5-5.1 $mm$), mass flux (651-3662 $kg/(m^2s)$) and heat flux (310-3500 $kW/m^2$). For the heat transfer correlation, 400 measuring points were considered. As a remark from Bishop et al. [73], it was stated that the deviation with the other heat transfer correlations is due to the difference of the used thermophysical and transport properties.

A generalized heat transfer correlation for forced convection heat transfer to water at supercritical state was proposed by Swenson et al. [76]. The fluid properties were calculated for wall temperature as such taking into account that the thermal conductivity of water is gradually decreasing in regard to the temperature. The prediction of the proposed heat transfer correlation Eq.(2.32) is within 15% for 80% of the measurement data. Furthermore, this heat transfer correlation predicted the data of supercritical $CO_2$ with good accuracy.

$$Nu_w = 0.00459 Re_w^{0.923} \overline{Pr}_w^{0.613} \left(\frac{\rho_w}{\rho_b}\right)^{0.231} \tag{2.32}$$

This heat transfer correlation was derived based on 2951 measuring points for the following conditions: pressure (228-414 $bar$), bulk temperature (70-576°C), wall temperature (93-649°C) tube diameter (9.4 $mm$), mass flux (542-2150 $kg/(m^2s)$) and heat flux (200-2000 $kW/m^2$). It covered 72.5% of the data within one standard deviation and it showed good prediction accuracy for $CO_2$.

Yamagata et al. [54] proposed a heat transfer correlation Eq.(2.33) for forced convection in vertical and horizontal flow in circular tubes, by excluding the DHT region.

$$Nu_b = 0.0135 Re_b^{0.85} Pr^{0.8} F_c \tag{2.33}$$

By using the Eckert number Eq.(2.38) the data was classified in three different regions

$$E = \frac{T_{pc} - T_b}{T_w - T_b} \tag{2.34}$$

$F_c = 1.0$ for $E > 1$;

$F_c = 0.67 Pr_{pc}^{-0.05} (\overline{c_p}/c_p)^{n_1}$ for $0 \leq E \leq 1$, $n_1 = -0.77(1 + 1/Pr_{pc}) + 1.49$;

$F_c = (\overline{c_p}/c_{pb})^{n_2}$ for $E < 0$ and $n_2 = 1.44(1 + 1/Pr_{pc} - 0.53$.

This heat transfer correlation has an accuracy of ± 20% and was derived for the following conditions: pressure (22.6-29.4 $MPa$), temperature (230-540°C), tube diameter (7.5-10 $mm$), length (1.5-2 $m$) mass flux (310-1830 $kg/(m^2 s)$) and heat flux (116-903 $kW/m^2$).

Recently, Mokry et al. [61] derived a heat transfer correlation for vertical bare tubes, by considering the bulk fluid temperature. The heat transfer correlation is of Dittus-Boelter type and is presented with Eq.(2.35)

$$Nu_b = 0.0061 Re_b^{0.904} \overline{Pr}_b^{0.684} \left(\frac{\rho_w}{\rho_b}\right)^{0.564} \tag{2.35}$$

The uncertainty of the heat transfer coefficient is ± 25% and about ± 15% for calculated wall temperatures. Furthermore, Mokry and Pioro incorporated a correction factor in order to account for the entrance effect Eq.(2.36)

$$Nu_b = 0.0061 Re_b^{0.904} \overline{Pr}_b^{0.684} \left(\frac{\rho_w}{\rho_b}\right)^{0.564} \left(1 + 0.9\frac{D}{x}\right) \tag{2.36}$$

Gupta et al. [75] proposed a heat transfer correlation Eq.(2.37), based on the experimental data for upward flow of water and considering 6336 measuring points.

$$Nu_w = 0.004 Re_w^{0.923} \overline{Pr}_w^{0.773} \left(\frac{\rho_w}{\rho_b}\right)^{0.186} \left(\frac{\mu_w}{\mu_b}\right)^{0.366} \tag{2.37}$$

The heat transfer correlation is derived for NHT and the data points of the DHT are considered as outliers. Furthermore, the entrance/exit effect is discarded by excluding the first and last readings of the thermocouples from the calculations. The proposed heat transfer correlations predicted with an uncertainty of ± 25% of the HTCs and is valid for the following range pressure (24-25 $MPa$), inlet bulk temperature (320-350°C), tube diameter (10 $mm$), mass flux (200-1500 $kg/(m^2 s)$) and heat flux (70-1250 $kW/m^2$).

Moreover, the newly derived heat transfer correlation of Gupta et al. [75] was compared with the heat transfer correlation of Mokry et al. [61]. The new

heat transfer correlation showed better fit with the experimental data that it was derived for. Furthermore, the heat transfer correlation was compared with heat transfer correlations from literature. The Dittus-Boelter heat transfer correlation overestimates the HTC's in the pseudocritical region. On the other hand, the heat transfer correlations of Bishop et al. [73] and Jackson show substantial deviation when compared with the experimental data of Gupta et al. [75] in the pseudocritical region.

### 2.4.2 Supercritical refrigerants

Forced convection heat transfer to R12 in a vertical annulus near the critical state was done by Holman et al.[121]. The experiments were conducted in a wide range of pressures (34.5-65.5 $bar$) and bulk fluid temperatures (65.6-204.4°C) in a tube diameter of 10.92 $mm$. A new empirical heat transfer correlation was derived from the experimental data:

$$Nu_w = 0.00175 Re_f^{1.02} Pr_w^{0.55} \tag{2.38}$$

The heat transfer correlation is derived for the following condition $T_b > T_{pc}$ and $T_w > T_{pc}$. It was emphasized that when the bulk fluid temperature was in the vicinity of the critical region the heat transfer correlation is inadequate to describe the data of the heat transfer coefficient. Furthermore, when the bulk fluid temperature is within a few degrees difference of the pseudocritical temperature then the heat transfer is deteriorated.

Gorban' et al. [92] derived a heat transfer correlation for R12. The test section was a circular tube with a diameter of 10 $mm$ and length of 1 $m$. From the experimental data a heat transfer correlation was proposed by considering the bulk fluid properties:

$$Nu_b = 0.00945 Re_b^{0.86} Pr_b^{-0.15} \tag{2.39}$$

The tests were obtained by varying the heat flux (6-290 $kW/m^2$), the mass flux (500-2000 $kg/(m^2 s)$), the inlet temperature (20-140°C) and the pressure (10.8-44.6 $bar$).

Another heat transfer correlation was derived for R134a by Kang and Chang [39]. The experimental data was obtained in a vertical test section with an inner diameter of 9.4 $mm$.

$$Nu_w = 0.02445 Re_b^{0.762} Pr^{0.552} \left(\frac{\rho_w}{\rho_b}\right)^{0.0293} \tag{2.40}$$

The tests were performed at pressures 1.01, 1.06 and 1.11 times the critical pressure of R134a, mass fluxes in the range of 600-2000 $kg/(m^2 s)$ and maximum heat flux of 160 $kW/m^2$. Applicability of the heat transfer correlation derived in steady-state conditions to the transient pressure sequences was evaluated by Kang and Chang [39]. It was found out that this heat transfer correlation overestimates the Nusselt number measured in the pressure transient by 10-40%.

Zhao and Jiang [101] experimentally investigated the heat transfer and pressure drop characteristics of R134a in a horizontal tube-in-tube test section with an inner diameter of 4.01 $mm$ at supercritical pressures during cooling. The experiments were done by varying the inlet temperature (80-140°C), the pressure (45-55 $bar$) and the mass flux (70-140 $kg/(m^2s)$) of R134a. A new heat transfer correlation was developed by modifying the Gnielinski's heat transfer correlation by accounting for the property variations of R134a at the inlet and at the outlet of the test section:

$$Nu = CNu_G\left(\frac{\overline{c_p}}{c_p}\right)^a\left(\frac{\rho_w}{\rho_b}\right)^b \tag{2.41}$$

The heat transfer correlation predicted more than 90% of the experimental data within an accuracy of ± 15%.

Zhang et al. [96] did an experimental investigation of R134a at supercritical pressures flowing upward in a circular tube with an inner diameter of 7.6 $mm$. A heat transfer correlation of Dittus-Boelter type for single-phase flow is considered by introducing an additional acceleration parameter $F$:

$$Nu_b = 0.023Re_b^{0.8}Pr_b^{0.4}F \tag{2.42}$$

The proposed heat transfer correlation by Zhang et al. [96] is compared with heat transfer correlations from literature.

Heat transfer correlations suitable for designing heat exchangers (vapour generators) applicable for transcritical ORC were derived from the experimental data obtained for R134a at supercritical pressures [98]. The tests were conducted in upward and downward flow in a test section with a length of 3 $m$ and an inner tube diameter of 8 $mm$. Hence, the heat transfer correlation for upward flow is:

$$Nu = 0.0291Re_b^{0.762}\overline{Pr}_b^{0.706}\left(\frac{\rho_w}{\rho_b}\right)^{0.353}(100,000Bu)^{-0.046} \tag{2.43}$$

The heat transfer correlation for downward flow is:

$$Nu = 0.0189Re_b^{0.812}\overline{Pr}_b^{0.685}\left(\frac{\rho_w}{\rho_b}\right)^{0.394}(100,000Bu)^{0.0176} \tag{2.44}$$

In the heat transfer correlations the buoyancy effects are encountered with the Bu dimensionless number. The heat flux (20-100 $kW/m^2$), the inlet pressure (43-48 $bar$) and the mass flux (500-1500 $kg/(m^2s)$) of the working fluid were varied during the measurements.

Experimental investigation of the heat transfer characteristics of R134a in a horizontal flow at supercritical pressures for a transcritical ORC condition was done by Tian et al. [43]. The test section was with a diameter of 10.3 $mm$ and the experiments cover a wide ranges of heat fluxes (20-100 $kW/m^2$), mass fluxes (400-1500 $kg/(m^2s)$) and the pressure was 1.02 to 1.2 times the critical pressure of R134a. New heat transfer correlations are proposed from the experimental data, that are as well compared with heat transfer correlations

from literature. The heat transfer correlation derived for the bottom surface is:

$$Nu_{b,bot} = 0.00186 Re_b^{0.9951} \overline{Pr}^{0.5799} \left(\frac{\rho_w}{\rho_b}\right)^{0.1248} \tag{2.45}$$

while the heat transfer correlation for the top surface is

$$Nu_{top} = 0.023 Re_b \overline{Pr}^{0.669} \left(\frac{\rho_w}{\rho_b}\right)^{0.219} Gr_q^{-0.1119} \tag{2.46}$$

Heat transfer characteristics of R134 were determined in a horizontal ribbed tube at different parameter ranges [44]. The aim was to derive a heat transfer correlation for designing heat exchangers suitable to be used in a transcritical ORC. The following heat transfer correlations is derived in order to account for heat transfer deterioration that occurs at the top surface:

$$Nu_{top} = 0.0395 Re_b^{0.63} \overline{Pr}_b^{0.72} \left(\frac{\rho_w}{\rho_b}\right)^{0.25} \pi_c^{-0.004} \tag{2.47}$$

The heat transfer correlation for the bottom surface is

$$Nu_{bot} = 4.314 Re_b^{0.33} \overline{Pr}_b^{0.65} \left(\frac{\rho_w}{\rho_b}\right)^{-0.12} \pi_c^{-0.22} \tag{2.48}$$

Determining the local heat transfer coefficients and heat transfer correlations of R22 flowing in vertical upward flow by use of a thermal camera was done by Dubey et al. [62]. The test sections with a height of 1.8 m and inner diameters of 6 $mm$ and 13.5 $mm$ were electrically heated by using the Joule heating. The derived heat transfer correlation resembles the Dittus-Boelter type which is multiplied with a correction factor.

$$Nu_b = 0.023 Re_b^{0.8} Pr_b^{0.4} \left(\frac{Cp_{ref}}{Cp_b}\right)^x \tag{2.49}$$

where $x$ is an exponent in $ND_{0m}$ that is a new modified non-dimensional number that incorporates the effects of the changes of the system pressure and is defined as:

$$ND_{0m} = \left(\frac{q\mu_{pc}}{GPr_{pc}^{0.5} k_{pc} \Delta T_o}\right) \left(\frac{Cp_{pc}}{Cp_{pc}^*}\right)^{0.55} \tag{2.50}$$

With this modified non-dimensional number the onset of the EHT and DHT can be determined as well as the transition region between the EHT and DHT.

As already mentioned, the heat transfer correlations are derived for various geometries and dimensions, but mainly focusing on vertical flow in small tube diameters.

### 2.4.3 Evaluation of heat transfer correlations

There are many heat transfer correlations available in literature derived for certain operating conditions and parameters that have a significant effect on the heat transfer.

Many researchers did comparisons of the different heat transfer correlations. The results show substantial discrepancies when validating heat transfer correlations in different conditions. This proofs that the heat and mass flux, the flow direction, tube diameters and the large variations of the thermophysical properties of a fluid at supercritical state are parameters that have an essential impact. Moreover, the results from the previous work do not show a good agreement with the refrigerants because they are characterized with unique heat transfer and pressure drop features.

As already mentioned Zhang et al. [96] evaluated different heat transfer correlations with his own experimental data at high and at low heat fluxes at pressure of 43 *bar* and mass flux of 2000 $kg/(m^2s)$, presented on Figure 2.13.

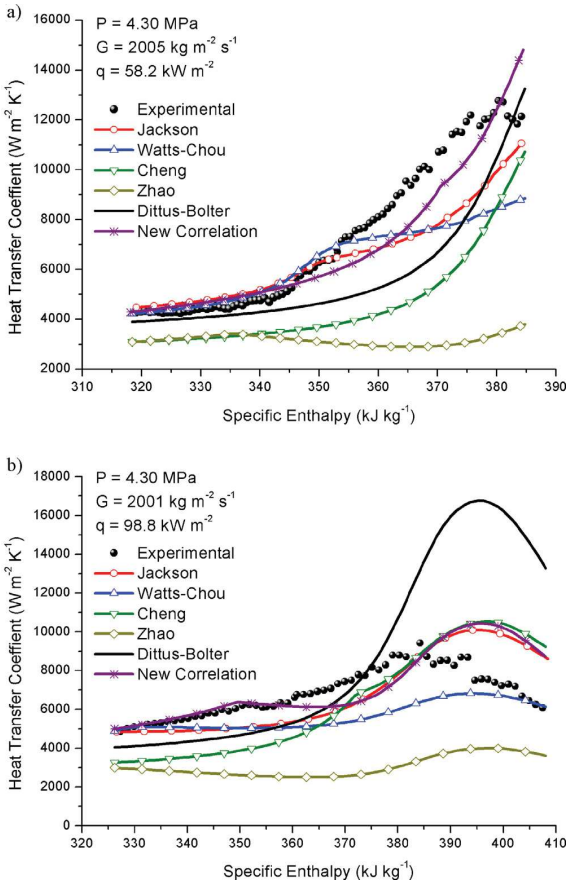


**Figure 2.13:** Comparison of heat transfer correlations with the experimental data of Zhang et al. [96] a) low heat flux, b) high heat flux.

When considering the measurements obtained at low heat flux, the heat transfer correlations of Jackson and Watts-Chou show good agreement with the experimental data of Zhang et al. [96] in the low enthalpy region. However,

there is a significant discrepancy as the enthalpy is approaching the pseudo-critical point. The heat transfer correlation of Zhang et al. [96] shows as well a good match with the experimental data far from the pseudocritical region and the difference between the measured and predicted heat transfer coefficient is significantly reduced near the critical region (Figure 2.13 a).

At high heat flux, the heat transfer correlation of Zhang et al. [96] also has the best agreement in the low specific enthalpy region. Figure 2.13 (b) shows that the prediction is nearly the same with Jackson's and Cheng's heat transfer correlations in the vicinity of pseudocritical value. These three heat transfer correlations over-predict the heat transfer coefficient with about 30%, but the one of Zhang [96] shows better prediction in the near critical region.

### 2.4.4 Approach to follow when developing a general heat transfer correlation

It can be concluded that the heat transfer correlations do not have universal application. All heat transfer correlations compared in the study [96] are unable to predict the heat transfer coefficients (HTCs) for the entire experimental range. The disagreement is most likely because the heat transfer correlations are applicable only for the working conditions that they were derived for.

Most of the heat transfer correlations fail to give accurate predictions of the HTCs for the entire operational regime (NHT, EHT, DHT). As can be seen from the elaborated example (Section 2.4.3) the HTCs show higher discrepancies in the vicinity of the pseudocritical region. While in the low enthalpy region (single phase - compressed fluid) show good match with the experimental data. Near the pseudocritical region the HTCs can be either under-predicted of over-predicted by even 30% [96] or even 50% [93]. Therefore, it is very important to define the width of the pseudocritical region. Additionally, it will be beneficial to analyse the three regions ($T < T_{pc}$; $T_{pc}$; $T_{pc} > T$) separately.

In order to account for the rapid variations of the thermophysical properties in the pseudocritical region, the ratios of the these properties should be included in the heat transfer correlations. Therefore, the general form of the heat transfer correlation (Section 2.4) given with Eq.(2.18) is expressed in the following form Eq. (2.51):

$$Nu = CRe^{m}\overline{Pr}^{n}\left(\frac{\rho_w}{\rho_b}\right)^{n_1}\left(\frac{\mu_w}{\mu_b}\right)^{n_2}\left(\frac{\kappa_w}{\kappa_b}\right)^{n_3}\left(\frac{c_{pw}}{c_{pb}}\right)^{n_4} \tag{2.51}$$

This heat transfer correlation is valid for forced convection to fluids at supercritical state. Furthermore, the ratios of the thermophysical properties can be calculated either at wall or film temperatures as function of the bulk temperature. The dimensionless numbers can be determined at either bulk, film or wall temperatures. However, it should be highlighted that there is no consensus in deciding which ratio is the best to be incorporated in the heat transfer correlations (Section 2.4). This is because all thermophysical properties are already included in the dimensionless numbers ($Nu = (HTC/D)\kappa$;

$Re = (\rho u D)/\mu$; $Pr = (c_p \mu)/\kappa$). Therefore, one possible solution for deriving general heat transfer correlation is to incorporate the entering effect and the dimensionless numbers to be calculated at film fluid temperatures which will consider the changes of the thermophysical fluid properties at wall and bulk temperatures ($T_f = (T_b + T_w)/2$).

Moreover, when developing a new general heat transfer correlation wider conditions and experimental data should be considered. Otherwise, the heat transfer correlations will show good agreement only with very limited data sets.

## 2.5 Conclusions

From the comprehensive literature review it can be concluded that most of the experimental work was done for supercritical water and $CO_2$. Hence, most of the heat transfer correlations that are developed are validated for these two fluids (Table 2.2). It has to be highlighted that the work done for supercritical water and $CO_2$ is very important and valuable. However, due to the peculiar fluid properties in the critical region, there is a need of additional investigation for other fluids as well. Moreover, there is very limited experimental data for supercritical heat transfer to refrigerants, potential fluid candidates for transcritical ORC's (Table 2.3). This is especially valid for supercritical heat transfer to refrigerants in heated horizontal tubes. Thus, adding experimental data for the refrigerant R125 is valuable.

In literature there is data for wide experimental ranges, in terms of tested heat fluxes, mass fluxes, pressures, tube diameters. It was concluded that the mass flux, the heat flux and the pressure are one of the most dominant parameters [100], [101], [110]. Moreover, the effect of buoyancy was not always encountered. Several researchers [40, 64] [77] [79] defined the boundary conditions for the onset of the buoyancy effect. However, in most of the studies it is not reported if the buoyancy effect or natural convection is encountered. Considering this effect, is especially important when deriving a heat transfer correlation.

In order to be able to study the effect that each parameter (mass flux, heat flux, pressure, buoyancy) has on the supercritical heat transfer a new test facility 'iSCORe' was built at Ghent University (Chapter 3). To avoid non-controlled wall temperature increase that might have an effect on the temperature measurements, the test section was constructed as a tube-in-tube heat exchanger. Strict steady-state criteria (Section 3.5) was followed during the measurement, due to the rapid changes of the thermophysical fluid properties with small temperature changes near the critical region.

As already mentioned (Section 2.2.2), the experimental range of interest in this study is the following: heat fluxes of 15-28 $kW/m^2$, mass fluxes of 400–650 $kg/m^2s$, and inner diameter of 24 $mm$ in pressure ranges of 38-42 $bar$.

For deriving new heat transfer correlation wider sets of experimental data should be considered. Otherwise, the heat transfer correlation will have limited

application and could be used for the conditions that was derived for. Therefore, three heat transfer correlations (Dittus-Boelter, Mokry et al. [61], Domin et al. [82]) (Section 2.2) were selected to be compared with the experimental data (Chapter 4). Both correlations, Mokry et al. [61] and Domin at al. [82] are of Dittus-Boelter type that have incorporated a correction factor. The correction factor is to account for the drastic thermophyscal changes at (near)critical region.

# 3. Experimental facility

Chapter 3 describes the experimental facility that was designed and built particularly for this thesis. The first three sections will describe in detail the test facility "iSCOre". Then in the next two sections the control strategy and the steady-state criteria will follow. In the last section the data reduction and the test methodology will be specified.

The new test facility 'iSCORe', was designed and constructed at Ghent University. The experimental facility is dedicated for investigating forced convection heat transfer to fluids at supercritical state. It consists of three different loops presented in Figure 3.1: a cooling, a heating and an experimental loop that are described in detail in the text below.

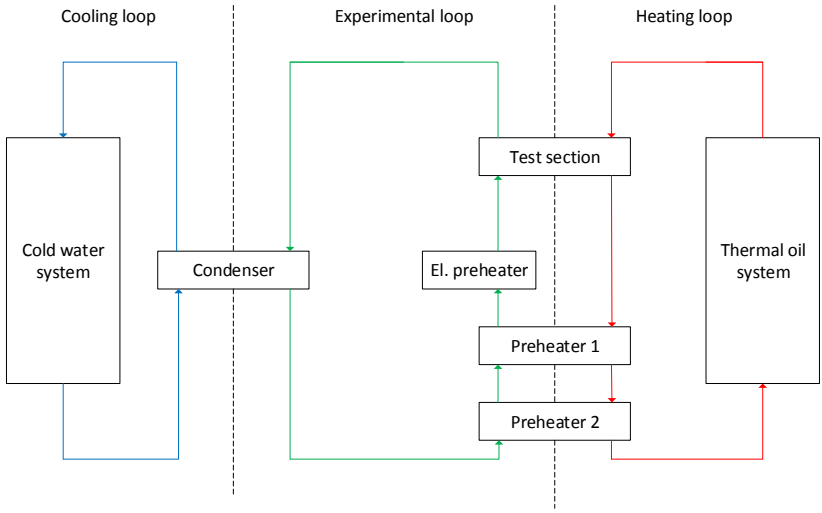


**Figure 3.1:** Simplified schematic diagram of the fluid loops in the experimental facility.

The 'iSCORe' test facility can be compared with a transcritical ORC, where instead of an expander an electronically controlled expansion valve is used. Furthermore, the maximum operational temperature of the heating fluid is

<200°C. On the other hand, the designed pressure limitation of the working fluid (in the high pressure side) is 60 $bar$.

Several fluids R125, R134a, R1234yf have been indicated as potential candidates for operation at supercritical pressures under ORC conditions [18], [21], [22], [32], [37], [122]. However, R125 was chosen as a target fluid in this work due to the low critical pressure and temperature of 36.18 $bar$ and 66.02°C, respectively [12], [19], [35–38]. The desired test pressures and temperatures are above the critical point of the working fluid with a mass flow rate in the range of 0.2-0.35 $kg/s$. Data acquisition systems, CompactRIO, type cRIO-9072/3/4 from National Instruments [123], Keithley, type 2700 from Tektronix [124] are used to monitor and gather all the measurement signals. With a specially coded LabView 11.0 programme, the measurement and control procedures are obtained at certain test conditions. In section 3.4, the control strategy and the experimental procedures are elaborated. In addition, in Appendix A and Appendix B, details about the measurement devices and their uncertainty analysis are included.

## 3.1 Cooling loop

In Figure 3.2, a schematic diagram of the cooling loop is presented. The cooling loop consists of a buffer vessel with capacity of 900 litre. A fixed-speed centrifugal pump (Grundfos, TPD) is used to pump a mixture of water/glycol (70/30% by volume) in the cooling loop. In order to maintain and control the desired temperature of the cooling fluid in the buffer vessel, a chiller (Daikin, EUWAP16KAZW1) with power of 37 $kW$ is included in the system. Reaching the set temperature of the cooling fluid is possible with an On-Off thermostat that is positioned on the vessel. A 3-way mixing valve (Danfoss, VRB 3) was installed in front of the condenser in order to control the water/glycol flow rate to the condenser. The condenser is a plate heat exchanger (Alfa Laval, CBXP) that cools down the working fluid to a temperature just below the entrance conditions of the circulation pump.

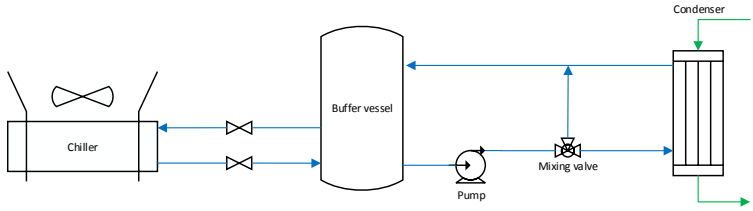


**Figure 3.2:** Schematic diagram of the cooling loop.

## 3.2 Heating loop

An electrical heater of 20 $kW$, (Vulcanic, Vulcatherm 10813) is used to heat the thermal oil by a current stabilized 3-phase power source. The thermal oil, (Therminol ADX10 [125]) is pumped by a built-in centrifugal pump to the test section where it provides a continuous heat flux (constant inlet temperature) over the heated test section. The oil is a low viscosity synthetic organic heat transfer fluid particularly recommended for indirect liquid phase process heating at medium temperature up to 250°C.

Figure 3.3 depicts a schematic overview of the heating loop.

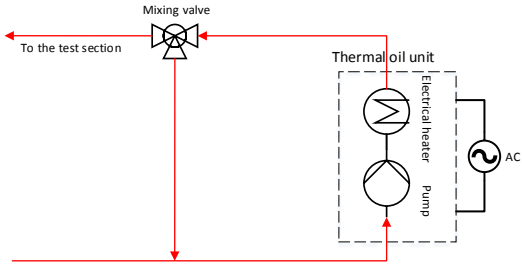


**Figure 3.3:** Schematic diagram of the heating loop.

An expansion vessel of 28 litre is installed in the unit to compensate for the thermal expansion of the heating fluid. The temperature of the thermal oil is PID controlled and is monitored at the control panel positioned on the unit itself. Two temperature sensors, type Pt100, are used during the temperature measurements at the inlet and the outlet of the test section. A 3-way mixing valve (Danfoss, VRB 3) is placed before the inlet of the test section in order to control the mass flow rate of the heating fluid. One Coriolis type mass flow meter (GE, RHM20) (360-8400 kg/h, ±0.2%) measures the mass flow rate of the heating fluid.

## 3.3 Experimental loop

Figure 3.4 presents a schematic overview of the experimental loop. The horizontally positioned test section for obtaining the heat transfer measurements to fluids at supercritical state is located in this loop.

A positive displacement (volumetric) pump (Hydra-Cell, G15) is used for circulating the working fluid (R125). The circulation pump provides almost pulse-less operation. Moreover, there is no mix between the working fluid and the oil of the pump, used for cooling purposes of the pump itself.

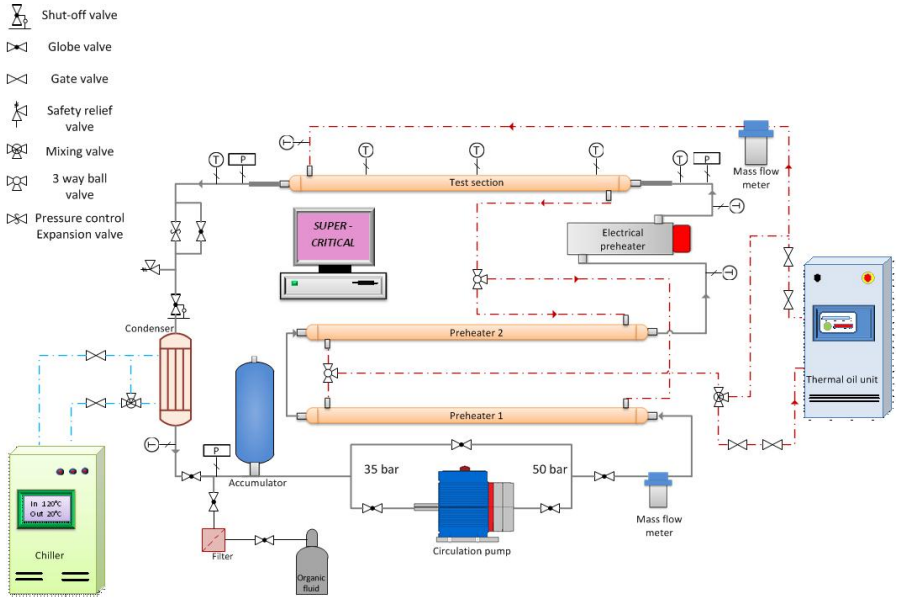


**Figure 3.4:** Schematic diagram of the experimental facility.

**Figure 3.5:** Experimental test facility.

The characteristic curve of the pump shows linear function of the volumetric flow rate and the rotational speed of the pump. For controlling the pump speed a variable frequency drive (VFD) is used. One Coriolis mass flow meter (GE, RHM12) (120-1800 kg/h, ±0.2%) is installed after the circulation pump, for measuring the actual mass flow rate. Furthermore, the experimental loop is divided into a high pressure and low pressure side, which is determined by the pump's inlet pressure of 35 *bar*. Therefore, after the test section, an electronically controlled expansion valve (Danfoss, ICMTS) reduces the pressure below 35 *bar*. Then the working fluid is subcooled in the condenser and brought up to the target inlet conditions of the circulation pump. A picture of the experimental test facility is depicted in Figure 3.5.

In the experimental loop, the pressurized working fluid is heated up to the desired inlet test conditions in two tube-in-tube preheaters and in an electrical preheater (Vulcanic, 10 *kW*). The test section and the two tube-in-tube preheaters have the same configuration. The working fluid circulates in the central tube and is heated by the thermal oil (heating fluid) that flows in the annulus. The complete installation is equipped with a number of pressure and temperature sensors. Two pressure transducers (GE, UNIK 5000) measure the pressure at the inlet and the outlet of the test section, while the pressure drop over the test section is determined by using a differential pressure sensor (GE, UNIK 5000). Three other pressure sensors are employed for monitoring and control purposes of the components at the high pressure and the low pressure side of the experimental loop.

In order to stabilize and control the system pressure and to compensate for the thermal expansion of the working fluid an accumulator is included in the installation as well. A filter is installed in front of the circulation pump to prevent particles to penetrate inside the pump and from damaging the installation. Additionally, there are many components (valves, bursting disc, sensors, side glass, etc.) installed, in order to secure safe operation of the test set-up. The complete installation was successfully pressure and leak tested with nitrogen at 40 *bar* but not higher due to the pressure limitation of the safety relief valve (Danfoss, SFA).

### 3.3.1 Test section

The test section is constructed as a tube-in-tube heat exchanger with a counter-current configuration. The annulus is galvanized tube with an outer and inner tube diameter of 88.72 *mm* and 80.26 *mm*, respectively. The inner tube is a copper alloy tube (CuFe2P) with an outer diameter of 28.58 *mm*, thickness of 1.9 *mm* and heating length of 4 *m* ($L/d_i$=162). Furthermore, the inner tube was cautiously centered by using three center bolts at four different locations along the test section. Table 3.1 presents the corresponding dimensions of the test section:

At the inlet of the test section the working fluid (R125) is brought up to supercritical pressure and heated up to supercritical temperature.

**Table 3.1:** Dimensions of the test section.

| *Dimensions* | *Unit* | *Value* |
|---|---|---|
| Copper tube outer diameter, $d_o$ | [mm] | 28.58 |
| Copper tube inner diameter, $d_i$ | [mm] | 24.78 |
| Copper tube thickness, $t$ | [mm] | 1.9 |
| Galvanized steel tube outer diameter, $D_o$ | [mm] | 88.72 |
| Galvanized steel tube inner diameter, $D_i$ | [mm] | 80.26 |
| Galvanized steel tube thickness, $t_s$ | [mm] | 4.44 |
| Length, $L$ | [m] | 4 |
| Total heat transfer surface area, $A_o$ | $[m^2]$ | 0.359 |
| Insulation outer diameter $D_{ins}$, | [mm] | 143 |

The test section is fitted with a number of thermocouples and pressure sensors. Figure 3.6 displays a layout of the test section.

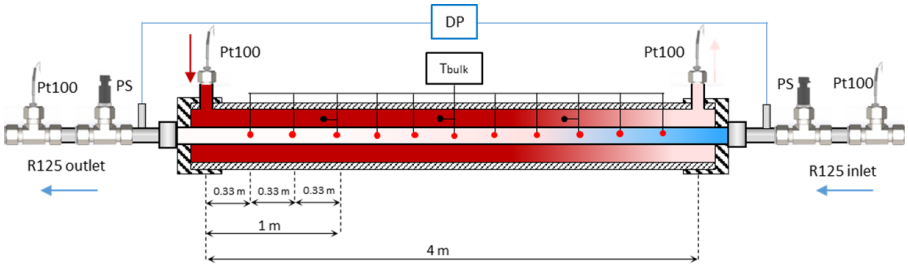


**Figure 3.6:** Schematic layout of the test section.

The bulk fluid temperature of the working fluid is measured by T-type thermocouples with a diameter of 1 $mm$. They are positioned along the test section on eleven equal distances of 0.33 $m$. Furthermore, three K-type thermocouples with a diameter of 1 $mm$ measure the bulk temperatures of the heating fluid and are positioned at even distances of 1 $m$. The bulk temperature at the inlet and at the outlet of the test section of both fluids is measured with temperature sensors, Pt100's. All the thermocouples were individually calibrated to 0.064°C against a precision Pt100-thermometer (Fluke 1523 with an absolute accuracy of 0.064°C).

Figure 3.7 shows the cross-section of the test section with the corresponding dimensions.

Additionally, an adiabatic section with a length of 1 $m$ is connected with the test section. The aim is to ensure fully-developed flow of the working fluid in the central tube at the inlet of the test section.

To reduce the heat losses to the environment the test section (and the tube-in-tube preheaters) is insulated by an insulation material (Isover, 1000 S alu) with a thickness of 55 $mm$ and thermal conductivity of 0.04 $W/mK$. While

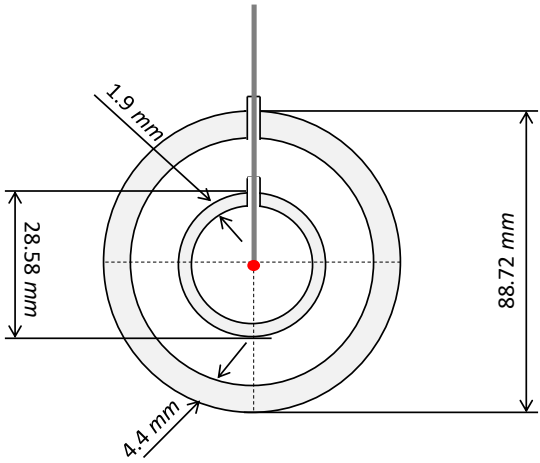


**Figure 3.7:** Cross-section of the inner tube with a thermocouple.

Kaiflex, (ZPDMPlus) is used as an insulation material for the rest of the tubing in the system with a thermal conductivity of 0.042 $W/mK$.

All the measurements were done by ensuring steady-state (thermal stability) of the test section where the measurements were within their uncertainties. Section 3.5 elaborates in detail the criteria for acquiring steady-state measurements.

### 3.3.2 Preheaters

In order to bring the working fluid up to the target inlet test conditions, two preheaters with a tube-in-tube configuration and one in-line electrical heater are included in the experimental loop.

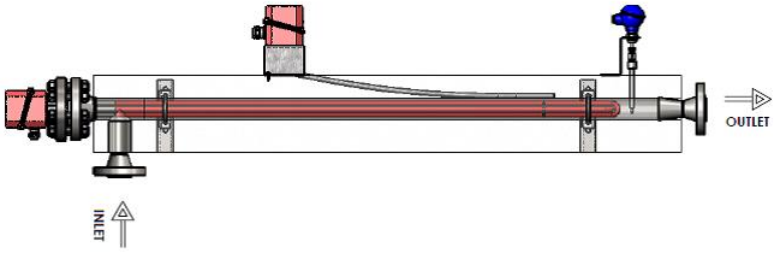


**Figure 3.8:** Schematic overview of the electrical preheater.

The tube-in-tube preheaters have a counter-current configuration and length of 4 $m$ each, same like the test section. The heating fluid circulating through the preheaters is used to preheat the working fluid. Each of the two preheaters can be by-passed individually, in step of 0-4-8 $m$. This is possible by using the mechanical three way valves.

The electrical in-line heater (Vulcanic, 10 $kW$), illustrated in Figure 3.8, controls accurately the set temperature of the working fluid at the inlet of the test section. The working fluid is directly heated by flowing through the electrical heating elements. The maximum power of the preheater is 10 $kW$ and is PID controlled. An integrated temperature sensor type Pt100 measures the temperature of the working fluid at the outlet of the electrical preheater. This sensor is used to control the electrical power going to the heating elements.

### 3.3.3 Challenges during design and construction of the test facility 'iSCORe'

In different research centers worldwide there are many test facilities that deal with supercritical heat transfer (including $CO_2$ as well) [26], [83], [86], [95, 96], [101], [104], [110]. Common for most of the test facilities is that the experimental loop consists of several stages. In practice, this means that some of the test rigs use either internal heat exchangers, compressors, decompression valves, multi stage pumps, etc. This is in order to bring the supercritical fluid (the vapour) to the desired condition at the inlet of the pump (after leaving the test section). However, even though at first sight it might look that the test facilities resemble each other, all of them have their unique design points.

The new test facility 'iSCORe' has several important differences with the existing test rigs. One major difference is the incorporation of an electronic expansion valve in the experimental loop. Including an expansion process in the design enabled depressurization of the working fluid up to the maximum required limitation at the inlet of the pump of 35 $bar$. This made the design 'simple' without having multiple stages.

Additionally, the new test facility is designed to be used for heating of the working fluid, where several other test rigs are built to study heat transfer in cooling processes [86], [101], [104].

A third difference is the layout of the test section, in terms of the flow direction and the tube diameter. Most of the test sections are positioned vertically with small tube diameters [95, 96], [101], [104], [110]. Furthermore, an electrically heated test section was not considered because it might lead to an uncontrolled wall temperature increase, that could have an effect on the temperature measurements. As already mentioned, the current test section is made as a tube-in-tube heat exchanger in order to represent real operating condition. In the current layout of the test section the effect that the horizontal flow and the large tube diameter have on the heat transfer at supercritical state can be determined.

Furthermore, very strict criteria were followed when considering the choice of the components. All components were selected according to the designed pressure and temperature limitations. An additional requirement was the accuracy and compatibility of each component with the working fluids.

One example is the use of T-type thermocouples for measuring the temperature of the working fluid along the test section. This decision was envisaged because the T-type thermocouples are more accurate than the K-type thermocouples (by 35%). This decision was justified by the fact that near the pseudocritical temperature, at very small temperature variation of the working fluid, the specific heat capacity has a drastic change. The aim was to obtain more accurate temperature and pressure measurements.

Another challenge was the positioning of the thermocouples in the test section. Each thermocouple is measuring the bulk fluid temperatures. The T-type thermocouples go through two fittings (annulus and inner tube) and are positioned in the center of the inner tube. Special care was paid for the correct positioning of the thermocuples in the center of the inner tube and at the same time to ensure that the test section is leak tight.

Additional work was dedicated in order to reach energy balance over the test section $\leq 5\%$ at subcritical testing conditions. It was detected that the mass flow meters were the reason for having larger discrepancies in the energy balance. Therefore, both mass flow meters were re-calibrated in-house by using proper software delivered by the manufacturer.

## 3.4 Control strategy and experimental procedure

There are several parameters (mass flow rate, temperature and pressure) that need to be controlled in order to assure safe operation of the test facility and for obtaining accurate (steady-state) measurements. For acquiring steady-state (Section 3.5), all components from the heating, the cooling and the experimental loop should be in operation. Additionally, a good pressure control is necessary to guarantee safe operation. Moreover, a reliable experimental procedure (elaborated in the text below in Section 3.5) was followed for validating the results from the measurements obtained at steady-state conditions.

### 3.4.1 Mass flow rate control

The circulation pump in the experimental loop, is a volumetric (positive displacement) pump that is controlled by setting the frequency of the pump's rotor. Once it is ensured that all the components and control devices of the experimental loop respond appropriately, the frequency of the pump and correspondingly the mass flow rate can be set. For each set of measurements, this was done by adjusting the frequency of the rotor's pump between 15-25 $Hz$, in a step of 5 $Hz$. This yields an actual mass flow rate of the working fluid in the range of 0.2–0.32 $kg/s$. An output card (module NI9207) from

CompactRio provides 0-10 V signal to the Variable Frequency Drive (VFD) of the pump. The setting of the new frequency was done in the main LabView programme. Reaching stable mass flow rate of the working fluid is strongly dependent on all other components that are in operation (thermal oil heater, chiller, in-line electrical preheater). A Coriolis mass flow meter was used to measure the mass flow rate $\dot{m}_{wf}$ of the working fluid.

Furthermore, the nominal mass flow rate of the heating fluid was 2.2 $kg/s$ (10 $m^3/h$ (T=20°C; p=2 $bar$)) and is determined by the specifications of the centrifugal pump that is built-in in the thermal oil heater. A 3-way valve combined with an electrical actuator controls the mass flow rate of the heating fluid at the inlet of the test section. The mass flow rate of the heating fluid is measured by a Coriolis mass flow meter and was kept stable at 2 $kg/s$.

However, attaining a stable flow of the working fluid was mostly influenced by the cooling fluid. The maximum mass flow rate of the cooling fluid was (6.3 $m^3/h$ (T=20°C; p=2 $bar$)) 2 $kg/s$ and was electronically controlled with a 3-way valve.

### 3.4.2 Temperature control

Three types of temperature sensors are used in the complete test facility: Pt100 resistive temperature sensors, K-type and T-type thermocouples. They have different accuracy, temperature range and responsive time scale. The temperature control is done by auto-tuned PID controllers integrated in the heaters. Moreover, one Pt100 temperature sensor is used for monitoring and controlling the temperature of the working fluid at the outlet of the condenser/ inlet of the circulation pump.

The electrical in-line preheater can be turned on after providing the minimum flow rate of the working fluid. The aim of this component is to heat-up the working fluid to the desired set temperature during the measurements. Additionally, it provides a stable temperature at the inlet of the test section. This unit has a self-adaptive (autotuned) PID controller that accurately controls the temperature of the fluid that corresponds to the set point value.

The heating fluid (thermal oil) is provided to the experimental loop by an electrical thermal oil heater. This unit has a management control system installed on the unit itself with an integrated PID temperature controller. The temperatures of the heating fluid for all set of measurements were in the range of 95–125°C. In general, reaching the set point temperature of the heating fluid was obtained in ∼15 minutes.

According to Gusev et al.[126] stabilizing the temperature in the condenser usually takes longer compared to the other components of an ORC installation. The temperature control of the cooling fluid at the inlet of the condenser was possible by adjusting the chillers' thermostat. The temperature of the cooling fluid was in the range of 15-20°C, ensuring that the inlet temperature of the working fluid in the pump was ∼40°C.

### 3.4.3 Pressure control

In the experimental loop there are in total six pressure sensors, used for measurements and control purposes. The pressure of the working fluid depends on the operational conditions and is determined by the pump's frequency, the position of the expansion valve and by the fluid's temperature in the system.

A valve system, consisting of an expansion valve, a safety relief valve and a shut-off valve precisely control the pump's inlet pressure below the operational limitation of 35 *bar*. These three components provide a clear distinction between the high pressure and the low pressure side of the experimental loop. The maximum operational pressure at the high pressure side is 55 *bar* and at the low pressure side this is 35 *bar*. Therefore, three pressure sensors are employed for monitoring and controlling the pressure of the working fluid. It has to be in the operational range of the components' limitation. The set value of the PID controller of the expansion valve is compared with the measured value of a pressure sensor placed right after it.

A pressure sensor positioned at the pump's outlet is connected to a process controller mounted on a control panel. In case that the pressure is above the threshold, the circulation pump is automatically shut down by the process controller. While the third pressure sensor is used to monitor the pressure after the condenser and before the inlet of the circulation pump.

During the measurements the supercritical pressure was in the range of 38-42 *bar* ((1.05-1.15)$p_{cr}$), this was obtained by controlling the expansion valve.

After establishing good operating conditions of all components in the three different loops, the next step was to perform measurements at steady-state. The thermocouples measuring the local temperature along the test section are connected to DAQ Keithley, that reads out the thermoelectric voltages. All other components and measuring equipment are connected to the CompactRIO (DAQ from NI) that together with a LabView programme, control and monitor the set-points and measured values.

## 3.5 Steady-state conditions

All measurements were obtained after reaching steady-state in the experimental facility. This means that the state variables (pressure, temperature, mass flow rate) which define the system are constant in time ($\frac{\partial N}{\partial t} = 0$). However, when doing an experimental investigation there is also an uncertainty on the repeated measurements. Therefore, it is important to isolate the effect of measurement uncertainty and transient (or non steady-state) operation.

In order to perform reliable heat transfer measurements and to develop a heat transfer correlation which is applicable to supercritical pressures it is important to define and obtain steady-state data. However, there is lack of predefined criteria for acquiring steady-state for heat transfer measurements at supercritical state. In most of the articles linked to supercritical heat

transfer, it is highlighted that the measurements were performed at steady-state conditions, without identifying the variation of the state parameters and the duration of each measurement.

In the text below, some of the articles that provide detailed information for determining steady-state (for supercritical heat transfer) is elaborated. Jiang et. al. [85] [127] assumed that the system was at steady-state when the variation of the temperatures (wall, inlet and outlet) were within ±0.1°C and the inlet pressure and the mass flow rate variations were 0.2% for at least 10 minutes. In the experimental study of Kang and Chang [39] measurements at supercritical pressures were recorded for 300s after reaching steady-state. Furthermore, their work was related to heat transfer during pressure transients and the data was averaged for 200 measurements. Oh and Son [86] collected the data at steady-state for 2 minutes in each run when doing experiments in order to predict the heat transfer coefficient by using supercritical $CO_2$ in a in-tube cooling. However, the criteria for steady-state identification was not clearly indicated. Forooghi and Hooman [108] accepted in their work that steady-state was reached when there were no time-dependency in the measured quantities, except for random fluctuations. The experimental investigation was done in a plate heat exchangers when the working pressure varied ±0.1 $MPa$. In order to reduce the uncertainty, 100 measurement points were collected in the steady-state data set. In the study of Zhao et al. [101] supercritical R134a was tested in-tube cooling and steady-state was determined when the inlet pressure variation was within ±0.9%. Wen et.al. [128] determined steady-state when the temperatures varied within a band of ±0.2°C and the mass flow rate and the system pressure were in the range of ±0.4%. In the experimental investigation of R134a a steady-state was considered when the fluctuation of the temperatures was ±0.5°C, the mass flux of ±2% and the pressure of 0.05 $MPa$ [43]. The book of Pioro and Duffey [23] elaborate a detailed overview of the variations of different parameters at steady-state conditions. One example is the experimental data recorded over 1 minute in 5 seconds intervals and the pressure fluctuation was ±0.2%, the temperatures and mass flux variations were within ±1%.

Table 3.2 gives an overview of the steady-state parameters of some of the data available in literature obtained at supercritical pressures that is relatively complete.

**Table 3.2:** Steady-state parameters defined in literature.

| *Reference* | *Temperature* | *Pressure* | *Flowrate* | *Time* |
|---|---|---|---|---|
| [23] | ± 1% | ± 0.2% | ± 1% | 1 min |
| [85] [127] | ± 0.1°C | ± 0.2% | ± 0.2% | 10 min |
| [43] | ± 0.5°C | ± 0.05 $MPa$ | ± 2% | |
| [128] | ± 0.2°C | ± 0.4% | ± 0.4% | |

Furthermore, Corlett [129] defined a steady-state conditions when the wall temperature variation was ±0.3°F or the pressure drop across the test section of

±0.2%. The experiments were done for heat transfer characteristics of liquid-liquid dispersion flowing in the annulus. Additionally, Woodland et. al. [130] proposed a standard for ORC steady-state measurement detection. A steady-state detecting model of a residential air conditioner was done by Kim et.al. [131]. Moreover, a new algorithm for identifying steady-state conditions in a 11 $kWe$ ORC installation was proposed by Lecompte et al. [132].

It can be concluded from the text above, that there is no systematic defined way on acquiring steady-state conditions for supercritical heat transfer measurements. Furthermore, there is a significant difference when comparing the defined criteria in the work of different authors.

Accurate steady-state prediction is however important because of the rapid changes of the thermophysical properties in the near-critical region with small temperature and pressure variations. This is uniquely relevant near the pseudo-critical temperature and the critical pressure of the fluid of interest ($\leq 1.05p_{cr}$). A relevant example that can be reported is the variation of the specific heat capacity of R125 at temperatures of 68°C (24.2 $kJ/(kgK)$) and 69°C (10.4 $kJ/(kgK)$) at the critical pressure of 37.98 $bar$ ($1.05p_{cr}$). The percentage difference of the specific heat capacity with a temperature change of only 1°C can reach up to 80%.

Therefore, there is a need for predefined (strict) steady-state criteria to be followed. This is important in order to obtain reliable heat transfer measurements at supercritical state.

### 3.5.1 Acquiring steady-state in 'iSCORe'

In the test facility 'iSCORe', steady-state conditions were achieved after 2 hours of the initial start of all components. Furthermore, there were usually 20-30 minutes needed to reach a new steady-state between different set of measurements.

**Table 3.3:** Defined steady-state criteria for the test facility 'iSCORe'

| *Parameter* | *Variation*[1] | *Range*[2] | *Deviation*[3] '$\sigma$' | *Threshold*[4] '$2\sigma$' |
|---|---|---|---|---|
| $T_{hf,in}$ | 0.5°C | $\leq 0.4$ % | 0.1°C | 0.2°C |
| $T_{wf,in}$ | 0.5°C | $\leq 0.8$ % | 0.11°C | 0.2°C |
| $p_{wf,in}$ | 0.5 $bar$ | $\leq 0.5$ % | 0.05 $bar$ | 0.1 $bar$ |
| $\dot{m}_{hf}$ | $< 2\%$ | $\leq 1.5$ % | 0.0025 $kg/s$ | 0.005 $kg/s$ |
| $\dot{m}_{wf}$ | $< 2\%$ | $\leq 1.5$ % | 0.001 $kg/s$ | 0.02 $kg/s$ |

[1]Variation: limit defined in literature
[2] Range: percentage difference between the measured maximum and minimum value
[3] Deviation: '$\sigma$' standard deviation about the mean value
[4] Threshold: calculated '$2\sigma$' standard deviation

In Table 3.3, the criteria for reaching steady-state conditions in the experimental facility 'iSCORe' is enlisted, representing the highest deviation

calculated from the measurements. The observed and calculated data are tabulated in the Appendix B.

The inlet temperature and the mass flow rate of the heating fluid presented in Figure 3.9 are an indicator for steady-state condition at the hot side.

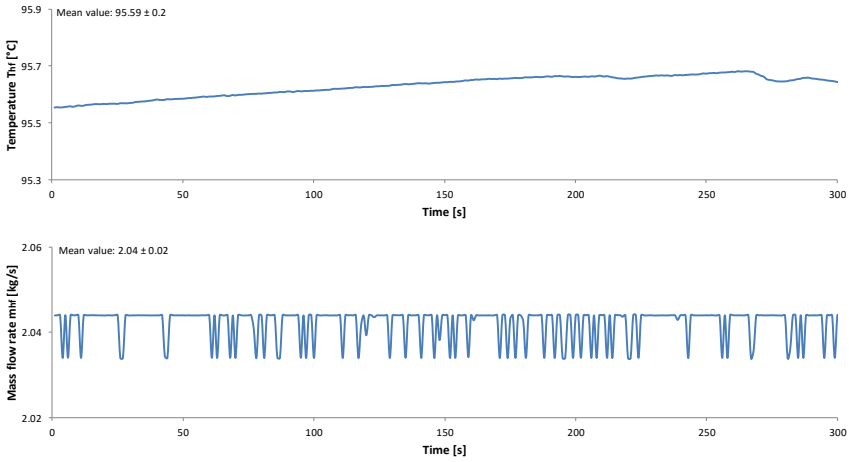


**Figure 3.9:** Parameters of the heating fluid at steady-state conditions, inlet temperature $T_{hf,in}$, mass flow rate $\dot{m}_{hf}$.

While the inlet pressure, temperature and mass flow rate of the working fluid are parameters used for detecting steady-state conditions of the working fluid. Figure 3.10 presents the variation of these parameters over time.

A time window of 300 measurements (5 minutes) was averaged and compared with the predefined criteria illustrated in Table 3.3. Additionally, a steady-state threshold for the selected parameters was defined to be within two times standard deviation '$\pm 2\sigma$' of the averaged value from the measurements. The particular approach considers more than 95% of the values assuming normal (Gaussian) distribution. This means that all the values fall within '$\pm 2\sigma$' of the average value. The decision to use two standard deviation, $\pm 2\sigma$, instead of one standard deviation, '$\pm\sigma$', is to avoid a too strict definition of steady-state. The measurements were done in a controlled laboratory environment within a temperature range of 20-25°C.

After obtaining steady-state conditions, the measurements were registered, and all data from the sensors connected to the DAQ CompactRIO and Keithley was saved on the computer. The duration of one set of measurement was over 300 seconds. It was recorded in 1 second interval.

Each sensor has its own shift register in which all measured values are stored. At the same time Keithley was recording the data from the 11 T-type thermocouples evenly positioned on a distance of 0.33 $m$, measuring the bulk temperatures of the working fluid and 3 K-type thermocouples, measuring the

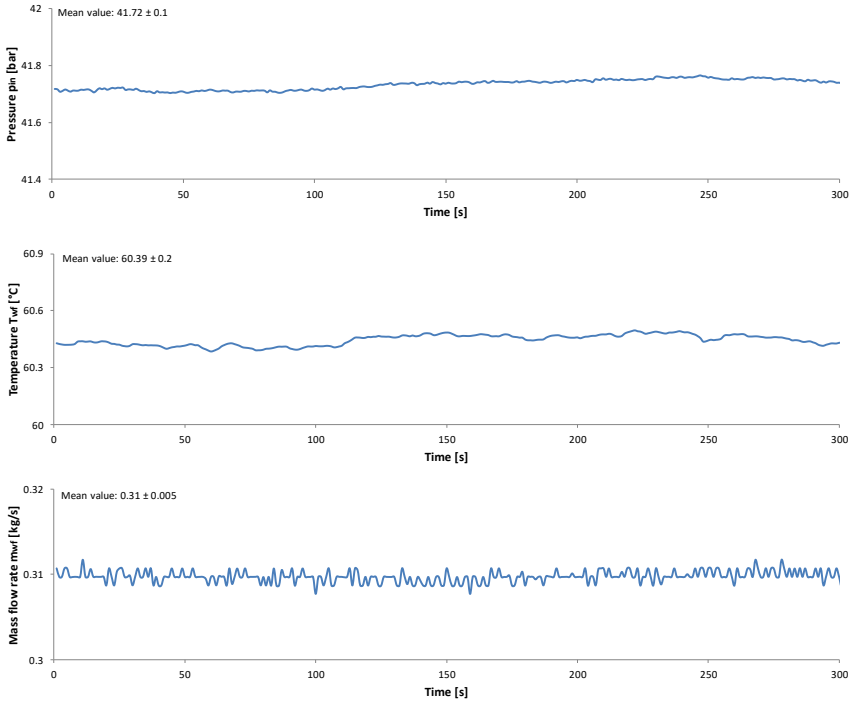


**Figure 3.10:** Parameters of the working fluid in steady-state conditions, inlet pressure $p_{wf,in}$, inlet temperature $T_{wf,in}$, mass flow rate $\dot{m}_{wf}$.

bulk temperature of the heating fluid, placed at a distance of 1 $m$. During the measurements, the PID controllers try to maintain the steady-state operation, which is continuously checked by the program. The program also keeps checking if any of the component operating limits is exceeded. The measurement is aborted if single measured value differs more than 1% from its set point.

### 3.5.2 Validation of the experimental facility 'iSCORe'

Validation of the experimental facility was done by obtaining different sets of measurements and by repeating the same set of measurements on a different day. The repeated tests show good agreement with the initial measurements and are within the uncertainty margins. In Appendix B an overview of the measurement data is included.

The inlet test conditions are determined by directly measuring the mass flow rate, the temperature and the pressure of the heating and the working fluid, respectively. At first, the validation of the test facility 'iSCORe' was done by checking the energy balance over the test section by acquiring measurements at single-phase (liquid-liquid) flow. The inlet temperature of the heating fluid was 60°C, while the inlet temperature and the inlet pressure of the working fluid

were 40°C and 25 *bar*, respectively. During the measurements the mass flow rates were varied at both sides. Hence, the heat transfer over the test section was compared.

Figure 3.11 presents the energy balance over the test section for measurements at single-phase (liquid-liquid) flow of the heating and the working fluids. Overall, the heat balance closes within 5% (determined with Eq.(3.3)). However, the energy balance is on average within 2.9%. Furthermore, the error margins of the working fluid fall within the uncertainty of the heating fluid.

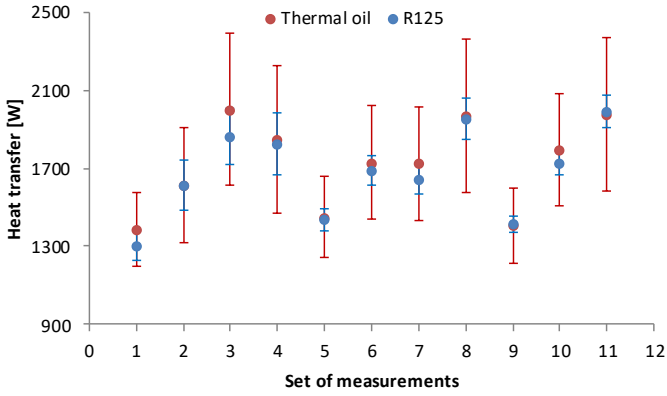


**Figure 3.11:** Energy balance over the test section for a single-phase (liquid-liquid) flow.

Additionally, the measured heat transfer coefficients are compared with the calculated HTCs by the Dittus-Bolter heat transfer correlation Eq. (2.19). The measurements agree well with the calculated results and the relative errors are within ± 6%, presented in Figure 3.12.

Conservation of energy over the test section was checked with liquid- supercritical flow (Thermal oil-R125) as well. Due to the strong variations of the thermophysical properties of R125 at supercritical state the energy balance was closing on average within 10%. This is illustrated on Figure 3.13.

When the inlet or the outlet temperatures of the working fluid (depending on the measurement conditions) are near (≤1%) the (pseudo)critical temperature $T_{pc}$ (determined for R125 with Eq.(4.1)), then the variance of the energy balance can reach deviations of up to even 20%. This conclusion is especially prominent to pressures closer to the critical pressure of the working fluid. The reason is (probably) associated to the strong variations of the thermophysical properties at the near-critical region (Figure 1.9 and Figure 4.1). Therefore, evaluating the energy balance near the critical point of R125 was avoided.

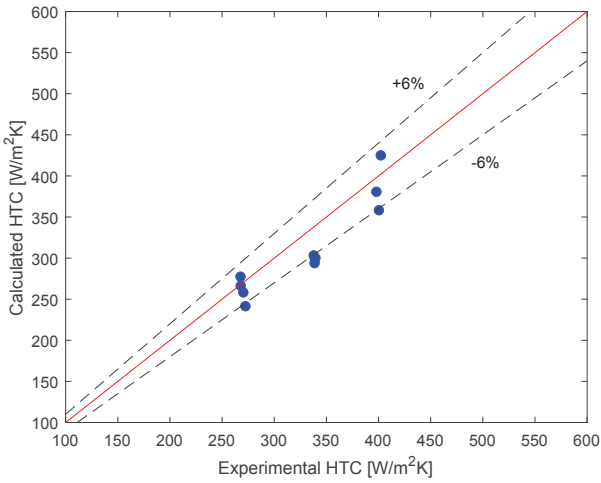


**Figure 3.12:** Energy balance over the test section for a single-phase (liquid-liquid) flow.

## 3.6 Data reduction

The LMTD (log mean temperature difference) method was used to determine the (local) convection heat transfer of the working fluid from the data sets.

### 3.6.1 Energy balance

Energy balance over the test section is obtained when the heat transfer to the working fluid (R125) $\dot{Q}_{wf}$ Eq.(3.1) flowing in the central tube is equal to the heat transfer of the heating fluid (Therminol ADX10) $\dot{Q}_{hf}$ Eq.(3.2), circulating in the annulus.

The heat transfer rate at the working fluid side was determined with the enthalpy changes at the inlet and the outlet of the test section.

$$\dot{Q}_{wf} = \dot{m}_{wf}(h_{wf,out} - h_{wf,in}) \tag{3.1}$$

On the other hand, the heat transfer rate of the heating fluid was calculated considering the temperature differences at the inlet and the outlet of the test section, Eq.(3.2).

$$\dot{Q}_{hf} = \dot{m}_{hf}c_{p,hf}(T_{hf,in} - T_{hf,out}) \tag{3.2}$$

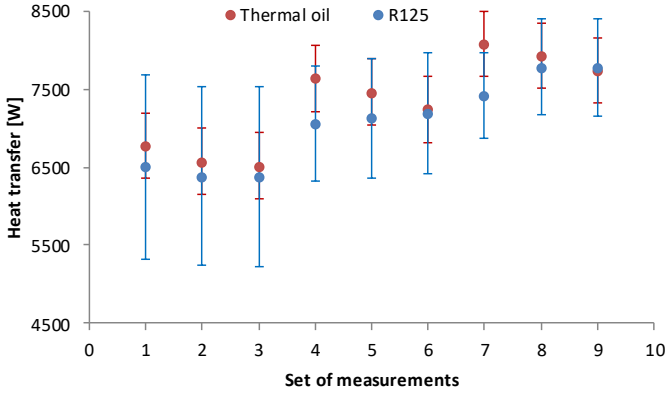


**Figure 3.13:** Energy balance over the test section for measurements at supercritical state.

Hence, the energy balance was determined by using the percentage difference between the $\dot{Q}_{hf}$ and the $\dot{Q}_{wf}$, illustrated with Eq.(3.3).

$$EB(\%) = \frac{\dot{Q}_{hf} - \dot{Q}_{wf}}{\frac{\dot{Q}_{hf} + \dot{Q}_{wf}}{2}} \cdot 100 \tag{3.3}$$

For the single-phase measurements the difference of the energy balance was lower than 5% and on average 3.8%. However, the energy balance showed larger discrepancies for the measurements at supercritical state. Particularly, the deviation was significant when the outlet temperature of the working fluid $T_{wf,out}$ was close to the pseudocritical temperature $T_{pc}$.

Furthermore, the heat losses to the environment are less than $\leq$3% and were neglected in the calculations.

### 3.6.2 Determining the heat transfer coefficient at the heating fluid side

In order to determine the convection heat transfer coefficient of the heating fluid, the heat transfer (Nusselt) correlation of Dirker and Meyer [133], derived for annular flow was used Eq.(3.4). The selected heat transfer correlation is appropriate for determining the Reynolds numbers $Re$ and the annular diameter ratio '$a$' for the particular test section because both properties are within the proposed ranges (4,000 $< Re <$ 30,000; 1.7 $<$ '$a$' $<$ 3.2).

$$Nu = \frac{HTC_{hf} D_h}{k_{hf}} = C Re_{D_h}^{P} Pr^{1/3} \left( \frac{\mu_{hf}}{\mu_{hf,w}} \right)^{0.14} \tag{3.4}$$

where $C$ and $P$ are constants that account for the geometry effect and depend on the annular diameter ratio '$a$' ($D_i/d_o$). They can be determined with Eq.(3.5) and Eq.(3.6).

$$P = 1.013e^{-0.067a} \tag{3.5}$$

$$C = \frac{0.003a^{1.86}}{0.063a^3 - 0.674a^2 + 2.225a - 1.157} \tag{3.6}$$

The Nusselt numbers were calculated by using the hydraulic diameter ($D_h = D_i - d_o$). The heat transfer correlation predicts the Nusselt numbers within an uncertainty of 3%.

For determining the thermophysical properties (specific heat capacity $c_{p,hf}$, thermal conductivity $k_{hf}$, density $\rho_{hf}$ and kinematic viscosity $\nu_{hf}$) of the heating fluid at particular (bulk) temperatures (Eq.(3.10)), equations from the manufacturer were used [125], included in Appendix A. The dynamic viscosity $\mu$ was obtained from the product of the kinematic viscosity and the density ($\mu_{hf} = \nu_{hf}\rho_{hf}$). Moreover, the dynamic viscosity $\mu_w$ was determined by considering the temperature of the inner annular wall. Furthermore, the dimensionless Reynolds number and the Prandtl number were calculated by using Eq.(3.7) and Eq.(3.8).

$$Re = \frac{4\dot{m}_{hf}}{\mu_{hf}\pi(D_i + d_o)} \tag{3.7}$$

where $A_{o,c}$ is the cross sectional area determined with $A_{o,c} = \pi(D_i^2 - d_o^2)/4$.

$$Pr = \frac{\mu_{hf}c_{p,hf}}{k_{hf}} \tag{3.8}$$

Equation (3.9) was used to determine the overall heat flux from the measurements.

$$q = \frac{\dot{Q}_{hf}}{A_o} \tag{3.9}$$

where $A_o$ is the total heat transfer surface area determined with $A_o = \pi d_o L$.

For determining the bulk fluid temperatures at certain location (heating fluid and working fluid) Eq.(3.10) is used.

$$T_{b,(n)} = \frac{T_n + T_{n+1}}{2} \tag{3.10}$$

### 3.6.3 Determining the local heat transfer coefficient of the working fluid and the local heat flux

Equation (3.11) is used for calculating the local heat transfer coefficient of the working fluid at the inside of the tube.

$$HTC_{wf,loc,(n)} = \frac{q_{loc,(n)}}{T_{wf,w,i,(n)} - T_{wf,b,(n)}} \tag{3.11}$$

Furthermore, the local heat flux can be determined with Eq.(3.12).

$$q_{loc,(n)} = \frac{\dot{m}_{hf} c_p \Delta T_{(n)}}{\pi d_o L_{(n)}} \tag{3.12}$$

The outer wall temperature of the central tube at each location was determined with the thermal resistances at the heating fluid side Eq.(3.13).

$$T_{wf,w,o,(n)} = T_{hf,b,(n)} - \dot{Q}_{(n)} R_{o,(n)} \tag{3.13}$$

where $R_{o,(n)} = 1/HTC_{hf,(n)} A_o$ is the thermal resistance.

Hence, the local inner wall temperature of the central tube was estimated with Eq.(3.14)

$$T_{wf,w,i,(n)} = T_{wf,w,o,(n)} + \frac{q_{loc,(n)} d_i ln(d_o/d_i)}{2\kappa} \tag{3.14}$$

The test section was discretised into 4 control volumes so that the properties variation in each step is small and an average constant value, different for each step, can be assigned within each volume.

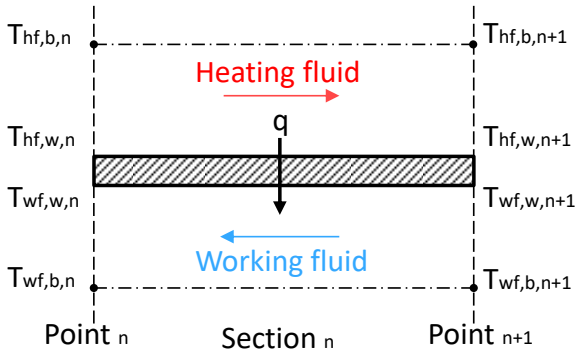


**Figure 3.14:** Control volume depicting the inlet/outlet temperatures of the heating and the working fluids.

The number of control volumes was determined by the actual temperature sensors measuring the bulk temperature of the heating fluid. A single control volume with the main variables and parameters is presented on Figure 3.13.

where $q_n$ is the heat flux in one control volume, $T$ are the temperatures of the fluids and the subscripts $wf$ is working fluid, $hf$ is heating fluid, $b$ is bulk conditions, $w$ is wall conditions and $n$ is the iteration step.

### 3.6.4 Overall heat transfer coefficient and heat transfer correlation

A *logarithmic mean temperature difference* $LMTD$ method Eq.(3.15) was used to calculate the overall convection heat transfer coefficient at the working fluid side.

$$LMTD = \frac{(T_{hf,in} - T_{wf,out}) - (T_{hf,out} - T_{wf,in})}{ln\frac{T_{hf,in} - T_{wf,out}}{T_{hf,out} - T_{wf,in}}} \tag{3.15}$$

The overall heat transfer coefficient was determined with Eq.(3.16)

$$U = \frac{\dot{Q}_{wf}}{A_o LMTD} \tag{3.16}$$

Furthermore, the overall thermal resistance $R_{ov}$ is expressed with Eq.(3.17). It represents a sum of the thermal resistances corresponding to outer convection resistance $R_o$, the tube wall resistance $R_w$ and the internal convection resistance $R_i$, while the inner $R_{f,i}$ and outer $R_{f,o}$ fouling resistances are neglected (due to the new installation).

$$R_{ov} = R_o + R_w + R_i \tag{3.17}$$

The thermal resistances substituted with the convection heat transfer coefficients are expressed with Eq.(3.18)

$$\frac{1}{HTC_{wf} A_i} = \frac{1}{U A_o} - \frac{1}{HTC_{hf} A_o} - \frac{ln\left(\frac{d_o}{d_i}\right)}{2\pi L k_{cu}} \tag{3.18}$$

where $A_i$ is the total heat transfer surface area of the central tube calculated with $A_i = \pi d_i L$, considering the inner diameter $d_i$. Hence, the heat transfer coefficient of the working fluid can be determined.

The local Nusselt number of the working fluid can be expressed with Eq.(3.19)

$$Nu = \frac{HTC_{wf} d_i}{k_{wf}} \tag{3.19}$$

### 3.6.5 Determining the pseudocritical temperature

Figure 3.14 illustrates the variation of the pseudocritical temperatures and the maximum values of the specific heat at different inlet pressures (1.0-1.25)$p_{cr}$ of R125. Both, the specific heat capacity and the pseudocritical temperatures are determined based on data retrieved from CoolProp 6.3.0 [134]. In the experimental results, the pseudocritical temperature $T_{pc}$ was determined with the third order polynomial fitting Eq.(3.20)

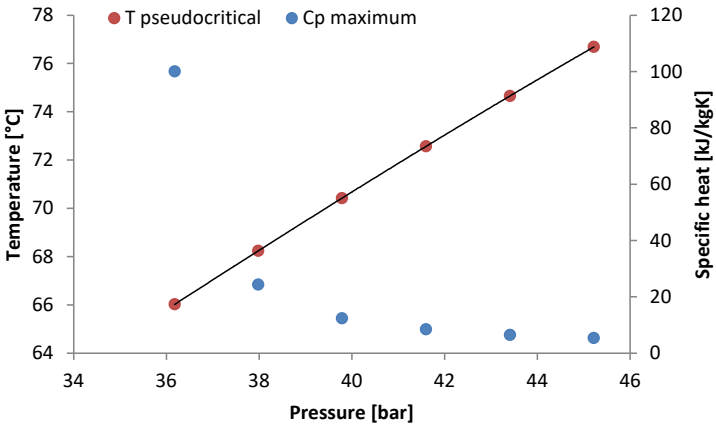


**Figure 3.15:** Pseudocritical temperatures at different inlet pressures with corresponding maximum values of specific heat capacity.

$$T_{pc} = 58.79 - 1.84p + 0.084p^2 - 0.0008p^3 \tag{3.20}$$

where the pseudocritical temperature $T_{pc}$ is in '°C' and the pressure in *bar*.

# 4. Experimental results and discussion

This chapter is dedicated for discussing the results from different sets of measurements that were performed at various conditions. The important characteristics and thermophyscial property variations of R125 at supercritical pressure ($1.02p_{cr}$) is presented in Figure 4.1. The rapid changes of the density, the viscosity and the thermal conductivity occur at the location where the specific heat reaches its maximum value ($T_{pc}$ Eq. (3.20)). These variations have significant effect on the heat transfer at supercritical pressures. The changes of the thermophysical properties at various pressures was elaborated in Chapter 2.

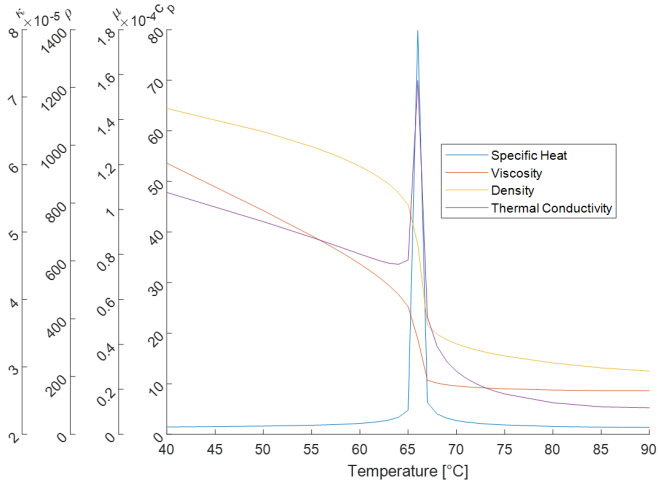


**Figure 4.1:** Variation of the thermophysical properties of R125 at pressure of $1.02p_{cr}$.

The main target of this study was to experimentally determine the heat transfer characteristics at supercritical pressures of R125 circulating in a horizontal flow and in a large tube diameter ($d_o = 28.58mm$). The main motivation to consider the horizontal flow direction and the large tube diameters is because

these are one of the parameters that have a significant effect on the supercritical heat transfer and there is very limited data in literature for these conditions (Chapter 2).

A brief overview of the measurement inlet conditions is given in Table 4.1. The critical pressure for all set of measurements was in the range of 38-42 *bar* (1.05-1.15)$p_{cr}$. The mass flux of the working fluid was between 400-600 $kg/m^2s$ and the inlet temperature of 60°C. The working fluid temperature at the outlet of the test section was in the vicinity of the critical temperature of R125. The heating fluid temperature was in the range of 95-125°C that gave a relatively low heat fluxes (14 - 28 $kW/m^2$).

**Table 4.1:** A brief overview of the measurement inlet conditions

| *Parameter* | *Unit* | *Heatingfluid* | *Workingfluid* |
|---|---|---|---|
| $T_{inlet}$ | °C | 95-125 | 60 |
| $p_{inlet}$ | *bar* | 2 | 38-42 |
| $\dot{m}_{inlet}$ | $kg/s$ | 2 | 0.2-0.3 |

Moreover, in Appendix B, in Table B.1 a detailed overview of the experimental data at inlet conditions of the heating and the working fluid is given. Furthermore, Figure B.1 depicts a good reproducibility of the measurements done in the test facility 'iSCORe' on three different days.

## 4.1 Heat transfer at supercritical pressures

Evaluating the dominance of enhanced heat transfer or deteriorated heat transfer in certain operating conditions is important. Therefore, the effects of various control variables were elaborated and the results were compared in this section. The presence of these heat transfer regimes is based on the following temperature conditions ($T_b < T_{pc} < T_w$). In this work, the local wall temperatures were calculated based on the local bulk temperature measurements. This is elaborated more in detail in Section 3.3.1 (Test section) and Section 3.6 (Data reduction).

Additionally, the buoyancy effect is one of the reasons for DHT in horizontal flow and large tube diameter. This could be concluded from the literature review (Chapter 2). Therefore, the significance of the buoyancy effect on the heat transfer was verified with a criterion from literature [81]. Furthermore, the experimental Nusselt number determined for R125 was compared with heat transfer correlations from literature.

The heating process of the working fluid R125, from compressed fluid (liquid) to supercritical fluid (vapour) after crossing the (pseudo)critical point is presented on the T-s diagram, Figure 4.2. The plotted data is from the measurements done at a pressure of 38 *bar* (1.05$p_{cr}$) and inlet temperature of 60°C. The red dotted line is actually represented by the 11 measuring points,

thermocouples located along the test section. With the blue dashed line is represented the pseudocritical line determined for the pressure range of 36.02-46 *bar*. The changes occuring on the thermophysical properties of the fluid near the (pseudo)critical point and their impact on the supercritical heat transfer is very significant and is presented in Figure 4.3.

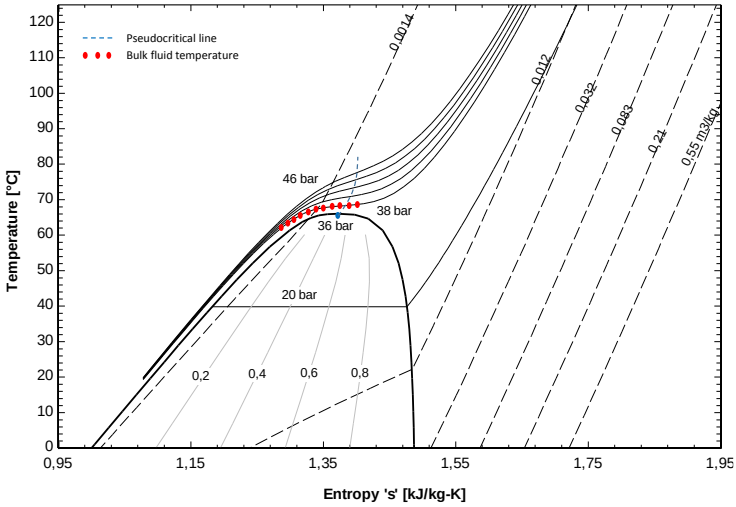


**Figure 4.2:** Heating process of R125 at a pressure of 38 *bar* presented on a T-s diagram.

### 4.1.1 Enhanced and deteriorated heat transfer

Usually, near the critical region there is enhanced heat transfer because of the substantial property changes of the fluid, where the specific heat has the most dominant effect. In this region the working fluid R125 is heated from liquid-like to vapour-like state that is followed by drastic changes of the thermophysical properties Figure 4.1 and Figure 4.2.

In Figure 4.3, the wall and bulk fluid temperature changes along the test section as function of the bulk enthalpy are presented. For these operating conditions ($1.05p_{cr}$, 413 $kg/(m^2s)$, 14 $kW/m^2$) the critical region starts where the enthalpy is 302.4 $kJ/kg$. As can be seen from Figure 4.3, after the critical temperature the HTC's have risen significantly. When approaching the pseudocritical temperature (at $1.05p_{cr}$ $T_{pc} = 68°C$), the temperature difference between the wall and the bulk fluid is the lowest, and the specific heat capacity and the thermal conductivity have their peak in that region. Thus, the heat

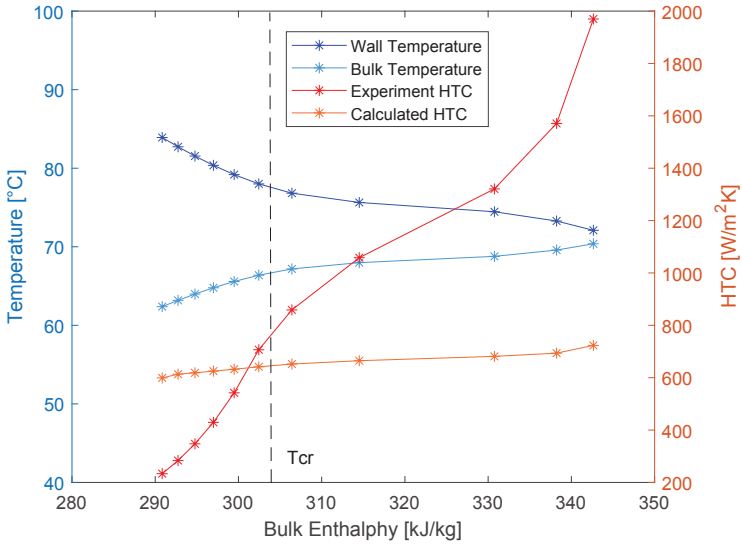


**Figure 4.3:** Wall and bulk fluid temperature profiles and enhanced heat transfer coefficients at near critical region at $1.05p_{cr}$, mass flux of 413 $kg/(m^2s)$ and heat flux of 14 $kW/m^2$.

transfer coefficients in this region are higher. Furthermore, the experimental HTCs are compared to the calculated HTCs determined by using Eq. (3.20). From the results it can be seen that in the region before the critical temperature (290-300 $kJ/kg$) the deteriorated heat transfer regime DHT is present because the following condition is fulfilled $T_b < T_{pc} < T_W$. In this region the HTCs are lower than the ones determined with Dittus-Bolter. After leaving the critical temperature and approaching the pseudocritical temperature the HTCs are higher than the ones determined with Dittus-Boelter. Hence, there is EHT. In a vey small region the experimental HTCs and calculated HTCs have same (similar) values which means in that region there is NHT regime.

Furthermore, there are criteria in literature that were used in order to quantitatively express when one of the two (EHT or DHT) heat transfer mechanisms is present. The following ratio $\dot{q}/\dot{G}$ is one of the used criterion. When the ratio $\dot{q}/\dot{G}$ is low, then the bulk fluid temperature $T_b$ is closer to the pseudocritical temperature $T_{pc}$ and the wall temperature $T_w$ is slightly higher than the $T_{pc}$. At these operating conditions the heat transfer coefficients HTCs are higher which leads to EHT. Additionally, at these conditions the temperature difference between the top and bottom surface is relatively small. At higher ratio $\dot{q}/\dot{G}$ the bulk fluid temperatures $T_b$ are lower than the pseudocritical temperature $T_{pc}$ and the wall temperatures $T_w$ are higher than the pseudocritical temperature $T_{pc}$. Furthermore, at these operating conditions the temperature difference between the top and bottom surfaces is higher, due to the changes of the

thermophysical properties. According to the results from the experimental investigation the ratio $\dot{q}/\dot{G}$ is in the range of 0.022 - 0.058 $kJ/kg$.

## 4.2 Effects of mass flux

The effect of mass flux is presented in Figure 4.4 shows. The variations of the heat transfer coefficients at mass fluxes were in the range of 410-640 $kg/(m^2s)$. The results presented in Figure 4.4 are at a pressure of $1.05p_{cr}$, while the results presented in Figure 4.5 are at a pressure of $1.15p_{cr}$. For both results the heat flux was 15 $kW/m^2$.

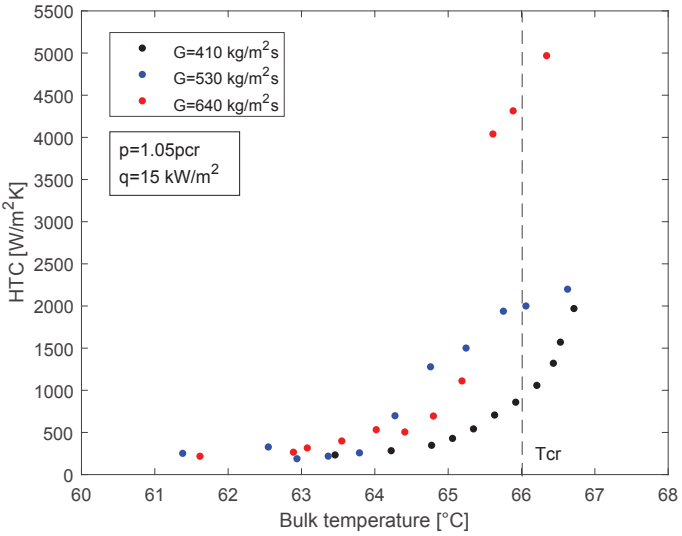


**Figure 4.4:** Heat transfer coefficients at various mass fluxes, pressure of $1.05p_{cr}$ and heat flux of 15 $kW/m^2$.

Higher mass fluxes (Reynolds numbers) lead to lower wall temperatures that result in higher heat transfer coefficients. These results are valid for the entire range of the assessed bulk fluid temperatures. However, in Figure 4.5 there is an occurrence that might lead to a conclusion that the HTC is higher at lower mass fluxes. This is evident when comparing the HTC's at 410 $kg/(m^2s)$ and 530 $kg/(m^2s)$. For this set of measurements the pseudocritical temperature is 72°C (determined with Eq. (3.20)). As it can be seen, the effect of mass flux is more dominant when the bulk fluid temperature is near the pseudocritical temperature. At these conditions (as already highlighted) the fluid undergoes extreme property changes in the vicinity of the pseudocritical region. The drop of viscosity leads to higher turbulence and velocity of the fluid and with

the peak of the specific heat capacity lead to higher HTC. The heat transfer coefficient at lower mass flux (410 $kg/(m^2s)$) is 25% higher compared with the HTC at higher mass flux (530 $kg/(m^2s)$).

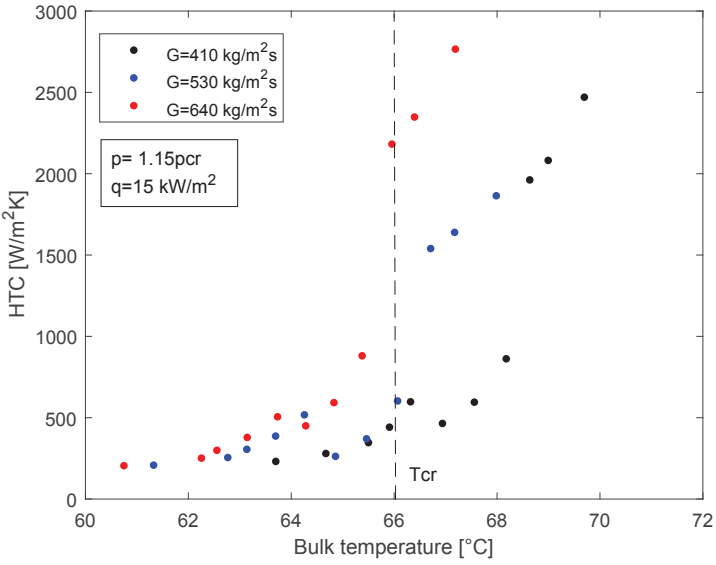


**Figure 4.5:** Heat transfer coefficients at various mass fluxes, pressure of $1.15p_{cr}$ and heat flux of 15 $kW/m^2$.

## 4.3 Effects of heat flux

Figure 4.6 shows the variation of the local HTC's along the test section at three different heat fluxes (15 $kW/m^2$; 23 $kW/m^2$ and 27 $kW/m^2$) for a mass flux of 535 $kg/(m^2s)$ and a pressure of $1.05p_{cr}$. At lower heat fluxes the temperature difference between the wall and the bulk fluid is smaller which yields higher HTC's. These findings are relevant for 15 $kW/m^2$. By increasing the heat flux the temperature difference between the wall and the bulk fluid increases up 20 $K$ for heat flux of 23 $kW/m^2$ and up to 30 $K$ for heat flux of 27 $kW/m^2$. This shows that higher heat fluxes result in increased local wall temperatures and accordingly to lower HTC's.

However, the magnitude of the heat transfer coefficients strongly depends on the heat flux, especially in the pseudocritical region. The heat transfer coefficients at lower heat fluxes (15 $kW/m^2$) have higher values when the bulk fluid temperature (66.3°C) is near the pseudocritical temperature (68.6°C). In these conditions the specific heat capacity of the fluid reaches a peak and the magnitude of the viscosity and the density have a significant drop. This leads to higher heat transfer coefficients, hence to enhanced heat transfer. However,

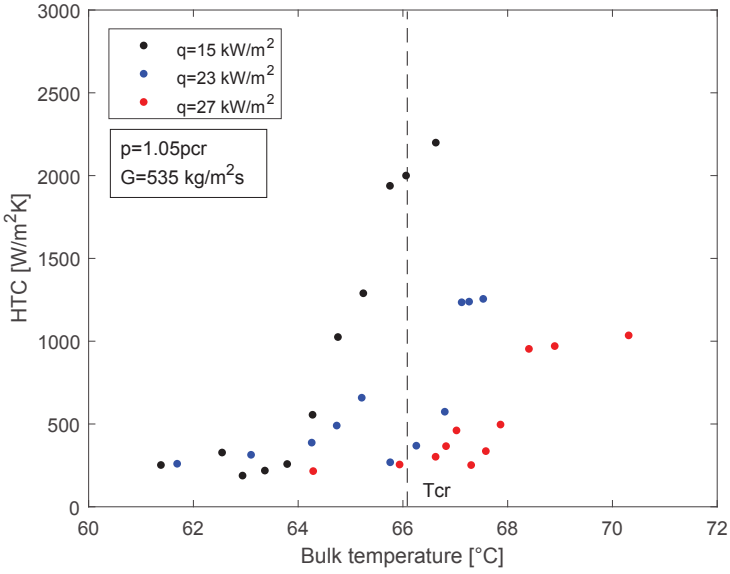


**Figure 4.6:** Variations of the heat transfer coefficients as function of bulk temperature presented at different heat fluxes.

when the wall temperature $T_w$ is higher than the pseudocritical temperature $T_{pc}$, the specific heat, the density and the thermal conductivity of the fluid are quite low which reduces the heat transfer between the wall and the fluid. This occurrence is relevant for the higher heat fluxes (23 $kW/m^2$ and 27 $kW/m^2$) where the temperature difference between the wall $T_w$ and the pseudocritical temperature $T_{pc}$ is 12 $K$ and 22 $K$ accordingly. Therefore, the magnitude of the HTC's is lower and that can be one of the reasons for the appearance of deteriorated heat transfer in this working condition.

## 4.4 Effects of pressure

The heat transfer coefficients increase at pressures close to the critical pressure of the working fluid when other conditions are fixed. The pressure effects on the HTC's are of equal importance to the effects of the heat flux $\dot{q}$ and the mass flux $\dot{G}$.

In Figures 4.7 and 4.8 the heat transfer coefficients of R125 are presented for pressures in the range of (1.05-1.15)$p_{cr}$, at different heat fluxes and fixed mass fluxes (640 $kg/(m^2s)$ and 650 $kg/(m^2s)$). It is evident from the experimental investigation that at higher pressures the HTC's is lower.

However, the HTC increases at pressures close to the critical pressure of a fluid when the other conditions are fixed. This can be associated to the drastic thermophysical property changes at pressures near the critical pressure. At

constant values of mass flux and heat flux the wall $T_w$ and the bulk fluid $T_b$ temperatures change insignificantly with pressure. However, the pseudocritical temperature $T_{pc}$ is affected by the pressure changes and the most significant deviation of the thermophysical properties are occurring in this region. Hence, the heat transfer coefficient changes at different pressures.

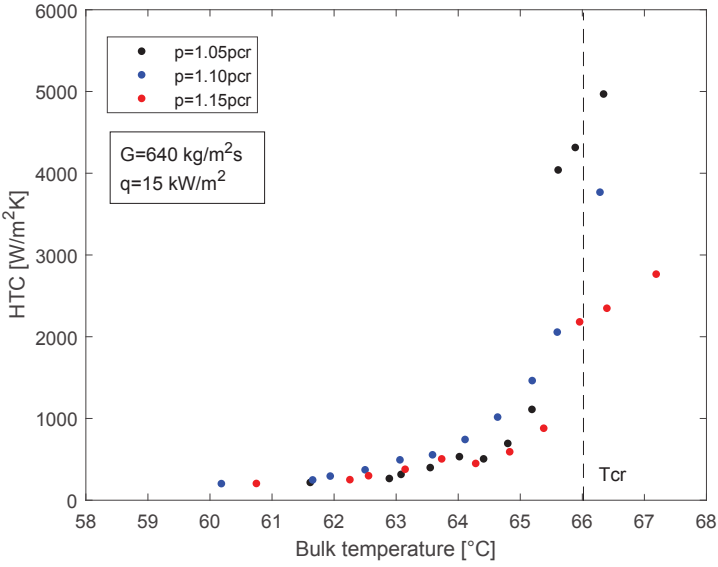


**Figure 4.7:** Heat transfer coefficient at different pressures in horizontal flow of R125 and mass flux of 640 $kg/(m^2s)$.

At pressures close to the critical pressure of the working fluid and when the ratio of $\dot{q}/G$ is low, then the bulk temperature $T_b$ is closer to the pseudocritical temperature $T_{pc}$ and the wall temperature $T_w$ is slightly higher than the $T_{pc}$. Therefore the variations of the thermophysical properties is stronger at lower pressure (closer to the critical pressure) than at higher pressures. Thus, the magnitude of the HTC is higher at lower pressures. On the other hand, at different pressures, when the ratio $\dot{q}/G$ is relatively high the bulk fluid temperatures $T_b$ are near the pseudocritical temperature $T_{pc}$, but the wall temperatures $T_w$ are higher than the pseudocritical temperature $T_{pc}$ at lower pressures. At these conditions there is a possibility of local deteriorated heat transfer.

## 4.5 Determination of the buoyancy effect

In order to determine the buoyancy-free and buoyancy-dependent flow at supercritical conditions it is necessary to use a proper buoyancy criterion. The buoyancy effect can become especially prominent in horizontal flow and large

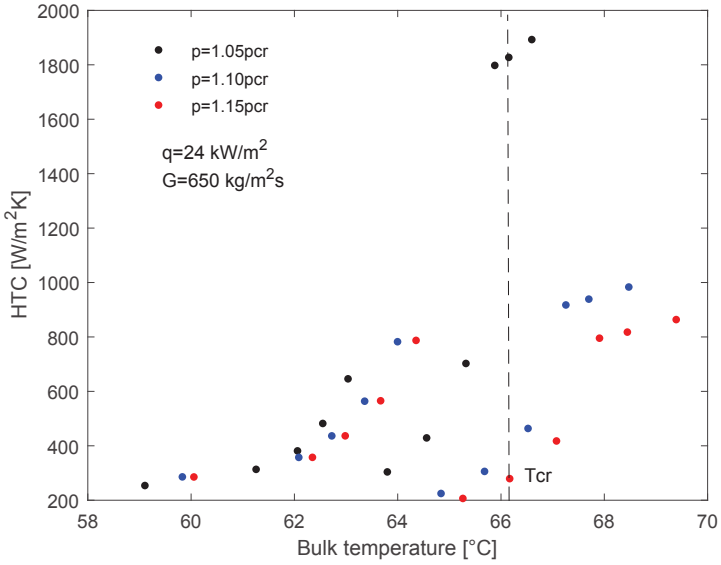


**Figure 4.8:** Heat transfer coefficient at different pressures in horizontal flow of R125 and mass flux of 650 $kg/(m^2s)$.

tube diameters because the temperature difference between the top and bottom tube surfaces can become extremely large. Consequently, wall temperature measurements are necessary for determining if there is an occurrence of local deteriorated heat transfer on the top or bottom tube surface. That occurrence can be represented by local wall temperature $T_w$ rise (local temperature peaks on the tube).

As already mentioned in Section 2.3.6, there are different criteria in literature to quantify the onset of the buoyancy effect. However, most of the criteria are determined for vertical flow. Furthermore, in order to use one of these criteria from literature, it is important to indicate if the temperature at the top or the bottom surface is used.

In this thesis, the simple criterion $Gr/Re^2$ is used for evaluating if the flow is buoyancy dependant or not. Bazargan et al. [81] used this criterion for supercritical water in horizontal flow, described in Section 2.3.6. When the ratio $Gr/Re^2 \geq 1$ then the buoyancy effect becomes dominant.

Three different sets of experiments with different mass fluxes in the range of 410-650 $kg/(m^2s)$ were considered in this analysis. The inlet pressure was $1.10p_{cr}$ and the heat flux was 14 $kW/m^2$. The density and the kinematic viscosity were estimated at bulk temperatures of the working fluid. At low mass flux (410 $kg/(m^2s)$) the ratio $Gr/Re^2 \geq 1$ is in the range 1.2-0.6. The highest value of the ratio $Gr/Re^2 \geq 1$ is noticed at the entry of the test section until the fluid goes through the critical point. Then the value of the ratio declines. The high values show that there could be a buoyancy effect because

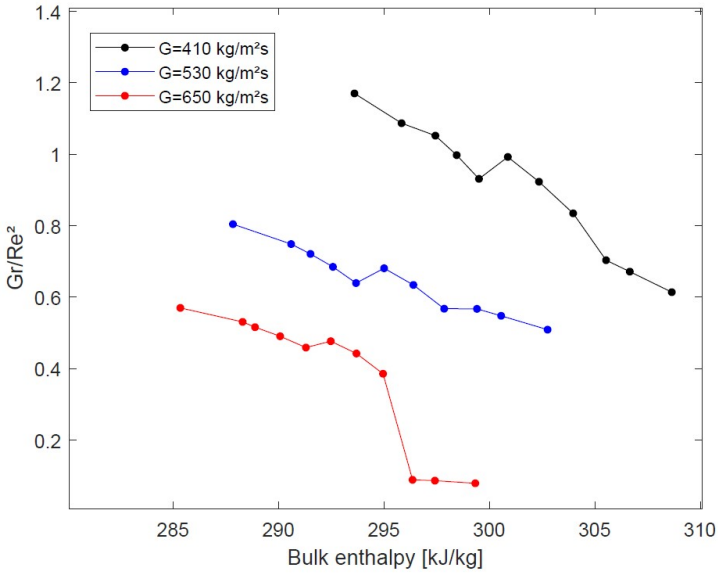


**Figure 4.9:** Variation of $Gr/Re^2$ as function of the bulk enthalpy at heat flux of 14 $kW/m^2$.

there is a substantial density gradient between the wall temperature $T_w$ and the bulk fluid temperature $T_b$. At the exit of the test section both temperatures become closer and the buoyancy effect is less prominent. Thus the ratio of $Gr/Re^2$ is declining.

At higher mass fluxes (510 and 650 $kg/(m^2s)$) the buoyancy effect is decreased. The temperature difference between the wall $T_w$ and the bulk fluid $T_b$ is reduced. For instance, at mass flux of 650 $kg/(m^2s)$ the temperature difference at the exit of the test section is $3K$ which yields density difference of less than 20%. Hence, the value of the ratio $Gr/Re^2$ is 0.08 and the buoyancy effect should be insignificant.

In Figure 4.9 the results of the experiments are presented. Based on this analysis it can be concluded that the buoyancy effect is present when following the criterion $Gr/Re^2 \geq 1$. However, for a more detailed evaluation it is mandatory to use either the measured wall temperature at the top or the bottom surface. That way it is possible to better evaluate the criteria available in literature. Additionally, due to time restrictions this wall temperature measurements could not be done. This leaves room for further investigations and improvements of the test facility.

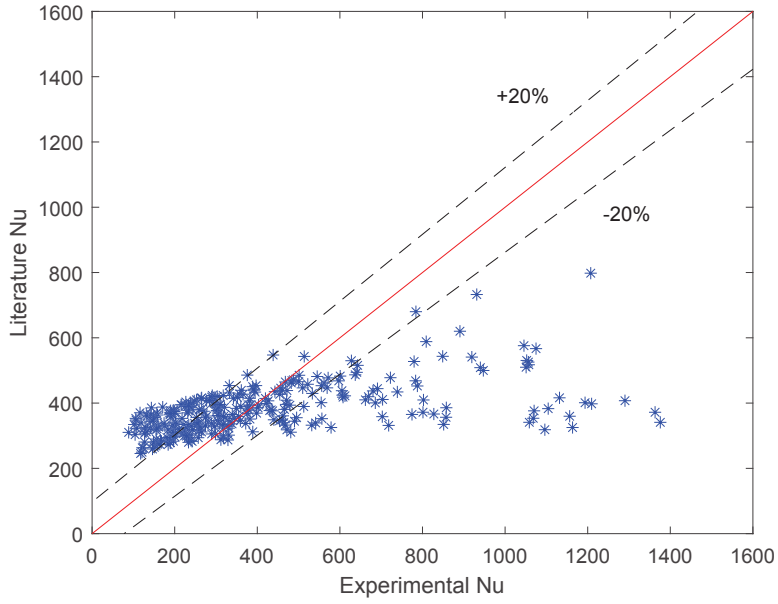


**Figure 4.10:** Comparison of the experimental Nusselt number with the Dittus-Boelter correlation.

## 4.6 Comparison with heat transfer correlation from literature

Despite the large number of experimental investigations and derived heat transfer correlations available in literature, it is according to the knowledge of the author not possible to find one with similar test conditions as in this study. Most of the studies were done with fluids (water, $CO_2$) other than refrigerants (R125). Furthermore, another difference is the flow direction and the tube diameter. Also, this study is one of the rare that considers low heat fluxes (14 -28 $kW/m^2$) compared to other investigations.

In the present study, three heat transfer correlations (Dittus-Boelter, Mokry et al. [61], Domin et al. [82]) included in the literature review (Chapter 2) were compared with the experimental data. The comparisons between the experimental Nusselt numbers and the predicted ones (from literature) are presented with parity plots. The heat transfer correlations of Mokry et al. [61] and Domin et al. [82] have a correction factor in order to account for the drastic property changes of the fluid. This correction factor is represented as ratio of different thermophysical properties. The heat transfer correlation of Mokry et al. [61] is derived for vertical flow while the one of Domin et al. [82] for horizontal flow.

The results presented in Figure 4.10 show that the Dittus-Boelter heat trans-

fer correlation is not suitable for predicting the Nusselt number in the whole experimental range. The Dittus-Boelter heat transfer correlation is derived for a single phase and does not account for the drastic thermophysical property changes of the fluid near the critical region. Furthermore, the experimental and the predicted Nusselt numbers show good agreement in a very limited range. Many of the points from the experimental data do not fall within the error band of ±20%.

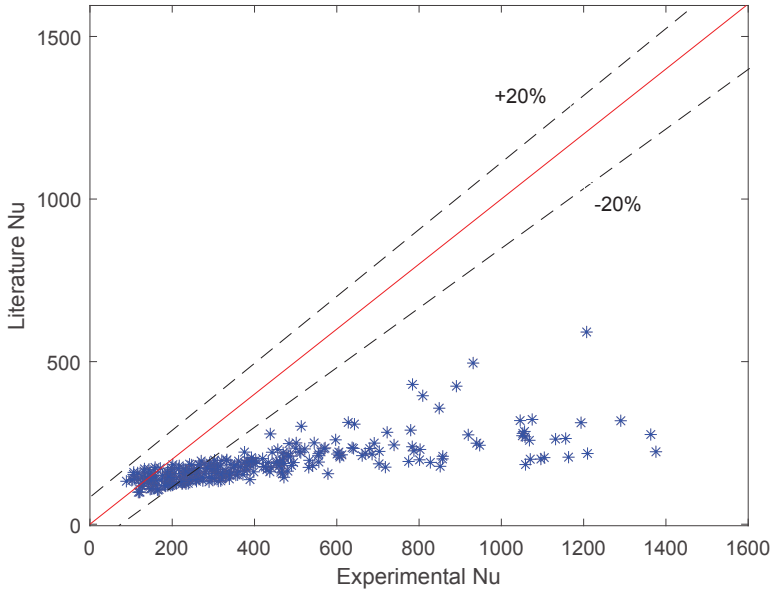


**Figure 4.11:** Comparison of the experimental Nusselt number with the Mokry et al. [61] heat transfer correlation, derived for vertical flow.

The heat transfer correlation of Mokry et al. [61] is considered as one of the most accurate heat transfer correlations in literature for supercritical flow. It is of Dittus-Boelter type with an incorporated correction factor in order to account for the property changes. The correction factor is given as function of wall to bulk properties ($\rho_w/\rho_b$). In Figure 4.11 the comparison of the Mokry et al. [61] heat transfer correlation with experimental Nusselt number is given. Very limited data from the experiments is within the error margins of ±20%. The Mokry et al. [61] heat transfer correlation was derived for vertical flow. This might be one of the reasons that it is unsuitable to predict the experimental Nusselt number for the entire range.

On the other hand, the heat transfer correlation of Domin et al. [82] was derived for horizontal flow. It is also of the Dittus-Boelter type with an incorporated ratio of the viscosity in order to account for the fluid property changes at wall to bulk conditions. In Figure 4.12 the comparison of the Domin et al. [82] heat transfer correlation with the experimental Nusselt

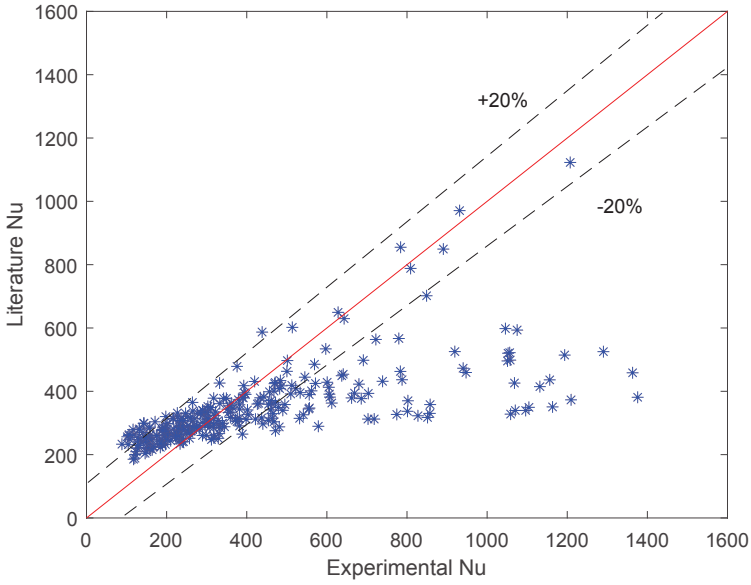


**Figure 4.12:** Comparison of the experimental Nusselt number with the Domin et al. [76] heat transfer correlation, derived for horizontal flow.

number is illustrated. This heat transfer correlations shows the best agreement with the experimental data, when compared with the other two heat transfer correlations. However, this heat transfer correlations fails to predict the Nusselt numbers for the entire experimental range. The reason might be caused by the fact that the experimental data were affected by the buoyancy. However, the heat transfer correlation of Domin et al. [82] hadn't accounted for the buoyancy effect. There is a certain range (especially valid for the pseudocritical region) of experimental data where the heat transfer correlation does not provide acceptable results.

The heat transfer correlations compared in this study are unable to predict the Nusselt numbers for the entire experimental range. The disagreement is most likely because the heat transfer correlations are applicable only for the working conditions that they were derived for.

As already proposed in Section 2.5.4, when developing a general heat transfer correlation it is the best to consider three regions ($T < T_{pc}$; $T_{pc}$; $T_{pc} > T$) separately. In this way, the drastic changes of the pseudocritical properties in the temperature region $T_{pc}$ are not going to be neglected. Moreover, when developing a new general heat transfer correlation wider conditions and experimental data should be considered. Otherwise, the heat transfer correlations will show good agreement only with very limited data sets. Therefore, more data points are required for deriving new heat transfer correlation for R125. This can be considered as part of future work.

# 5. Conclusions

The main objective of this thesis is to get a better understanding of the supercritical heat transfer characteristics of R125. Therefore, in order to increase the knowledge and the understanding of the supercritical heat transfer a comprehensive literature review was done. In this way it was possible to determine which are the parameters that have an influence on the supercritical heat transfer. On the other hand it was possible to detect the gap that exists in literature. From the review two major conclusions can be made:

1. most of the experimental data on supercritical heat transfer is for water and $CO_2$ while investigations for refrigerants including R125 is limited.

2. the flow direction and the tube diameters are one of the parameters that have a significant influence on the supercritical heat transfer. In literature, the focus is in vertical flow and small tube diameters. However, a heat exchanger with horizontal layout and large tube diameters is considered as most suitable for transcritical ORC.

In order to be able to better understand the supercritical heat transfer, there was a need for an experimental investigation. Thus, a novel test facility was designed and built to measure the supercritical heat transfer to refrigerants (R125) in horizontal flow and large tube diameter. On component level, the new test facility 'iSCORe' resembles like a transcritical ORC, but instead of an expander an expansion valve is used. Before performing measurements at supercritical pressures, the new test facility was experimentally validated.

Thus, it was then possible to experimentally determine the effects that different parameters have on the supercritical heat transfer. The influence of mass flux, heat flux, pressure and buoyancy are one of the most significant for horizontal flow. Based on the effect of each parameter it was possible to detect which heat transfer mechanism (enhanced heat transfer EHT or deteriorated heat transfer DHT) is present at particular operating conditions. The heat transfer mechanisms, occur simultaneously when the following temperature conditions are fulfilled $T_b < T_{pc} < T_w$. It was concluded that the effect of mass flux becomes especially dominant near the pseudocritical region. Enhanced heat transfer EHT could be noticed at lower mass fluxes when the bulk fluid temperature was near the pseudocritical temperature. Additionally,

the combination of higher mass flux and lower heat flux leads to DHT. The effect of pressure is significant near the critical pressure of the working fluid. The criterion $Gr/Re^2$ was used in order to determine the buoyancy effect in this study. When the ratio $Gr/Re^2 \approx 1$ then it is combined forced and free convection. Considering the results in this study, the flow is buoyancy dependent at low mass fluxes and low heat fluxes.

Moreover, three heat transfer correlations Dittus-Boelter, Mokry et al. [61], Domin et al. [82] were compared with the measured data. The heat transfer correlations of Mokry et al. [61] and Domin et al. [82] have incorporated correction factors with the aim to account for the thermophysical property changes at wall and bulk temperatures near the (pseudo)critical temperature. However, the three heat transfer correlations do not predict the Nusselt numbers for the entire experimental range. The disagreement is most likely because the heat transfer correlations are only applicable for the working conditions they were derived for.

However, the heat transfer correlation of Domin et al. [82] shows the best agreement with the experimental data most probably because it was derived for horizontal flow. Moreover, in most of the heat transfer correlations it is not indicated if the buoyancy effect was encountered. This should be certainly indicated when developing a new heat transfer correlation. Moreover, it is important that a new general heat transfer correlation is derived and is applicable for wider operating ranges. More accurate heat transfer correlation will lead to better design of the main heat exchanger (vapour generator) that presents a vital part of a (transcritical) ORC. This would be beneficial in terms of improved performance and lower cost of the heat exchanger and the ORC installation.

## 5.1 Future work

As already mentioned, it is very important to develop a heat transfer correlation that is applicable for supercritical fluids. Due to time constraints it was not possible to obtain experimental data in wider operating ranges and a new heat transfer correlation was not proposed. This can be considered as a part of future work.

Furthermore, the test section could be improved by positioning the thermocouples to measure the wall temperatures. It would be beneficial to have these sets of measurement in order to determine the temperature difference at the top and bottom tube surface. This would enable to detect if there is occurrence of local EHT or DHT. As part of the future work it is possible to evaluate the effect of higher heat fluxes on the supercritical heat transfer. Additionally, a part of the future work can be obtaining experimental data for other refrigerants as well. Moreover, the effect of tube diameters is very important in horizontal flow and such data is limited in literature. Additional tests can be done in fin and corrugated tubes to check the effects on heat transfer. The results can be compared with the test data for smooth tubes.

# Bibliography


[1] International Energy Agency. Key World Energy Statistics. Technical report, Intergovernmental organization, 2017.

[2] Ozone Secretariat UNEP. Montreal Protocol on Substances that Deplete the Ozone Layer. Technical Report September, 1987.

[3] Michel De Paepe. Situation of ORCNext project. Technical report, International Symposium of Advanced Waste Heat Valorization Technologies, Kortrijk, Belgium, 2012.

[4] Clemens Forman, Ibrahim Kolawole Muritala, Robert Pardemann, and Bernd Meyer. Estimating the global waste heat potential. *Renewable and Sustainable Energy Reviews*, 57:1568–1579, 2016.

[5] Michael Papapetrou, George Kosmadakis, Andrea Cipollina, Umberto La Commare, and Giorgio Micale. Industrial waste heat: Estimation of the technically available resource in the EU per industrial sector, temperature level and country. *Applied Thermal Engineering*, 138(April):207–216, 2018.

[6] Elisa Trujillo-Baute, Pablo del RÍo, and Pere Mir-Artigues. Analysing the impact of renewable energy regulation on retail electricity prices. *Energy Policy*, 114(June 2017):153–164, 2018.

[7] European Council. Energy roadmap 2050. Technical Report December 2011, European Commission, 2012.

[8] Hilel Legmann. Recovery of industrial heat in the cement industry by means of the ORC process. *IEEE Cement Industry Technical Conference (Paper)*, pages 29–35, 2002.

[9] G. David, F. Michel, and L. Sanchez. Waste heat recovery projects using Organic Rankine Cycle technology - Examples of biogas engines and steel mills applications. *World Engineers Convention*, 2011.

[10] Sylvain Quoilin, Martijn Van Den Broek, Sébastien Declaye, Pierre Dewallef, and Vincent Lemort. Techno-economic survey of organic rankine cycle (ORC) systems. *Renewable and Sustainable Energy Reviews*, 22: 168–186, 2013.

[11] J. Michael Moran and N. Howard Shapiro. *Fundamenals of Engineering Thermodynamics*. Wiley, fifth edit edition, 2006.

[12] Bahaa Saleh, Gerald Koglbauer, Martin Wendland, and Johann Fischer. Working fluids for low-temperature organic Rankine cycles. *Energy*, 32 (7):1210–1221, 2007.

[13] Zhen Wang Jian Zhang Fubin Yang Enhua Wang Baofeng Yao Kai Yang, Hongguang Zhang. Study of zeotropic mixtures of ORC (organic Rankine cycle) under engine various operating conditions. *Energy*, 58:494–510, 2013.

[14] A. Schuster, S. Karellas, and R. Aumann. Efficiency optimization potential in supercritical Organic Rankine Cycles. *Energy*, 35(2):1033–1039, 2010.

[15] Jiangfeng Wang, Zhixin Sun, Yiping Dai, and Shaolin Ma. Parametric optimization design for supercritical CO2 power cycle using genetic algorithm and artificial neural network. *Applied Energy*, 87(4):1317–1324, 2010.

[16] Ernest G. Feher. The Supercritical Thermodynamic Power Cycle. *Energy Conversion*, 8(2):85–90, 1968. URL `http://linkinghub.elsevier.com/retrieve/pii/0013748068901058`.

[17] Y. Chen, P. Lundqvist, A. Johansson, and P. Platell. A comparative study of the carbon dioxide transcritical power cycle compared with an organic rankine cycle with R123 as working fluid in waste heat recovery. *Applied Thermal Engineering*, 26(17-18):2142–2147, 2006.

[18] Bo Tau Liu, Kuo Hsiang Chien, and Chi Chuan Wang. Effect of working fluids on organic Rankine cycle for waste heat recovery. *Energy*, 29(8): 1207–1217, 2004.

[19] Junjiang Bao and Li Zhao. A review of working fluid and expander selections for organic Rankine cycle. *Renewable and Sustainable Energy Reviews*, 24(August):325–342, 2013.

[20] J. Larjola. production economics Electricity from industrial waste heat using high-speed organic Rankine cycle (ORC). *International Journal of Production Economics*, 41:227–235, 1995.

[21] S. Lecompte, B. Ameel, D. Ziviani, M. Van Den Broek, and M. De Paepe. Exergy analysis of zeotropic mixtures as working fluids in Organic Rankine Cycles. *Energy Conversion and Management*, 85:727–739, 2014.

[22] T .C. Hung, T. Y. Shai, and S. K. Wang. A review of organic Rankine cycles (ORCs) for the recovery of low-grade waste heat. *Energy*, 22(7): 661–667, 1997.

[23] Igor L. Pioro and Romney B. Duffey. Heat transfer and hydraulicresistance at supercritical pressures in power engineering applications. *New York, NY, USA, asme press edition*, 2007.

[24] Igor Pioro and Sarah Mokry. Heat Transfer to Fluids at Supercritical Pressures. *Heat Transfer- Theoretical Analysis, Experimental Investigations and Industrial Systems*, pages 481–504, 2011.

[25] I L Pioro and R B Duffey. Literature Survey of Heat Transfer and Hydraulie Resistance of Water, Carbon Dioxide, Helium and Other Fluids at Supercritical and Near-Critical Pressures. Technical Report April, 2003.

[26] S Liao. An experimental investigation of convection heat transfer to supercritical carbon dioxide in miniature tubes. *International Journal of Heat and Mass Transfer*, 45(25):5025–5034, 2002.

[27] H. J. Haskins, R. M. Taylor, and D. B. Osborn. Development of solar receiver for an organic Rankine cycle engine. In *Proceedings of the 16th Intersociety Energy Conversion Engineering Conference. Technologies for the Transition*, volume 2, pages 1764 – 1769, 1981.

[28] TAS Energy. Project profile US Geothermal 22 MW Neal Hot Springs Geothermal Power Plant. *Renewable Energy Systems*, 2012.

[29] Copco Atlas. Renewable power play. (December), 2013.

[30] Marija Lazova, Henk Huisseune, Alihan Kaya, Steven Lecompte, George Kosmadakis, and Michel De Paepe. Performance Evaluation of a Helical Coil Heat Exchanger Working under Supercritical Conditions in a Solar Organic Rankine Cycle Installation. *Energies*, 9(6):432, 2016.

[31] Pedro J. Mago, Louay M. Chamra, Kalyan Srinivasan, and Chandramohan Somayaji. An examination of regenerative organic Rankine cycles using dry fluids. *Applied Thermal Engineering*, 28(8-9):998–1007, 2008.

[32] Huijuan Chen, D. Yogi Goswami, and Elias K. Stefanakos. A review of thermodynamic cycles and working fluids for the conversion of low-grade heat. *Renewable and Sustainable Energy Reviews*, 14(9):3059–3067, 2010.

[33] Christian Vetter, Hans Joachim Wiemer, and Dietmar Kuhn. Comparison of sub- and supercritical Organic Rankine Cycles for power generation from low-temperature/low-enthalpy geothermal wells, considering specific net power output and efficiency. *Applied Thermal Engineering*, 51 (1-2):871–879, 2013.

[34] Zhaolin Gu and Haruki Sato. Performance of supercritical cycles for geothermal binary design. *Energy Conversion and Management*, 43(7): 961–971, 2002.

[35] Zhang Shengjun, Wang Huaixin, and Guo Tao. Performance comparison and parametric optimization of subcritical Organic Rankine Cycle (ORC) and transcritical power cycle system for low-temperature geothermal power generation. *Applied Energy*, 88(8):2740–2754, 2011.

[36] Young Jin Baik, Minsung Kim, Ki Chang Chang, Young Soo Lee, and Hyung Kee Yoon. A comparative study of power optimization in low-temperature geothermal heat source driven R125 transcritical cycle and HFC organic Rankine cycles. *Renewable Energy*, 54:78–84, 2013.

[37] Young Jin Baik, Minsung Kim, Ki Chang Chang, and Sung Jin Kim. Power-based performance comparison between carbon dioxide and R125 transcritical cycles for a low-grade heat source. 88(3):892–898, 2011.

[38] Gequn Shu, Lina Liu, Hua Tian, Haiqiao Wei, and Xiaofei Xu. Performance comparison and working fluid analysis of subcritical and transcritical dual-loop organic Rankine cycle (DORC) used in engine waste heat recovery. *Energy Conversion and Management*, 74:35–43, 2013.

[39] Kyoung Ho Kang and Soon Heung Chang. Experimental study on the heat transfer characteristics during the pressure transients under supercritical pressures. *International Journal of Heat and Mass Transfer*, 52(21-22):4946–4955, 2009.

[40] J. D. Jackson and W. B. Hall. Forced convection heat transfer to fluids at supercritical pressure, In book: Turbulent Forced Convection in Channels and Bundles. 2:563–612, 1979.

[41] W. B. Hall. Heat transfer near the critical point. *Advances in Heat Transfer*, 7:1–86, 1971.

[42] Sotirios Karellas, Andreas Schuster, and Aris Dimitrios Leontaritis. Influence of supercritical ORC parameters on plate heat exchanger design. *Applied Thermal Engineering*, 33-34(1):70–76, 2012.

[43] Ran Tian, Dabiao Wang, Yue Zhang, Yuezheng Ma, Hui Li, and Lin Shi. Experimental study of the heat transfer characteristics of supercritical pressure R134a in a horizontal tube. *Experimental Thermal and Fluid Science*, 103:49–61, 2019.

[44] Dabiao Wang, Ran Tian, Yue Zhang, Lanlan Li, Yuezheng Ma, Lin Shi, and Hui Li. Heat transfer investigation of supercritical R134a for transcritical organic Rankine cycle system. *Energy*, 169:542–557, 2019.

[45] Igor L. Pioro and Romney B. Duffey. Experimental heat transfer in supercritical water flowing inside channels (survey). *Nuclear Engineering and Design*, 235(22):2407–2430, 2005.

[46] Kenneth H. Wohletz. Water/Magma Interaction: Physical considerations for the deep submarine environment. *Earth and Environmental Sciences*, pages 25–49, 2003.

[47] Bruce Fegley, Mikhail Yu Zolotov, and Katharina Lodders. The Oxidation Station of the Lower Atmosphere and Surface of Venus. *Icarus*, 125: 416–439, 1997.

[48] Tristan Guillot. A Comparison of the Interiors of Jupiter and Saturn. *Planteray and Space Science*, 47:1183–1200, 1999.

[49] Zhouhang Li, Yuxin Wu, Guoli Tang, Dalong Zhang, and Junfu Lu. Comparison between heat transfer to supercritical water in a smooth tube and in an internally ribbed tube. *International Journal of Heat and Mass Transfer*, 84:529–541, 2015.

[50] Alireza Taklifi, Mohammad Ali Akhavan-Behabadi, Pedram Hanafizadeh, and Abbas Aliabadi. Effect of heat and mass flux on heat transfer characteristics of water forced convection inside vertical and inclined rifled tubes. *Applied Thermal Engineering*, 117:169–177, 2017.

[51] M. E. Shitsman. Impairment of the heat transmission at super-critical pressures. *Teplofiz. Vys. Temp. 1,*, 2, 1963.

[52] V Vikrev, Y.V.and Lokshin. An experimental study of temperature conditions in horizontal steam generating tubes at supercritical pressures. *Teploenergetika*, 1:12–16, 1964.

[53] Ackerman J W. Pseudoboiling Heat Transfer to Supercritical Pressure Water in Smooth and Ribbed Tubes. *ASME. J. Heat Transfer.*, 92(3): 490–497, 1970.

[54] K Yamagata, K Nishikawa, S Hasegawa, and S Yoshida. Forced convective heat transfer to supercritical water flowing in tubes. *Int. J. Heat Mass Transfer*, 15:2575–2593, 1972.

[55] Bharat S. Shiralkar and Peter Griffith. Deterioration in heat transfer to fluids at supercritical pressure and high heat fluxes. Technical report, 1968.

[56] Kondrat'ev N.S. *In Transactions of the IVth All-Union Conference on Heat Transfer and Hydraulics at Movement of Two-Phase Flow inside Elements of Power Engineering Machines and Apparatuses*, pages 71–74.

[57] N Koshizuka, S Takano and Y Oka. Numerical analysis of deterioration phenomena in heat transfer to supercritical water. *Engineering, Nuclear*, 38:1–8, 1995.

[58] V.S. Protopopov, I.V. Kuraeva, and A.M. Antonov. An approach to the determination of the conditions of occurrence of deteriorated heat transfer regimes at supercritical pressures. *High Temperatures*, 11(3):529—-532, 1973.

[59] V.S. Protopopov and V.A. Silin. Approximate method of calculating the start of local deterioration of heat transfer at supercritical pressure. *High Temperatures*, 11(2):399—-401, 1973.

[60] B.S. Petukhov, V.A. Kurganov, and V.B. Ankudinov. Heat-transfer and flow resistance in the turbulent pipe-flow of a fluid with near-critical state parameters. *High Temperatures*, 21(1):92–100, 1983.

[61] Sarah Mokry, Igor Pioro, Amjad Farah, Krysten King, Sahil Gupta, Wargha Peiman, and Pavel Kirillov. Development of supercritical water heat-transfer correlation for vertical bare tubes. *Nuclear Engineering and Design,*, 241(4):1126—-1136, 2011.

[62] Santosh Kumar, R P Vedula, Kannan N Iyer, and Avinash J Gaikwad. Local heat transfer coefficient measurements using thermal camera for upward flow of freon 22 in a vertical tube at supercritical conditions and development of correlations. *Nuclear Engineering and Design,*, 328:80–94, 2018.

[63] B. S. Petukhov. Heat Transfer and Friction in Turbulent Pipe Flow with Variable Physical Properties. *Advances in Heat Transfer*, 6(C):504–564, 1970.

[64] J.D. Jackson and W.B. Hall. Influences of buoyancy on heat transfer to fluids in vertical tubes under turbulent conditions. *Turbulent Forced Convection in Channels and Bundles*, 2:613–640, 1979.

[65] A. F. Polyakov. Heat transfer under supercritical pressures. *Advances in Heat Transfer*, 21:1–51, 1991.

[66] P. L. Kirillov. Heat and mass transfer at supercritical parameters. The short review of researches in Russia. Theory and experiments. *Proceedings of the first international symposium on supercritical watercooled reactors, design and technology*, pages 58–71, 2000.

[67] Igor L. Pioro, Hussam F. Khartabil, and Romney B. Duffey. Heat transfer to supercritical fluids flowing in channels - Empirical correlations (survey). *Nuclear Engineering and Design*, 230(1-3):69–91, 2004.

[68] Dan Huang, Zan Wu, Bengt Sunden, and Wei Li. A brief review on convection heat transfer of fluids at supercritical pressures in tubes and the recent progress. *Applied Energy*, 162:494–505, 2016.

[69] Luisa F. Cabeza, Alvaro de Gracia, A. Inés Fernández, and Mohammed M. Farid. Supercritical CO2 as heat transfer fluid: A review. *Applied Thermal Engineering*, 125:799–810, 2017.

[70] M. E. Shitsman. Heat transfer to water, oxygen and carbon dioxide in the approximately critical range. *Teploenergetiky*, 1:68–72, 1959.

[71] N. L. Dickinson and C. P. Weich. Heat transfer to supercritical water. *ASME*, 80:745–751, 1958.

[72] E.A. Krasnoshchekov and V.S. Protopopov. Heat transfer at supercritical region in flow of carbon dioxide and water in tubes, (In Russian). *Thermal Engineering*, 12:26–30, 1959.

[73] A.A. Bishop, R.O. Sandberg, and L.S. Tong. Forced convection heat transfer to water at near critical temperatures and supercritical pressures. Technical report, WCAP-2056, Westinghouse Electric Corporation, Atomic Power Division, 1964.

[74] Z.L. Miropol'skii and M.E. Shitsman. Heat transfer in super-critical flows through curvilinear channels. In N.A. Dollezhal, editor, *Investigation of Heat Transfer to Steam and Water Boiling in Tubes at High Pressures*, pages 54–70. Atomizdat Publishing House, Moscow, Russia, 1958.

[75] Sahil Gupta, Amjad Farah, Krysten King, Sarah Mokry, and Igor Pioro. Developing new heat-transfer correlation for supercritical-water flow in vertical bare tubes. *International Conference on Nuclear Engineering, Proceedings, ICONE*, 2(June 2016), 2010.

[76] H.S. Swenson, J.R. Carver, and C.R. Karakal. Heat transfer to supercritical water in smooth-bore tubes. *Journal of Heat Transfer, Transactions of the ASME, Series C*, 87(4):477–484, 1968.

[77] Yoon Yeong Bae, Hwan Yeol Kim, and Deog Ji Kang. Forced and mixed convection heat transfer to supercritical CO2 vertically flowing in a uniformly-heated circular tube. *Experimental Thermal and Fluid Science*, 34(8):1295–1308, 2010.

[78] I. I. Belyakov, L. Y. Krasyakova, and A. V. Zhukovskii. Heat transfer in vertical risers and horizontal tubes at supercritical pressure. *Therm. Eng.*, 18(11):55–59, 1971.

[79] G A Adebiyi and W B Hall. Experimental investigation of heat transfer to supercritical pressure carbon dioxide in a horizontal pipe. *International Journal of Heat and Mass Transfer*, 19(7):715–720, 1976.

[80] Shuiqing Yu, Huixiong Li, Xianliang Lei, Yongchang Feng, Yifan Zhang, Hong He, and Tai Wang. Influence of buoyancy on heat transfer to water flowing in horizontal tubes under supercritical pressure. *Applied Thermal Engineering*, 59(1-2):380–388, 2013.

[81] Majid Bazargan, Daniel Fraser, and Vijay Chatoorgan. Effect of buoyancy on heat transfer in supercritical water flow in a horizontal round tube. *Journal of Heat Transfer*, 127(8):897–902, 2005.

[82] G. Domin. Warmeubergang in kritischen und iiberkritischen Bereichen von Wasser in Rohren (Heat transfer to water in pipes in the critical/super-critical region). *Brennst.-Warme-Kraft*, 15(11), 1963.

[83] Zhi Hui Li, Pei Xue Jiang, Chen Ru Zhao, and Yu Zhang. Experimental investigation of convection heat transfer of CO2 at supercritical pressures in a vertical circular tube. *Experimental Thermal and Fluid Science*, 34 (8):1162–1171, 2010.

[84] Yoon Y. Bae. Mixed convection heat transfer to carbon dioxide flowing upward and downward in a vertical tube and an annular channel. *Nuclear Engineering and Design*, 241(8):3164–3177, 2011.

[85] Pei Xue Jiang, Yu Zhang, Yi Jun Xu, and Run Fu Shi. Experimental and numerical investigation of convection heat transfer of CO2 at supercritical pressures in a vertical tube at low Reynolds numbers. *International Journal of Thermal Sciences*, 47(8):998–1011, 2008.

[86] Hoo Kyu Oh and Chang Hyo Son. New correlation to predict the heat transfer coefficient in-tube cooling of supercritical CO2 in horizontal macro-tubes. *Experimental Thermal and Fluid Science*, 34(8):1230–1241, 2010.

[87] Nathan Kline, Florian Feuerstein, and Stavros Tavoularis. Onset of heat transfer deterioration in vertical pipe flows of CO2 at supercritical pressures. *International Journal of Heat and Mass Transfer*, 118:1056–1068, 2018.

[88] J. K Kim, K Jeon, J H, Y Yoo, and S Joon. Experimental study on heat transfer characteristics of turbulent supercritical flow in vertical circular/non-circular tubes. pages 992–995, 2005.

[89] B. S. Petukhov, E. A. Krasnoschekov, and V. S. Protopopov. An Investigation of Heat Transfer to Fluids Flowing in Pipes Under Supercritical Conditions. In *International Developments in Heat Transfer: Papers presented at the 1961 International Heat Transfer Conference, ASME, University of Colorado, Boulder, CO, USA*, pages 569–578. 1961.

[90] R.P. Bringer and J.M. Smith. Heat transfer in the critical region. *A.I.Ch.E. Journal*, 3(1):49–55, 1957.

[91] E. A. Krasnoshchekov and V. S. Protopopov. Some results of an experimental investigation of heat transfer to carbon dioxide at supercritical pressure and temperature heads of up to 850°C. *High Temperatures*, pages 992–995, 1971.

[92] L. M. Gorban', R. S. Pomet'ko, and O. A. Khryaschev. Modeling of water heat transfer with Freon of supercritical pressure, (In Russian), Institute of Physics and Power Engineering Obninsk, Russia. 2:19, 1990.

[93] G Richards, G D Harvel, I L Pioro, A S Shelegov, and P L Kirillov. Heat transfer profiles of a vertical , bare , 7-element bundle cooled with supercritical Freon R-12. *Nuclear Engineering and Design*, 264:246–256, 2013.

[94] J. P. Holman and J. H. Boggs. Heat Transfer to Freon 12 Near the Critical State in a Natural-Circulation Loop. *ASME. J. Heat Transfer*, 82(3):221–226, 1960.

[95] Sung deok Hong, Se-Young Chun, Se-Yun Kim, and Won-Pil Baek. Heat Transfer Characteristics of an Internally-Heated Annulus Cooled with R-134a Near the Critical Pressure. *Journal of the Korean Nuclear Society*, 36(3):403–414, 2004.

[96] Siyu Zhang, Hanyang Gu, Xu Cheng, and Zhenqin Xiong. Experimental study on heat transfer of supercritical Freon flowing upward in a circular tube. *Nuclear Engineering and Design*, 280:305–315, 2014.

[97] X Cheng, Y H Yang, and S F Huang. A simplified method for heat transfer prediction of supercritical fluids in circular tubes. *Annals of Nuclear Energy*, 36:1120–1128, 2009.

[98] Ya lin Cui and Huai xin Wang. Experimental study on convection heat transfer of R134a at supercritical pressures in a vertical tube for upward and downward flows. *Applied Thermal Engineering*, 129:1414–1425, 2018.

[99] Nicholas Tarsitano, Khalil Sidawi, and Pioro Igor. Development and Comparison of a Heat-Transfer Correlation for Supercritical Refrigerants. *In 25th International Conference on Nuclear Engineering*, page 10, 2017.

[100] F. Feuerstein, S. Coelho, D. Klingel, and X. Cheng. Experimental study on convection heat transfer of R134a at supercritical pressures in a vertical tube for upward and downward flows. *International Journal of Nuclear Power*, 62(2):121–125, 2017.

[101] Chen Ru Zhao and Pei Xue Jiang. Experimental study of in-tube cooling heat transfer and pressure drop characteristics of R134a at supercritical pressures. *Experimental Thermal and Fluid Science*, 35(7):1293–1303, 2011.

[102] Dabiao Wang, Xiaoye Dai, Ran Tian, and Lin Shi. Experimental investigation of the heat transfer of supercritical R134a in a horizontal micro-fin tube. *International Journal of Thermal Sciences*, 138:536–549, 2019.

[103] Hideo Mori, Takenobu Kaida, Masaki Ohno, and Suguru Yoshida. Heat transfer to a supercritical pressure fluid flowing in sub-bundle channels. page 3131, 2019.

[104] Pei xue Jiang, Chen ru Zhao, and Bo Liu. Flow and heat transfer characteristics of r22 and ethanol at supercritical pressures. *The Journal of Supercritical Fluids*, 70:75–89, 2012.

[105] Jiacheng He, Chaobin Dang, and Eiji Hihara. Experimental investigation of heat transfer to supercritical R245fa flowing vertically upward in a circular tube. *International Journal of Heat and Mass Transfer*, 127: 286–295, 2018.

[106] Jiacheng He, Chaobin Dang, and Eiji Hihara. Supercritical heat transfer characteristics of R1233zd ( E ) in vertically upward flow. *International Journal of Heat and Mass Transfer*, 127:2497–505, 2018.

[107] Srinivas Garimella, Biswajit Mitra, Ulf C. Andresen, Yirong Jiang, and Brian M. Fronk. Heat transfer and pressure drop during supercritical cooling of HFC refrigerant blends. *International Journal of Heat and Mass Transfer*, 91:477–493, 2015.

[108] Pourya Forooghi and Kamel Hooman. Experimental analysis of heat transfer of supercritical fluids in plate heat exchangers. *International Journal of Heat and Mass Transfer*, 74:448–459, 2014.

[109] Jiayue Chen, Hanyang Gu, Zhenqin Xiong, and Da Liu. Experimental investigation on heat transfer behavior in a tight 19 rod bundle cooled with supercritical R134a. *Annals of Nuclear Energy*, 115:393–402, 2018.

[110] Hongfang Gu, Hongzhi Li, Haijun Wang, and Yushan Luo. Experimental investigation on convective heat transfer from a horizontal miniature tube to methane at supercritical pressures. 58:490–498, 2013.

[111] M. E. Shitsman. The effect of natural convection on temperature conditions in horizontal tubes at supercritical pressures. *Teploenergetika*, 13(7):51–56, 1966.

[112] S. Garimella. Near-critical/supercritical heat transfer measurements of R-410A in small diameter tube. *Technical Report 20120-01*, 2008.

[113] J D Jackson, M A Cotton, and B P Axcell. Studies of mixed convection in vertical tubes. 10(1), 1989.

[114] Dan Huang and Wei Li. A brief review on the buoyancy criteria for supercritical fluids. *Applied Thermal Engineering*, 131:977–987, 2018.

[115] B. S. Petukhov and A. F. Polyakov. Heat transfer in turbulent mixed convection. *Heat Transfer in Turbulent Mixed Convection*, pages 115–146, 1988.

[116] Shenghui Liu, Yanping Huang, Guangxu Liu, Junfeng Wang, and Laurence K.H. Leung. Improvement of buoyancy and acceleration parameters for forced and mixed convective heat transfer to supercritical fluids flowing in vertical tubes. *International Journal of Heat and Mass Transfer*, 106:1144–1156, 2017.

[117] J D Jackson. *Supercritical heat transfer*, volume v. 1975.

[118] W. B. Hall, J. D. Jackson, and A. Watson. Paper 3: A Review of Forced Convection Heat Transfer to Fluids at Supercritical Pressures. *Proceedings of the Institution of Mechanical Engineers, Conference Proceedings*, 182(9):10–22, 1967.

[119] F. P. Incropera and D. P. DeWitt. *Fundamentals of Heat and Mass Transfer*. New York, NY, USA, 5th edition, 2002.

[120] E.A. Krasnoshchekov and V.S. Protopopov. About heat transfer in flow of carbon dioxide and water at supercritical region of state parameters, (In Russian). *Thermal Engineering*, 10:94, 1960.

[121] J. P. Holman, S. N. Rea, and C. E Howard. Forced convection heat transfer to Freon 12 near the critical state in a vertical annulus. *Int. J. Heat Mass Transfer*, 8(11):1095–1102, 1965.

[122] T. C. Hung, S. K. Wang, C. H. Kuo, B. S. Pei, and K. F. Tsai. A study of organic working fluids on system efficiency of an ORC using low-grade energy sources. 35(3):1403–1411, 2010.

[123] National Instruments. CompactRIO cRIO-9072/3/4 ™. Technical report, 2010.

[124] Tektronix. Multimeter / Data Acquisition / Switch Systems Multimeter / Data Acquisition / Switch Systems. Technical report, Tektronix Company, 2010.

[125] Solutia. Therminol ADX10. Technical report, Solutia Europe S.A/N.V., 1998.

[126] Sergei Gusev, Davide Ziviani, and Ian Bell. Experimental Comparison Of Working Fluids For Organic Rankine Cycle With Single-Screw Expander. *International Refrigeration and Air Conditioning Conference*, page 10, 2014.

[127] Pei xue Jiang, Bo Liu, Chen ru Zhao, and Feng Luo. Convection heat transfer of supercritical pressure carbon dioxide in a vertical micro tube from transition to turbulent flow regime. *International Journal of Heat and Mass Transfer*, 56(1-2):741–749, 2013.

[128] Jie Wen, Haoran Huang, Zhouxia Jia, Yanchen Fu, and Guoqiang Xu. Buoyancy effects on heat transfer to supercritical pressure hydrocarbon fuel in a horizontal miniature tube. *International Journal of Heat and Mass Transfer*, 115:1173–1181, 2017.

[129] Thomas L Corlett. *Heat transfer characteristics of liquid-liquid dispersion flowing in the annulus*. 1974.

[130] Brandon J Woodland, James E Braun, E. A. Groll, and W Travis Horton. Experimental Testing of an Organic Rankine Cycle with Scrolltype Expander. 2012.

[131] Minsung Kim, Seok Ho, Piotr A Domanski, and W Vance Payne. Design of a steady-state detector for fault detection and diagnosis of a residential air conditioner. *International Journal of refrigeration*, 31:790–799, 2008.

[132] Steven Lecompte, Sergei Gusev, Bruno Vanslambrouck, and Michel De Paepe. Experimental results of a small-scale organic Rankine cycle : Steady state identification and application to off-design model validation. *Applied Energy*, 82:80–106, 2018.

[133] J. Dirker and J. P. Meyer. Convective heat transfer coefficients in concentric annuli. *Heat Transfer Engineering*, 26(2):38–44, 2005.

[134] Ian H Bell, Wronski Jorrit, Sylvain Quoilin, and Vincent Lemort. Pure and Pseudo-pure Fluid Thermophysical Property Evaluation and the Open-Source Thermophysical Property Library CoolProp. *Industrial and Engineering Chemistry Research*, 53(6):2498–2508, 2014.

[135] Eric W. Lemmon and Richard T. Jacobsen. A new functional form and new fitting techniques for equations of state with application to pentafluoroethane (HFC-125). *Journal of Physical and Chemical Reference Data*, 34(1):69–108, 2005.

[136] Eric W. Lemmon. Enthalpy uncertainty. *RefProp 7*.

[137] Koichi Watanabe. Uncertainties in Enthalpy for the IAPWS Formulation. Technical Report 1, 2003.

[138] D. R. Goodwin, H. M. Roder, and G. C. Straty. Thermophysical Properties of Ethane, from 90 to 600 K at pressures to 700 Bar. Technical report, National Bureu of Standards, 1976.

[139] D. Robert McCarty and A. Lloyd Weber. Thermophysical Properties of Parahydrogen from the Freezing Liquid Line to 5000 R for Pressures to 10,000 Psia. Technical report, Cryogenics Division Institute fo Basic Standards, 1972.

# Appendices

# A. Uncertainty analysis

## A.1 Thermophysical properties of thermal oil Therminol ADX10

Therminol ADX10 is a low viscosity synthetic organic heat transfer fluid particularly recommended for indirect liquid phase process heating at medium temperatures up to 250°C. For determining the thermophysical properties of the heating fluid the technical data provided by the manufacturer (Solutia Inc.) was used [125]. Calculating the actual properties (density, $\rho$ $(kg/m^3)$, specific heat capacity $c_p$ $(kJ/kgK)$, thermal conductivity $\kappa$ $(W/mK)$ and the kinematic viscosity $\nu$ $(cSt)$) of the fluid at effective temperature measurements was done by using equations particularly derived for the Therminol ADX10, and are enlisted below.

$$\rho = 870.297 - 0.684497 \cdot T + 5.18441 \cdot 10^{-5} \cdot T^2 - 1.0695 \cdot 10^{-6} \cdot T^3 \quad \text{(A.1)}$$

$$c_p = 1.8363 + 0.00392 \cdot T - 1.5 \cdot 10^{-6} \cdot T^2 \quad \text{(A.2)}$$

$$\kappa = 0.1265 - 0.000123 \cdot T - 9.161 \cdot 10^{-8} \cdot T^2 \quad \text{(A.3)}$$

$$\nu = e^{\left(\frac{-4132.91}{T+149} + 13.93\right)} \quad \text{(A.4)}$$

where the temperature is in °C. All thermophysical properties were calculated at bulk temperatures of the thermal oil.

The dynamic viscosity $\mu$ is determined as a product of the kinematic viscosity and the density $\mu = \nu \cdot \rho$.

In order to determine the uncertainty of the specific heat capacity an experimental data provided by the manufacturer (Solutia Inc.) was used. The average heat capacity from the measurements was plotted as function of the temperatures between the range of 60-130°C. Hence, the heat capacity of Therminol ADX10 was estimated to be equal to $c_p = 0.0036T + 2.0647$ with an uncertainty of $\pm 0.0743$ $kJ/kgK$ (3.4%).

## A.2 Thermophysical properties of R125

An Open-Source Thermophysical Property Library, CoolProp 6.3.0 [134] was used for evaluating the thermophysical properties of R125 at each measurement conditions. The properties are evaluated by the Lemmon and Jacobsen model [135] and the uncertainties are illustrated as 0.1% for the density, 0.5% for the specific heat capacity and 0.1% in vapor pressure. On the other hand, the equation of state for R125 is valid for temperatures in the range of 175.52K (triple point) to 500K and pressures of 60 $MPa$. The uncertainty of all thermophysical properties is higher in the critical region. In the work of [136] was reported that as common practice in the literature is to assume that the enthalpy's uncertainty is the half of the specific heat capacity [136].

Furthermore, for estimating the uncertainty of the heat transfer rate at the working fluid side $\dot{Q}_{wf}$ (Eq.(3.1)) it is important to know the accuracy of the mass flow rate and the enthalpy. However, the uncertainty of the specific heat capacity (enthalpy) in the critical region is not quantitatively expressed in the article for R125 [135].

The reason lies in the difficulty to estimate the uncertainties near the critical region because of the rapid property changes. For instance, the specific heat capacity near the critical point becomes very large. Therefore, quantitative estimation of the specific heat uncertainty's is most of the time not reported. This is the case for most of the fluids. However, even though there is limited data in literature, the uncertainty of enthalpy difference (specific heat) is reported for water/steam [137] and ethane [138]. Also, the accuracy of the density near critical point for hydrogen is estimated in the report of McCarty et. al [139].

Furthermore, absolute uncertainties of the enthalpy difference for water/steam is reported as $\pm 15\%$ at 24 $MPa$ (the critical pressure of water is 22.01 $MPa$) and $\pm 8\%$ at 30 $MPa$ [137]. The uncertainty of the density of hydrogen near the critical point is estimated to be $\pm 6\%$ [139]. On the other hand, the uncertainty of the enthalpy near the critical point of ethane is $\pm 10\%$ [138].

In summary, because there is no quantitative data concerning the uncertainty of the enthalpy (specific heat) for R125 near the critical region, the author assumed for the data reduction and uncertainty analysis an error of $\pm 10\%$.

## A.3 Temperature measurement uncertainty

There are 3 types of temperature sensors used in the test facility 'iSCORe': Pt100, K-type and T-type of thermocouples. A precision data acquisition system (Keithley 2700) is used for reading out the thermoelectric voltages of the K-type and T-type of thermocouples. While the signals of the Pt100's are read out from DAQ NI CompactRio. In order to mitigate the uncertainty on the measured data the thermocouples are calibrated in-house. During the

calibration, the thermocouples were placed in a dry-block calibrator (Druck DBC 150) that was connected with a reference probe Pt100 thermometer (Fluke 1523) that has a very high absolute accuracy of 0.064°C. After stabilizing the calibrator in terms of temperature, the measurement started and it was in a range of 0-100°C with intervals of 10°C and a frequency of 1 $Hz$. At each interval the reference probe executed 10 measurements and the calibrated thermocouples 100 measurements. Then the average values of the reference probe are plotted with respect to the average values of the thermocouples (one at a time) at the appropriate measuring point. Using these measurements, a calibration curve is fitted. For the Pt100's is a linear calibration curve in a form $Y = Ax + B$ while for the K-type and T-type a least square polynomial regression $Y = Ax^2 + Bx + C$ of $2^{nd}$ order was used. For improved accuracy the measurements of all the thermocouples can be corrected by using the constants A, B or C, accordingly.

For linear regression used for the Pt100's the uncertainty of the fitted curve is determined with Eq.(A.5).

$$\delta T_{reg} = \sqrt{\frac{\sum_i (y_i - A \cdot x_i - B)^2}{n-2}} \tag{A.5}$$

A least square regression of $2^{nd}$ order was used for the K-type and T-type of thermocouples illustrated with Eq.(A.6).

$$\delta T_{reg} = \sqrt{\frac{\sum_i (y_i - A \cdot x_i^2 - B \cdot x - C)^2}{n-3}} \tag{A.6}$$

For calculating the total uncertainty Eq.(A.7) of the thermocouples both uncertainties (the thermocouple and the reference probe) have to be considered.

$$\delta T_{tot} = \sqrt{\left(\delta T_{reg}\right)^2 + \left(\delta T_{ref}\right)^2} \tag{A.7}$$

Determining the uncertainties by using Eq.(A.7) is shown in Table A.1.

**Table A.1:** Uncertainties of the temperature sensors

| | Average | Maximum |
|---|---|---|
| Pt100 | 0.0718 | 0.0871 |
| T-type | 0.0669 | 0.0699 |
| K-type | 0.1779 | 0.1866 |

## A.4 Pressure measurement uncertainty

There are 6 pressure sensors installed in the experimental loop, that are connected to DAQ NI CompactRio. The uncertainty of a pressure sensor accounts three values: accuracy, long-term stability (or ageing) and the thermal stability, expressed as a percentage of the measurement range. On the other hand, the accuracy of the pressure sensor considers the hysteresis, repeatability and non-linearity effects. The uncertainty of the thermal stability is defined for a specific temperature range and the long-term stability (ageing) is specified with the maximum drift per year.

Table A.2. gives the accuracy and the thermal stability of all pressure transmitters used in the experimental loop. However, for determining the pressure drop over the test section, 2 pressure sensors GE UNIK 5000 (PMP50G6-TD-A2-CA-H0-PR) with an accuracy of 0.1% FS BSL (Full Scale Best Straight Line) were used. The thermal stability is considered in the range of -40 - 125°C and is 1.5% for the pressure transmitters used for determining the pressure drop. For all pressure sensors the ageing is represented with 0.1% FS/year (Full Scale per year.). Additionally, the uncertainty of the DAQ NI CompactRio that is a sum of the given reading, the offset and the system noise is also considered.

**Table A.2:** Uncertainty of pressure sensors

| Sensor | Type GE UNIK 5000 | Range | Accuracy [FSBSL] | Thermal stability [FS/°C] |
|---|---|---|---|---|
| $P_{in}$ | PMP50G6-TD-A2-CA-H0-PR | 0 - 60 $bar$ | 0.1% | 1.5% |
| $P_{out}$ | PMP50G6-TD-A2-CA-H0-PR | 0 - 60 $bar$ | 0.1% | 1.5% |
| $P_{pump}$ | PMP50A2-TD-A3-CC-H0-PR | 0 - 60 $bar$ | 0.04% | 1% |
| $P_{cond}$ | PMP50G6-TD-A1-CA-H0-PR | 0 - 60 $bar$ | 0.2% | 2% |
| $P_{exp}$ | PMP50G6-TD-A1-CA-H0-PR | 0 - 60 $bar$ | 0.2% | 2% |
| $P_{diff}$ | PMP50G6-TD-A3-CA-H0-PB | 0 - 15 $kPa$ | 0.04% | 0.2% |

$$\delta p = \sqrt{(\delta p_{acc})^2 + (\delta p_{thermal})^2 + (\delta p_{age})^2} \tag{A.8}$$

The percentile error was determined for the operating pressure ($(1.05\text{-}1.15)p_{cr}$) and is in the range of 1.45%-1.55%. As already indicated the pressure drop was determined by using these two pressure transmitters. The pressure drop was in the range of 5-10 $kPa$ that yields an error of 6-12%.

## A.5 Mass flux uncertainty

Two Coriolis mass flow meters from 'Rheonik' were used to measure the mass flow rate of the heating fluid (GE, RHM20) and the working fluid (GE, RHM12). Both meters were calibrated by the manufacturer at temperatures in the range

of 20-130°C for the heating fluid and in the range of 20-110°C for the working fluid. The range of the mass flow rate and the absolute error of the heating fluid was 6-140 $kg/min$ ($\pm 0.16\%$) and for the working fluid 2-30 $kg/min$ ($\pm 0.16\%$).

$$G_{wf} = \frac{\dot{m}_{wf}}{A_{i,c}} \tag{A.9}$$

$$\begin{aligned} \delta G_{wf} &= \sqrt{\left(\frac{\partial G_{wf}}{\partial \dot{m}_{wf}} \cdot \delta \dot{m}_{wf}\right)^2 + \left(\frac{\partial G_{wf}}{\partial A} \cdot \delta A\right)^2} \\ &= \sqrt{\left(\frac{1}{A} \cdot \delta \dot{m}_{wf}\right)^2 + \left(-\frac{\dot{m}_{wf}}{A^2} \cdot \delta A\right)^2} \end{aligned} \tag{A.10}$$

The mass flux was in the range of 400-650 $kg/m^2s$ and the uncertainty is below 1.5%.

## A.6 Uncertainty in the energy balance in the test section

In this section the uncertainty of the energy balance is presented.

$$\dot{Q} = \dot{m}_{hf} c_{p,hf} \Delta T \tag{A.11}$$

$$\begin{aligned} \delta Q_{hf} &= \sqrt{\left(\frac{\partial Q_{hf}}{\partial \dot{m}_{hf}} \cdot \delta \dot{m}_{hf}\right)^2 + \left(\frac{\partial Q_{hf}}{\partial c_{p,hf}} \cdot \delta c_{p,hf}\right)^2 + \left(\frac{\partial Q_{hf}}{\partial \Delta T} \cdot \delta \Delta T\right)^2} \\ &= \sqrt{\left(c_{p,hf} \Delta T \delta m_{hf}\right)^2 + \left(\dot{m}_{hf} \Delta T \delta c_{p,hf}\right)^2 + \left(\dot{m}_{hf} c_{p,hf} \delta \Delta\right)^2} \end{aligned} \tag{A.12}$$

$$\dot{Q} = \dot{m}_{wf} \Delta h_{wf} \tag{A.13}$$

$$\begin{aligned} \delta Q_{wf} &= \sqrt{\left(\frac{\partial Q_{wf}}{\partial \dot{m}_{wf}} \cdot \delta \dot{m}_{wf}\right)^2 + \left(\frac{\partial Q_{wf}}{\partial \Delta h} \cdot \delta \Delta h\right)^2} \\ &= \sqrt{\left(\dot{m}_{wf} \delta \Delta h_{wf}\right)^2 + \left(\delta \dot{m}_{wf} \Delta h_{wf}\right)^2} \end{aligned} \tag{A.14}$$

## A.7 Uncertainty in the heat transfer coefficient and heat flux

The local heat transfer coefficient of the working fluid at the inside of the tube is calculated using Eq. (A.15) and the heat flux with Eq. (A.17).

$$HTC_{wf,loc,(n)} = \frac{q_{loc,(n)}}{T_{wf,w,i,(n)} - T_{wf,b,(n)}} - \frac{ln(D_i/d_o)d_o}{2\lambda} \tag{A.15}$$

$$q_{loc,(n)} = \frac{\dot{m}_{hf}}{\pi d_o}\frac{dh_{hf}}{dn} \tag{A.16}$$

$$\delta q = \sqrt{\left(\frac{\partial q}{\partial m_{hf}}\delta m_{hf}\right)^2 + \left(\frac{\partial q}{\partial d_o}\delta d_o\right)^2 + \left(\frac{\partial q}{\partial \frac{dh_{hf}}{d_n}}\delta\frac{dh_{hf}}{dn}\right)^2} \tag{A.17}$$

# B. Experimental data

## B.1 Experimental reproducibility

Experimental reproducibility validation of the measurement results was done by comparing data obtained at three different days. The measurements were done under similar inlet conditions of the working and the heating fluid. The inlet temperature of the working fluid differs less than 1% between the first (06.08.2019) and the second measurement (17.04.2019) and less than 0.2% between the first and the third measurements (19.08.2019). This trend is visible for the temperature profile along the test section. However, the temperature difference at the inlet and at the outlet of the test section is in the same order of magnitude ($\sim 6.5C$).

The good reproducibility of the measurements is presented on Figure B.2.

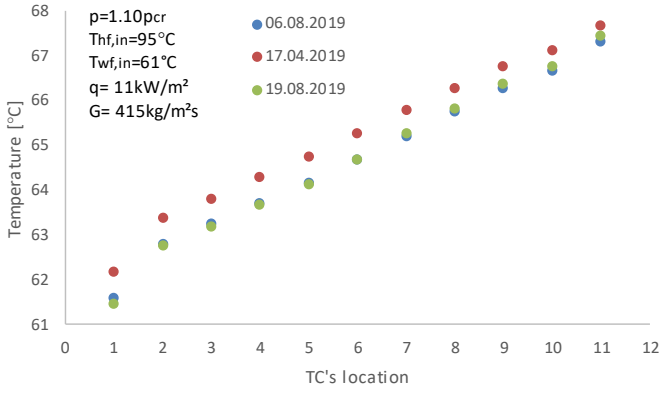


**Figure B.1:** Experimental reproducibility validation

#### B.1.0.1 List of experimental data.

**Table B.1:** An overview of the experimental data at inlet conditions

| $T_{hf,in}$ | $T_{wf,in}$ | $m_{hf}$ | $m_{wf}$ | $p_{wf,in}$ |
|---|---|---|---|---|
| 95°C | 60°C | 2 $kg/s$ | 0.2 $kg/s$ | 1.05<br>1.10<br>1.15 |
| 95°C | 60°C | 2 $kg/s$ | 0.25 $kg/s$ | 1.05<br>1.10<br>1.15 |
| 95°C | 60°C | 2 $kg/s$ | 0.3 $kg/s$ | 1.05<br>1.10<br>1.15 |
| 110°C | 60°C | 2 $kg/s$ | 0.2 $kg/s$ | 1.05<br>1.10<br>1.15 |
| 110°C | 60°C | 2 $kg/s$ | 0.25 $kg/s$ | 1.05<br>1.10<br>1.15 |
| 110°C | 60°C | 2 $kg/s$ | 0.3 $kg/s$ | 1.05<br>1.10<br>1.15 |
| 125°C | 60°C | 2 $kg/s$ | 0.2 $kg/s$ | 1.05<br>1.10<br>1.15 |
| 125°C | 60°C | 2 $kg/s$ | 0.25 $kg/s$ | 1.05<br>1.10<br>1.15 |
| 125°C | 60°C | 2 $kg/s$ | 0.3 $kg/s$ | 1.05<br>1.10<br>1.15 |

## B.2 Changes of the Reynolds number for the entire sets of measurement

Figure B.2 represents the variation of the Nusselt number as a function of the Reynolds number for the entire sets of measurements. As it can be seen from Table B.1, that there are $\sim 20$ different sets of measurements. Moreover, there are large changes of the Reynolds number especially when the working fluid

is in the vicinity of the pseudocritical region. The Reynolds number is in the range between 130,000 - 550,000.

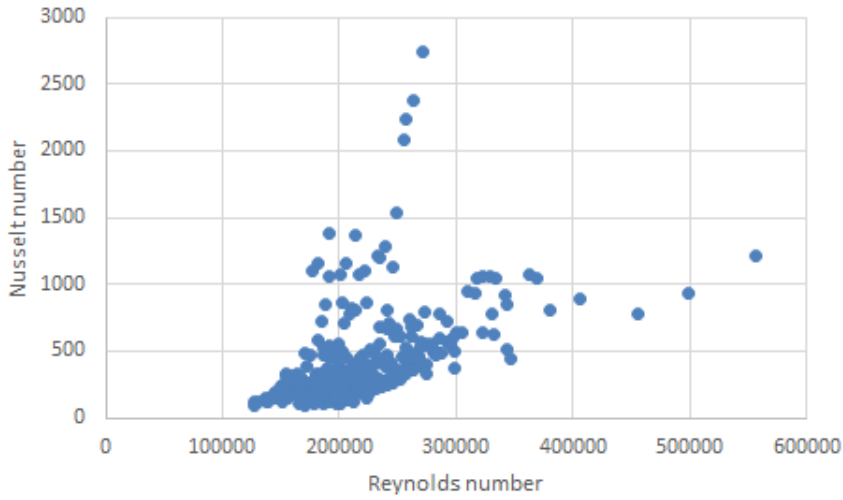


**Figure B.2:** Nusselt number as a function of the Reynolds number.

Because the data set is limited, it could not be used for developing a heat transfer correlation for general use. Therefore, it is mandatory to obtain measurements for wider ranges and to consider more refrigerants as working fluids.

# C. Publications

## C.1 Publications in peer reviewed journals

Lazova Marija, Kaya Alihan, Billiet Marijn, Lecompte Steven Manolakos Dimitris and De Paepe Michel, Experimental assessment of a helical coil heat exchanger operating at subcritical and supercritical conditions in a small-scale solar organic Rankine cycle, Energies, Vol. 10, 2017

Lazova Marija, Huisseune Henk, Kaya Alihan, Lecompte Steven, Kosmadakis George and De Paepe, Michel, Performance evaluation of a helical coil heat exchanger working at supercritical conditions in a solar ORC installation, Energies, Vol. 9, 2016

Kosmadakis George, Landelle Arnaud, Lazova, Marija, et al. Experimental testing of a low-temperature organic Rankine cycle (ORC) engine coupled with concentrating PV/thermal collectors : laboratory and field tests, Energy. Vol. 117, 2016

## C.2 Publications in proceedings of international conferences

Lazova Marija, Lecompte Steven and De Paepe Michel, Determining the heat transfer characteristics of R125 at supercritical pressures, Proceedings of the 5th International Seminar on ORC Power Systems, Athens, Greece, 2019

Lazova Marija, Lecompte Steven and De Paepe Michel, Heat transfer regimes of R-125 at supercritical pressures tested in horizontal flow and under organic Rankine cycle conditions, Proceedings of the 25th IIR International Congress of Refrigeration, Montreal, Canada, 2019

Lazova Marija, Kaya Alihan, Lecompte Steven and De Paepe Michel, Presentation of a test-rig for heat transfer measurements of a fluid at supercritical state for organic rankine cycle application, Proceedings of the 16th International Heat Transfer Conference, Beijing, China, 2018

Lazova Marija, Kaya Alihan, Lecompte Steven and De Paepe Michel, Supercritical heat transfer characteristics occurring in a heat exhanger operating under organic Rankine cycle conditions, 5th Annual engine ORC consortium workshop for the automotive and stationnary engine industries, Lyon, France, 2018

Lazova Marija and De Paepe Michel, Investigating the heat transfer characteristics of supercritical HFC-125 in low temperature organic Rankine cycles, 2nd European supercritical $CO_2$ Conference, Essen, Germany, 2018

Lazova Marija, Kaya Alihan and De Paepe Michel, Heat transfer characteristics of supercritical fluids operating under low-temperature organic Rankine cycle conditions, IV International Seminar on ORC Power Systems, ORC2017, Milano, Italy, 2017

Lazova Marija, Kaya Alihan and De Paepe Michel, Experimental study of supercritical heat transfer characteristics of the fluid R-125 applicable for organic Rankine cycle's, 9th World Conference on Experimental Heat Transfer, Fluid Mechanics and Thermodynamics, Foz do Iguazu, Brazil, 2017

Lazova Marija, Kaya Alihan, Billiet Marijn, Lecompte Steven and De Paepe Michel, Experimental investigation of a forced convection heat transfer of the organic fluid R-125 at supercritical pressures and under organic rankine cycle conditions, Proceedings of the 13th International Conference on Heat Transfer, Fluid Mechanics and Thermodynamics, Portoroz, Slovenia, 2017

Lazova Marija, Kaya, Alihan, Huisseune Henk and De Paepe Michel, Experimental investigation of a helical coil heat exchanger operating at sub- and supercritical state in a small-scale solar ORC installation, 12th International Conference on Heat Transfer, Fluid Mechanics and Thermodynamics, Malaga, Spain, 2016

Lazova Marija, Kaya Alihan, Huisseune Henk and De Paepe Michel, Experimental investigation at sub- and supercritical conditions of a helical coil heat exchanger particularly designed for a small-scale solar ORC, 7th European Thermal-Sciences Conference, Krakow, Poland, 2016

Lazova Marija, Kaya Alihan, Huisseune Henk and De Paepe Michel, Experimental investigation of heat transfer to supercritical organic fluid R125 in horizontal tubes for Organic Rankine Cycle applications, 1st European Seminar on Supercritical $CO_2$ Power systems, Vienna, Austria, 2016

Lazova Marija, Kaya Alihan, Huisseune Henk and De Paepe Michel, Heat transfer at supercritical state for organic Rankine cycle applications, 24th IIR International Congress of Refrigeration (ICR), 2015

Lazova Marija, Daenens Dieter, Kaya Alihan, Huisseune Henk and De Paepe Michel, Design of a supercritical heat exchanger for an integrated CPVT-Rankine cycle, Proceedings of the 3rd International Seminar on ORC Power Systems, Brussels, Belgium, 2015

Lazova Marija, Kaya Alihan, Huisseune Henk and De Paepe Michel, Supercritical heat transfer and heat exchanger design for organic rankine application, 11th International Conference on Heat Transfer, Fluid Mechanics and Thermodynamics, Kruger National Park, South Africa, 2015

Lazova Marija, Daelman Stijn, Kaya Alihan, Huisseune Henk and De Paepe Michel, Heat transfer in horizontal tubes at supercritical pressures for organic rankine cycle applications,10th International Conference on Heat Transfer, Fluid Mechanics and Thermodynamics, Proceedings, Orlando, Florida, USA, 2014

Full list of articles: https://biblio.ugent.be/person/000130708308